NOTE TO USERS

SWEEPRATE AND TEMPERATURE EFFECTS ON CRACKLING NOISE

BY

ROBERT ALLEN WHITE

B.S., California State University, Chico, 1998
M.S., University of Illinois at Urbana-Champaign, 2001

DISSERTATION

Submitted in partial fulfillment of the requirements
for the degree of Doctor of Philosophy in Physics
in the Graduate College of the
University of Illinois at Urbana-Champaign, 2005

Urbana, Illinois

CERTIFICATE OF COMMITTEE APPROVAL

University of Illinois at Urbana-Champaign
Graduate College

November 10, 2005

We hereby recommend that the thesis by:

ROBERT ALLEN WHITE

Entitled:

SWEEPRATE AND TEMPERATURE EFFECTS ON CRACKLING NOISE

Be accepted in partial fulfillment of the requirements for the degree of:

Doctor of Philosophy

Signatures:

Karin Dahmen
Director of Research - Karin Dahmen

John D Stack
Head of Department - John D. Stack

Committee on Final Examination*

Nigel Goldenfeld
Chairperson - Nigel Goldenfeld

Michael J. Weissman
Committee Member - Michael Weissman

Committee Member - Gary Gladding

Committee Member -

Committee Member -

Committee Member -

* Required for doctoral degree but not for master's degree

Abstract:

Crackling noise, defined as separate bursts characterized by power law behavior of the frequency histograms over many decades, is observed in many driven systems far from equilibrium. Examples of such systems pepper a remarkable range of length and energy scales from jerky domain wall motion of disordered magnets, to the sometimes devastating crackling of the earth to the bursty release of energy in the photosphere of the sun dwarfing that of our most horrible WMD.

Typically, crackling noise is modeled in the infinitely slow driving rate limit at zero temperature. In this dissertation I investigate the effects of relaxing these limits. First I consider the crackling system at zero temperature and finite sweeprate. I discuss how the temporal overlap of power law bursts can account for a wide range of scaling behavior and provide a criterion for sweeprate controlled exponents based on exponents obtained in the infinitely slowly driven limit. I also discuss scaling arguments for hitherto unexplained results in the power spectrum of crackling response in disordered magnets, commonly referred to as Barkhausen noise. Scaling arguments and numerical results are compared to Barkhausen noise measurements in two materials representing distinct adiabatically driven universality classes.

Relaxation of the zero temperature constraint cannot be done without considering finite sweeprates due to global relaxation timescales that arise at finite temperatures. We investigate the connection between sweeprate and thermal fluctuations in the far from equilibrium limit typical of crackling systems. Again, using scaling arguments and numerical simulations of the random field Ising model near a disorder-induced critical point we analyze interesting crossover phenomena in the power spectra which are also observed in Barkhausen noise but have yet to be explained.

To My Wife

Acknowledgments

The enrichment I experienced in my graduate life at UIUC can be broken into three categories: Research, Teaching and Social. In each of these areas there are people who had a significant impact on my development as a scientist and as a human being. I would like to acknowledge those contributions here.

Research:

I would first like to formally extend my gratitude to Karin Dahmen. Her impromptu "invitations" to speak with visiting scientists or give a talk about my research (when I wasn't sure I had much to talk about) gave me significant stress. As I wrap up my graduate career I look back at those experiences as formative and invaluable to my development as a scientist. I also spent countless hours attempting to explain to her my thought processes about particular aspects of research. These attempts were met with infinite patience even if, as was often the case, the explanations were muddled. When I eventually made a point, she was quick to suggest consequences of ideas I was presenting that I had not seen or how the idea was related to work already done in the literature. In short, I am sure that without her infectious enthusiasm, endless encouragement, and broad knowledge base this thesis would not exist.

I would also like to thank Mike Weissman. An expert in finding clarity in noise, his ability to find bottlenecks in understanding was inspirational. He told me once that "there is more to life than exponents" and although it is probably not evident

from this thesis, it is a statement that I took to heart and will remember everytime I see a talk or read a paper.

I also benefited from discussions and/or collaborations with Alex Travesset, Jim Sethna, Andy Mills, Aki Palanisami, Gianfranco Durin and John Carpenter. Funding for the work contained in this document was provided by: NSF DMR 03-25939 (Materials Computation Center), NSF DMR 03-14279 and a GAANN fellowship from the University of Illinois.

Teaching:

Aside from the prerequisite of valuing teaching, I think becoming a good teacher has three necessary requirements: 1.) Having good professors as a student that serve as a model for pedagogical clarity. 2.) Having bad professors as a student that reinforce the idea that most everything you learn is based on an independent search for clarity 3.) Teaching in an environment where excellence in teaching is prized and ideas *about* teaching are discussed. My experience at UIUC has provided me with each of these.

Although I did not have personal experience with all the professors in the physics department I would like to acknowledge two professors at UIUC that have served as positive models for me. In each lecture and homework set Paul Goldbart and Nigel Goldenfeld made an ernest attempt to distill whatever topic they were covering into essential features. While I believe the real learning happens in the struggle with homework sets, the lectures provide depth that can only be gleaned from the thoughtful exposition of a topic from a learned expert. The rarity of this experience is sad but true and that I experienced it from two people in my graduate course-work deserves note.

As a teacher of undergraduate courses, I was fortunate to work closely with Tim Stelzer and Gary Gladding. The benefit that I got from these interactions was a

perspective that teaching excellence is not something you either have or you don't, it is something that can be developed and improved with the same thought processes that we use to investigate Nature.

Social:

I gained many friends during my time at Illinois that have given me great joy on a personal level that I will not detail here. There are individuals, however, that I think have had significant impact through social interactions on my development as a scientist and person. First and foremost, Akilan Palanisami began with me as a graduate student and was a constant source of interesting conversation about an unbelievably broad selection of topics. It is largely through my interactions with him that I obtained a richer view of the world than I could have conceived of as a wide-eyed undergraduate in a small town in northern California.

I would also like to express appreciation for interactions with Andy Mills; The Rodeo Girl Collective (a.k.a. The Renormalization Group) Susan Kim, Dan Finkenstadt and Dylan Smith; and the Boys: Erik Draeger, Dan Sheehy and Mark Kleinschmit.

Table of Contents

List of Figures

Chapter 1

Introduction

Jerky response to slowly varying conditions is a common theme in nature. Mundane examples can be appreciated while sitting by the campfire, making popcorn, eating your morning cereal or crumpling up a piece of paper. Other, thankfully more rare, examples include the jerky response of the earth to tectonic forces and the collapse of large-scale power grids. Investigations at finer length scales as well as outside the confines of Earth reveal a multitude of more exotic examples from the jerky motion of a magnetic domain wall dragged through a disordered magnet to bursts of radiation emanating from the sun.

A large subset of these systems exhibit a peculiar type of jerky response called crackling noise (CN) [1]. The defining feature of CN is the lack of characteristic scale of the pulses up to a size that is much larger than the smallest pulse and sometimes even represents dynamics that extend to the size of the system. In between the largest and smallest pulses, a wide range of sizes are found. This broad range of size scales manifests itself as a power-law distribution of burst, or avalanche, sizes and durations. Efforts to understand CN in a broad sense center around two questions: 1.) (Origin) Why and how do the avalanche sizes scale? 2.) (Ubiquity) Why is CN so common even in systems over which we have no experimental control, such as earthquakes?

The answer to the first question appears to be that the system is being driven

near a continuous non-equilibrium phase transition and the CN is a signature of this (akin to equilibrium critical phenomena). The study of avalanches near a depinning transition in which a flexible (but connected) interface is dragged through a disordered medium by an externally applied driving force, has provided early progress toward this understanding [2]. Near the depinning transition, characterized by a critical force F_C, the domain wall moves in a jerky fashion with a broad distribution of displacement events and the average velocity of the domain wall ν exhibits scaling behavior for $F > F_C$ given by $\nu = (F - F_C)^\beta$.

Depinning transitions are observed in a number of experimentally controlled systems including charge density waves [3], weakly pinned flux lattices in type II superconductors [4, 5], domain walls in weakly disordered magnets [6] and fluids invading porous media [7]. The critical behavior of these far-from-equilibrium systems has been studied by functional renormalization group methods [8] as well as simulations [9]. These studies have provided a solid conceptual foundation for the scaling behavior as well as numerical values to compare to experiments.

For depinning transitions, however, the environmental parameter regime over which scaling is observed is typically very small (a feature shared by equilibrium critical phenomena). For example, CN arising from a depinning transition is observed in a forcing regime within $\sim 1\%$ of the critical force. As a result, it is unlikely that the mystery of CN ubiquity can be explained by a large number of systems coincidentally sitting near a depinning transition. Something is missing.

In the late 1980's a seminal series of papers [10, 11, 12] provided an argument for the ubiquity of scale invariant noise. The enduring idea from these papers was the notion of self organized criticality (SOC). Gaining inspiration from the tendency of sandpiles to maintain a constant angle of repose with the slow addition of grains to the pile, Bak, Tang and Wiesenfeld proposed a cellular automata "sandpile" model (other models followed). In these models, the angle of repose was the tuning parameter for

the given boundary conditions that was automatically maintained, on average, to sit at a critical value by the avalanches of sand down the pile. The distribution of these avalanches exhibit power law scaling of all sizes up to system spanning avalanches.

More recent studies of the reversal of magnetic domains in the limit of strong disorder [13] have uncovered another critical point that is tuned by an external driving field (or force) and the amount of disorder present in the system. The physical differences between weak disorder, giving rise to depinning transitions, and the strong disorder limit relate to the allowed configurations of the domain wall; In the strong disorder limit a domain wall may "tear" to get around a pinning site; and the creation of new domains is allowed as the external conditions are slowly changed. Unlike most previously studied critical phenomena, scaling in this model can be observed over a remarkably large range of disorders [14]. For example, even at 50% away from the critical disorder, simulations still show 2 decades of scaling in the distributions of the domain flipping size. The wide scaling regime places the disorder-induced critical behavior in line as a possible explanation for the ubiquity of crackling phenomena; one with a broad base of analytical support. Although initial comparisons with this model and real materials have been promising [15], further systematic comparisons relating the disorder induced phase transition and CN are needed.

The pieces of the puzzle required for qualitative understanding of the two broad questions posed above (origin and ubiquity) appear to be in place. However, challenges remain in applying this understanding to real systems by comparing data to quantitative outputs from the models (*i.e.*, exponents and scaling functions). Some of these challenges are borne out of limitations of available data. Large statistical error bars can preclude the selection of one model over another. When the error bars are as good as they can get, a common approach is to tweak the parameters with the hope of generating a gross feature that will aid in model discrimination.

In this dissertation I present our investigations on the effects of changing the

rate at which the system is driven as well as the effects of non-zero temperature on typically measured properties of crackling systems. We were interested in this for a number of reasons. For the sake of analytic clarity crackling systems are typically studied in the zero sweeprate zero temperature limit. Relaxing these constraints is an intellectually interesting exercise as it probes the gaps between a well-developed understanding of equilibrium systems and the still young science of extended systems far from equilibrium. Fruits of this investigation will benefit theory, experiment and applications alike. Furthermore, in systems that cannot be experimentally controlled, knowledge of the effects of relaxing theoretical idealizations is crucial for mapping theory to reality.

In the hope of creating a somewhat self-contained document I include, in the following chapter, an introduction to select examples of CN presenting two examples of experimentally controlled CN (Barkhausen Noise and vortex avalanches) and two examples of CN found on large length scales (earthquakes and solar flares).

In chapter 3 I give representative examples of models used to study crackling response: I present a somewhat detailed overview of the disorder induced critical point observed in the zero temperature random field Ising model as I will use the general form of the scaling features found in this model throughout the thesis. I also outline two well-studied models of Barkhausen noise: a one degree of freedom model; and a flexible domain wall model which represents a proven example of an SOC system.

In chapter 4 I give details about the numerical methods used throughout the thesis including the base algorithm for the numerical studies of the zero temperature random field Ising model at finite sweeprate and the random field Ising model at finite temperature but far from equilibrium. In this chapter I also elaborate on a numerical technique for investigating the consequences of generic assumptions applied to crackling systems put forth in chapter 5.

In chapter 6 I lay out the consequences of the generic assumptions for pulse statistics and spectral measurements in crackling systems and show how previously observed sweeprate effects in Barkhausen noise can be explained by model independent scaling arguments. To support the generality of the scaling arguments I provide examples from experimental measurements on two materials representing distinct Barkhausen universality classes.

In chapter 7 I present a study of the effects of temperature on spectral measurements of crackling noise and the possible implications this may have for Barkhausen noise measurements. This chapter has a related, extended appendix (appendix C) that presents a speculative scaling regime in a broader temperature and sweeprate regime found in the body of the dissertation.

Finally, in chapter 8 I conclude with a discussion of the results and future projects extending the work presented in this thesis.

Chapter 2

Examples of crackling noise

In this chapter I discuss systems that exhibit CN listed in order of the extent to which the loading or forcing mechanisms are understood, from most well-characterized to the most mysterious. The primary focus here is the introduction of Barkhausen noise (BN) observed in disordered magnets as it will be used throughout the dissertation as the primary experimental example of crackling response. The overt purpose of introducing other examples is to give an idea of the varied systems that exhibit CN.

The motivation for presenting the examples in order of increasing ignorance in the driving mechanisms is not arbitrary. At first glance, the presence of power law scaling in the noise characteristics may seem justification enough for neglecting details in the underlying forcing mechanism. After all, universality and the presence of power law scaling is often the harbinger of detail-irrelevance. Throughout this dissertation, however, we investigate how sensitive typically measured properties (*e.g.*, jump size and duration distributions) are to details in the driving characteristics.

In introducing a sketch of what is known in proto-typical crackling systems, as well as identifying points of ignorance in underlying mechanisms, we achieve important tangential goals. First, we identify a model system (the disordered magnet) with well-understood and controllable driving characteristics that can be probed to study how various features of the driving mechanism effect typically measured quantities.

Second, we identify systems that are less malleable, but are no less dependent upon the forces that drive them, with the hope that the lessons learned from model systems can aide in the understanding of more poorly characterized phenomena, such as earthquakes and solar flares that have significant impacts on life and property.

Besides crackling, these examples share other common characteristics: They have all received some attention as an example of self-organized criticality followed by arguments that they are not SOC; they have each suffered the pain of the measurement of exponents over a collection of non-stationary distributions in space and/or time and/or some other parameter followed by a search for stationary regions; they are each still under active investigation.

2.1 Barkhausen noise (BN)

In 1919, H. Barkhausen reported on the jerky response of iron to slowly varying external magnetic fields [16]. Historically, the significance of this discovery was derived from its relation to the theoretical prediction, a decade earlier, of the existence of magnetic domains [17]. Barkhausen speculated that this "peculiar behavior of iron" resulted from "individual molecular magnets group[ing] themselves into assemblies of various sizes with different degrees of stability". Almost two decades after Barkhausen's discovery, the origin of this noise was understood, not as a complete domain reversal of a distribution of various sizes of domains (or a reversal of molecular magnets), but as the irregular propagation of domain walls.

Theoretical and experimental work continued throughout the 20th century. As a result, the noise that Barkhausen discovered, the so-called Barkhausen noise (BN), has served as a useful probe for the magnetization dynamics of soft ferromagnetic materials as well as a widely used material engineering tool for non-destructive microstructure determination and testing (for an excellent review see [6] and references

therein). Over the last few decades, and particularly since the notion of SOC was introduced, BN has garnered significant attention due to the power law scaling routinely observed in the pulse area distributions (corresponding to the volume of material that has changed its magnetization orientation in each jump). As experimental setups have become more standardized and interpretation of the data has become more trustworthy, BN has become one of the most well-characterized examples of crackling phenomena with controllable parameters.

The experimental setup for BN measurements typically consist of a pick-up coil wound around a magnetic sample and connected to an oscilloscope. As a slowly increasing external magnetic field is applied to the sample, more and more of the magnetic domains in the sample align with the external field. This magnetization process proceeds in a jerky fashion where each jump in the magnetization corresponds to an "avalanche" of spin flips in the direction of the applied field. These avalanches are observed by induction in the search coil as voltage pulses. In a plot of induced voltage versus time, the propagation of such a pulse is recorded (see fig. 2.1). The integral of each voltage pulse over time is proportional to the total magnetization change during that pulse and is termed the "size" of the pulse. The amount of time it takes to complete the pulse (*i.e.*, the time between two zero voltage signals with nonzero induced voltages in-between) is termed the pulse duration. The distributions (histograms) of pulse size and durations are usually described by power laws of the general form $P(S) = S^{-\tau} f_s(\frac{S}{S^*})$ and $P(T) = T^{-\alpha} f_t(\frac{T}{T^*})$ respectively, where S^* and T^* are the large avalanche cutoffs to power law behavior. The exponents obtained from these distributions, insofar as the proper experimental and interpretive care is taken, determine the universality class to which the material belongs.

So far there are two distinct and cleanly-described universality classes of disordered magnets that crackle [18]. The classes are represented by polycrystalline $FeCo$ 7.8% wt. ribbon and amorphous $Fe_{21}Co_{64}B_{15}$ under moderate tensile stress. The pulse

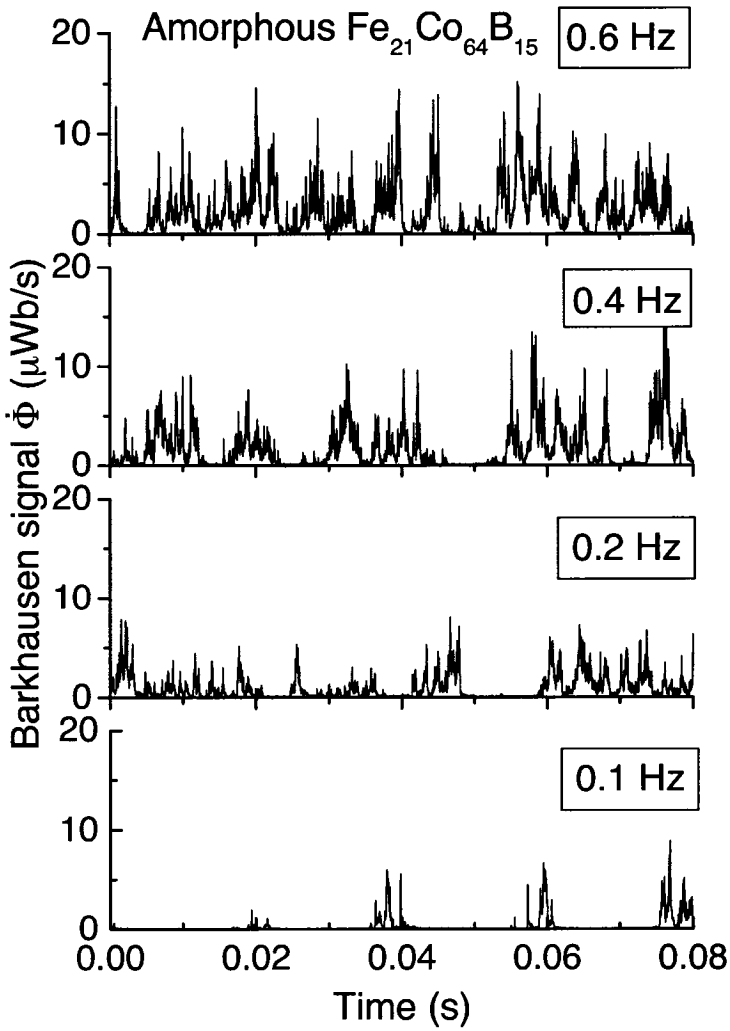

Figure 2.1: Experimental example of sweeprate effects on Barkhausen voltage trace. Shown for increasing sweeprate in the stressed amorphous alloy (taken with permission from [6]).

exponents for $FeCo$ are $\tau = 1.5$ and $\alpha = 2$; and for the stressed amorphous alloy $Fe_{21}Co_{64}B_{15}$ are $\tau \simeq 1.27$ and $\alpha \simeq 1.5$. $FeCo$ has shown sweeprate dependence of $\tau(\Omega) = 1.5 - \frac{\Omega}{2\Omega_t}$ and $\alpha(\Omega) = 2 - \frac{\Omega}{\Omega_t}$ where Ω is the time rate of change of external field and Ω_t marks the sweeprate beyond which individual pulses are not discernible. Exponents in the amorphous alloy under stress show no sweeprate dependence.

Power spectra in these two materials show broad band noise with high frequency scaling behavior of $P(\omega) \sim \omega^{-a}$ where $a = 2$ for the polycrystalline sample and $a = 1.78$ in the amorphous alloy under stress. The spectra also show a marked peak at a frequency at ω_{max} that scales with the sweeprate as Ω^{-b} where $b \simeq \frac{1}{2}$ for both materials. There also seems to be a regime of scaling between the peak and the high frequency regime with $P(\omega) \sim \omega^{-c}$ with $c \simeq 1$. The crossover from the ω^{-c} to ω^{-a} occurs near ω_L, where ω_L appears to have no sweeprate dependence. Below ω_{max}, another scaling regime appears- $P(\omega) \sim \omega$. It is generally accepted that the presence of a low frequency peak is due to the long range effects of the so-called demagnetizing field. In this dissertation I discuss the origin of the sweeprate scaling of ω_{max}, the origin of ω_L and the possible relation to temperature and the intermediate scaling regime between ω_L and ω_{max}.

Average pulse shapes, defined by averaging over all pulses of the same duration, in both of these materials show unambiguous asymmetry with the peak of the avalanche shifted toward the beginning of the pulse. Recently, this asymmetry has been attributed to Eddy currents and an effective negative mass of reversing domains [19]. Higher order spectra also point to breaking of time reversal symmetry [20] showing high frequency events preceding low frequency ones. There is also a marked flattening of the shapes for larger avalanches. The results on pulse shapes have been a long standing mystery since all known models of BN predict symmetric or approximately symmetric shapes.

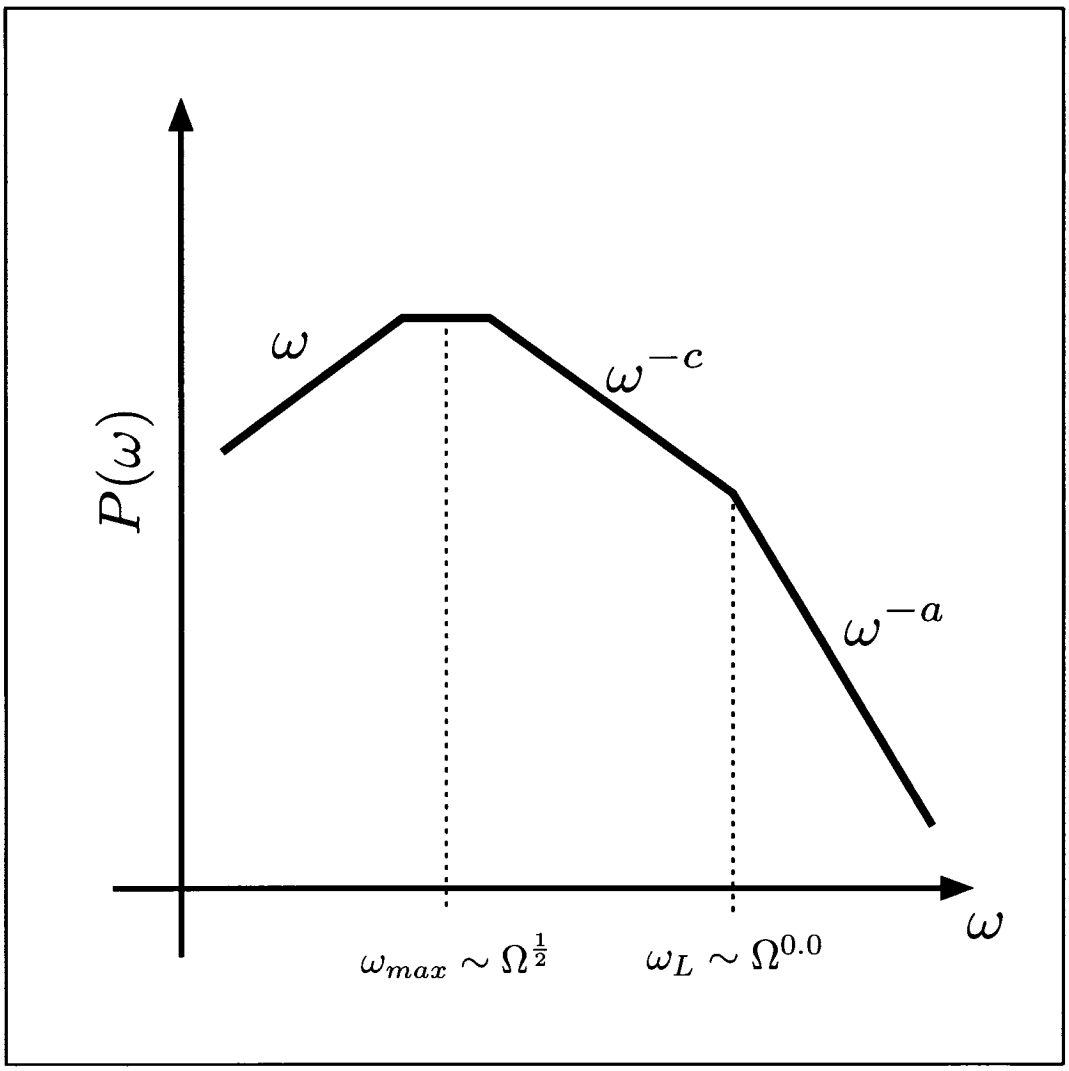

Figure 2.2: Schematic BN power spectrum with typically observed scaling regimes. Crackling Barkhausen spectra typically have a high frequency scaling regime with $P(\omega) \sim \omega^{-a}$ where a ranges from 1.7 to 2.0, an intermediate scaling regime below ω_H which scales as $P(\omega) \sim \omega^{-b}$ where $b \simeq 1$ and ω_H appears to be independent of the sweeprate Ω. The low frequency maximum in the PS at ω_{max} scales with the sweeprate as $\omega_{max} \sim \Omega^{\frac{1}{2}}$.

2.2 Superconducting vortex avalanches

Quanta of magnetic flux (vortices) enter type II superconductors from the edge and move toward the bulk as a critical field is exceeded. Increasing the field further forces more vortices into the material. The vortices themselves are a normal state core surrounded by rotating super current and are thought of as little solenoids with a radius $\sim 10nm$. In a perfect crystal the vortices order to minimize vortex-vortex repulsion but in real materials they become pinned by impurities in the material. As a result the dynamics of flux penetration in type II superconductors gives rise to jerky response upon slowly increasing the external magnetic field. This type of response was recognized in 1966 [21] but did not begin to get intense attention until the SOC era began.

There has been a wealth of experiments done on various materials and geometries (see summary table 2.1). The emerging picture from these studies is that power law scaling is common but the exponents are not. The range in exponents could be partly a consequence of measuring distributions over non-stationary regimes as it has been shown that the scaling behavior depends upon the value of the applied field [22] (a fact that is not always appreciated when analyzing data). The range can also be explained by differing universality classes. In any case, the resolution of ambiguities in interpretation of the data remains to be done to make such claims. Sweeprate and temperature effects are not systematically treated in most reported results. This thesis shows the necessity of these considerations.

The question of whether these phenomena are SOC or not will not be discussed in this thesis; however, it is curious to note how much tuning has been done to observe this criticality "with no tuning parameters". What is important is the field is interesting, there are well developed techniques for measuring the avalanche behavior [4] and, as a study of non-equilibrium critical behavior, there is still work to be done.

Reference	Geom.	Material	Sensor	Avalanche type	T/T_c	H range (kOe)	Rate (Oe/s)	Avalanche distribution
Heiden *et al.* (1968)	hollow cylinder	Pb-In	pickup coil	off-edge	0.6	0.55–0.85	10–100	exp
Field *et al.* (1995)	hollow cylinder	Nb-Ti	pickup coil	off-edge	0.3	2.25–7.55	5	power (1.4–2.2) (slow ramps)
Zieve *et al.* (1996)	planar	YBCuO crystal	Hall probe	internal	$\leq$0.01	0–80	7	peak
Nowak *et al.* (1997)	planar ring	Nb film	Hall probes	off-edge & internal	0.15–1.12	−0.5–0.5	0.002–20	peak/power (2.0)
Aegerter (1998)	planar	BSCCO crystal	SQUID	off-edge	0.06–0.8	?	0	exp/power (2)
Behnia *et al.* (2000)	planar	Nb film	Hall probes	internal	0.52	1.5	~1	peak/power (2.05) /stexp
Altshuler *et al.* (2002)	planar	Nb foil	Hall probes & MOI	internal	0.5	0–3.5	~1	power (3.0)
Aegerter *et al.* (2003)	planar	YBCO film	MOI	internal	0.05	0–0.15	$\leq$0.05	power (1.30)
Radovan and Zieve (2003)	planar	Pb film	Hall probes	internal	$\leq$0.7	0–0.04	0.2–3.3	peak/ power (1.1,2.0)

Table 2.1: Table of experimental results on vortex avalanches, illustrating the breadth of experimental results on vortex avalanches in type II superconductors (from [4])

2.3 Earthquakes

Long before the induction coil or the discovery of superconductivity the earth has exhibited crackling noise. In first half of the 20th century two empirical laws were put forth to describe expected data from earthquakes: Omori's law [23] and the Gutenberg-Richter law [24]. Omori's law relates the frequency of aftershock occurrence, n, to the time, t since a main shock, by $n(t) = t^{-\phi}$ where $\phi \simeq 1$. The Gutenberg-Richter law which (with suitable massaging) states that the distribution $D(M_o)$ of seismic moments M_o measured over a large area, like the earth, scales as $D(M_o) \sim M_o^{-(\beta+1)}$. (The seismic moment of an earthquake is $M_o = \mu AD$ where μ is the average shear modulus of the fault, A is the total area of slippage of the fault and D is the displacement during the earthquake.)

The study of earthquakes as a large scale example of non-equilibrium critical phenomena offers advantages and disadvantages in relation to the above examples. The length scales involved do not require sophisticated microscopy techniques to observe

the relaxations with fine spatial resolution on the scale set by the collective event; this leads to a relatively clear definition of the collective slip event, something that has not been done over many scales in BN. This benefit is partially offset by the difficulty of extracting seismic moments from seismic emissions, the relatively few recorded events, and the large statistical error bars that result. The presence of apparently uncoupled earthquake faults all over the globe with a range of disorder characteristics (such as geometrical inhomogeneities in the faults) offers the opportunity to study the effects that disorder may have on the event statistics [25]; however, quantifying the disorder distributions and other details of earthquake fault structures below the surface is a challenging task.

Another difficulty in modeling earthquakes is that the loading mechanism is not fully-characterized. Generally, it is known that slow continental drift is the driving mechanism with the root cause of convection currents in the underlying magma. It is generally believed that the surface waves caused by earthquakes are not strong enough to disrupt the magma currents (by virtue of the extremely high Rayleigh numbers in magma systems [26]); however, what is *not* known is how these currents change over time or how earthquakes themselves can affect other faults. It is assumed that the details of the loading mechanism are not important for many earthquake models. This may be a reasonable assumption but it is one made out of necessity and, as such, has yet to be fully justified. For practical purposes, it would be good to understand the detailed effects loading characteristics may have on wait time distributions between earthquakes and related statistical distributions.

Driven by the obvious benefits of understanding the crackling of the earth, it would be desirable to continue the study of this behavior until there is an earthquake website that gives the location and time of the next earthquake so people can plan vacations to or from the locales involved. If this sort of understanding is possible, it will no doubt include the interplay between currently unknown parameters and the

signature of universal behavior that has spawned the recent interest.

2.4 Solar flares

Solar flares are the bursty release of magnetic energy built up in the photosphere of the sun believed to result from magnetic reconnection events. The physics of magnetic reconnection is not fully understood and is an active area of research. As a result, the basic mechanisms for loading and instability criteria are still unknown (there are theories of course [27]). What is known is that the histograms of energy bursts emitted from solar flares are well described by power laws over 4 decades. It has been reasonably argued [28] that if an instability criteria exists, it will be local and have a characteristic length scale and hence not yield power law behavior. Consequently, the collective avalanche model seems consistent with the data. However, others have argued that the data is also consistent with the idea that the power laws come from some underlying mechanism and that the bursts themselves are not collective events [29]. The "universal" behavior *here* is that this state of affairs mimics the BN scientific history.

What can be observed from the data on solar flares is that bulk measurements on the sun show the possibility of temporal overlap of solar bursts depending on the 11 year cycle of solar flare activity. Understanding how this can affect the distributions of individual flare sizes and durations in relation to measurements made of spatially resolved flares may help in settling disputes between various camps claiming parameterized fits to the data.

Chapter 3

Models

In this chapter I introduce three models of crackling phenomena that are referred to throughout the thesis; the zero temperature nonequilibrium random field Ising model (ztneRFIM); a one degree of freedom domain wall model developed by Alessandro, Beatrice, Bertotti and Montorsi [30] called the ABBM model; and a flexible domain wall model developed by Ji and Robbins [7], and Cizeau, Zapperi, Durin and Stanley [31].

The ztneRFIM, and the disorder-induced critical behavior it exhibits, is discussed in detail to support discussion of extensive numerical calculations and scaling function definitions reported throughout this document. There are a number of real systems that appear to exhibit disorder-induced critical behavior [15, 32, 33] and the universality of the ztneRFIM has been shown to be unusually huge [1]. However, the focus on the ztneRFIM is borne, not merely out of its potential applicability to a large number of systems, but also from its simplicity. It gives a clear physical picture of the basic elements required for crackling phenomena (*e.g.*, an instability criterion and the importance of disorder and its competition with avalanche promoting interactions that result in collective dynamics). It is the hope that the generic features, exemplified by the ztneRFIM, provide the best perspective from which to view the arguments throughout this dissertation. Despite the focus on the ztneRFIM, the results of this

work are much more generally applicable than just to ztneRFIM-like systems.

The ABBM and flexible domain wall models are standard models in Barkhausen Noise studies. The heavy reliance on Barkhausen phenomenology throughout this thesis justifies this inclusion. Furthermore, the general results obtained in Section 6.6 are consistent with results that can be analytically obtained in these specific models in special cases. In the future, one may ask whether the analytic treatments of these models may be broadened to include the more general results reported here. Later in the dissertation (Sec. 6.7) we present comparisons of the general scaling arguments and numerical results obtained in this thesis to experimental results on materials that are well described by these specific models.

3.1 The zero temperature nonequilibrium random field Ising model (ztneRFIM)

The ztneRFIM is a variant of the Ising model in which quenched disorder is modeled by a random field h_i. The field h_i varies from site to site with no correlations, and is fixed in time. The model is classified by the following Hamiltonian-

$$\mathcal{H} = -J\sum_{\langle i,j\rangle} s_i s_j - \sum_i (H_{ext}(t) + h_i)s_i, \tag{3.1}$$

where the first term represents the ferromagnetically coupled nearest neighbors (with nearest neighbor coupling $J > 0$), $H_{ext}(t)$ is the external applied field, and h_i is the random magnetic field with Gaussian distribution having standard deviation R-

$$\rho(h_i) = \frac{1}{R\sqrt{2\pi}} \exp(-\frac{h_i^2}{2R^2}) \, .$$

This model has been studied extensively in thermal equilibrium. In hysteretic systems where the thermal relaxation time scale is much larger than the time scale imposed by the external sweeprate, $\frac{dH_{ext}(t)}{dt} \equiv \Omega$, the equilibrium state is never approached. As a result, in this regime it is a fair approximation for many systems

to first study the model at zero temperature and driven far from equilibrium. The dynamics typically defined for this model consist of local relaxation only, that is, thermal relaxation is completely neglected. One sweep in a simulation of this model through the so-called "saturation history" begins at $H_{ext} = -\infty$ causing all spins to be down. The external field is slowly increased and a spin, s_i, flips when its local effective field

$$H_i^{loc} = H(t) + \sum_{j_{n.n.}} J s_j + h_i \tag{3.2}$$

changes from negative to positive. In the basic RFIM the sum over j runs over the nearest neighbors of i. We take the microscopic amount of time it takes for the spin to flip, once the local field turns positive, to be $\delta\tau \equiv 1$.

3.1.1 Adiabatic loading and the disorder induced critical point

Following the local dynamics defined above, one can picture the emergent global dynamics for an infinitely slow or adiabatic field sweeprate $\Omega \to 0$. The field is raised until one spin flips (this is called the nucleation event or seed). In the next time step of duration $\delta\tau$ the external field is unchanged but some, none, or all of the unflipped nearest neighbors of the seed may be triggered to flip due to the nearest neighbor interaction (the resulting flips are referred to as the first shell). In the next time step some, none, or all of the unflipped nearest neighbors of the first shell may flip (forming the second shell) and the process continues until none of the nth shell's unflipped neighbors flip. The nearest neighbor interaction results in a iterative series of flipped shells that is connected in space and is called an "avalanche" (figure 3.1). At this point the field must be raised until another seed is flipped and the process repeats forming a jerky response to a smooth driving force (magnetization vs. external field).

The qualitative dependence of the avalanche statistics and the shape of the hys-

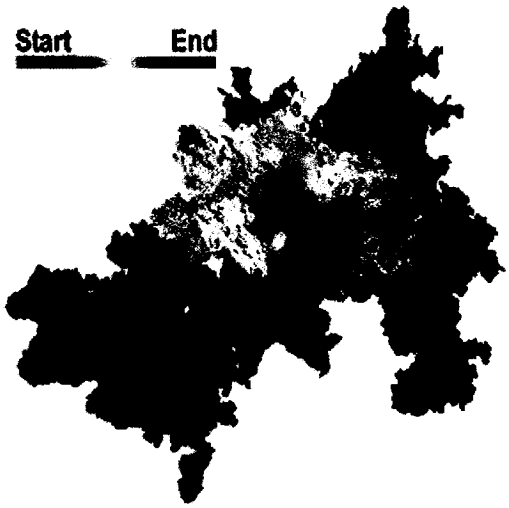

Figure 3.1: Spatial representation of an avalanche in the 3-d ztneRFIM. The colors represent the general order of flipping where the dark blue spins were the first to flip and the yellow the last. An avalanche is connected and able to nucleate anywhere in the sample in our model. (reproduced from [34])

teresis loop on the amount of disorder in the system is straight forward. In the low disorder regime we see one large avalanche with few small precursors due to the fact that there is nothing to stop an avalanche once it starts. For high disorder we see only small avalanches because the disorder halts the avalanche propagation. Between these two regimes we find the critical disorder where one observes avalanches of all sizes.

Combined analytical [35] and numerical [14] approaches have quantified the critical properties of the model in this adiabatic limit: There is a *disorder-driven* dynamical phase transition at a critical disorder $R = R_c = 2.16$ (in units of the nearest neighbor coupling J), separating a low disorder regime ($R < R_c$) characterized by hysteresis loops with a macroscopic jump (ΔM) in the magnetization, from a high disorder regime ($R > R_c$), in which the hysteresis loops look smooth (fig. 3.2). Here the magnetization M is defined as $M \equiv (\sum_{i=1}^{N} s_i)/N$, where N is the total number of spins in the system. The jump ΔM in the magnetization for $R < R_c$ scales to zero as $\Delta M \sim |R - R_c|^{\beta}$, where $\beta = 0.018$ is a universal prediction of the model for three

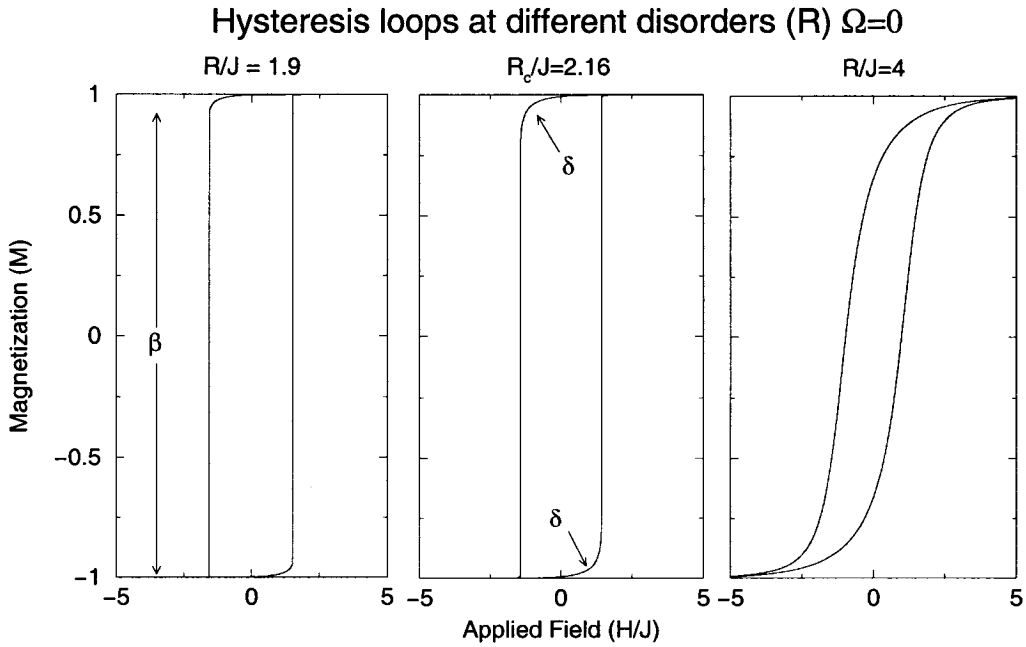

Figure 3.2: Magnetization loops in the ztneRFIM for increasing disorder. The left curve is for low disorder $R < R_c$, the center is at the critical disorder $R = R_c$, and the curve at the right is $R > R_c$. Approaching the critical disorder from above (*i.e.*, from $R > R_c$) results in the divergence of the maximum slope of the curve.

dimensional magnetic samples. At the critical disorder ($R = R_c$) the hysteresis loop has one point ($M_c(H_c)$) where the slope diverges, $\frac{dM(H_c)}{dH} \to \infty$; near that point the magnetization is described by a power law of the form $M(H) - M_c \sim |H - H_c|^{1/\delta}$, where δ is another universal prediction for experiments ($\beta\delta \simeq 1.8$ in 3 dimensions [14]), and $H_c = 1.435$ (in units of the nearest neighbor coupling J), and $M_c = 0.9$ are *nonuniversal* constants.

The apparently smooth parts of the hysteresis loops really consist of many microscopic steps that are not resolved in fig. 3.2. These steps are avalanches of spin flips, analogous to Barkhausen pulses in real materials. For $R > R_c$ the distribution of avalanche sizes $D(S, R, H)$ (which is proportional to the probability of observing an avalanche of S spin flips at disorder R and external field H in response to a small

increase in H) scales as

$$D(S,R,H,) \sim S^{-\tau}\mathcal{F}_s(S\,h^{\sigma\beta\delta}, \frac{h}{r^{\beta\delta}}),$$

and the distribution of avalanche durations scales as

$$D_t(T,R,H) \sim T^{-\alpha}\mathcal{F}_t(T\,h^{\frac{\nu z}{\beta\delta}}, \frac{h}{r^{\beta\delta}}),$$

where $\alpha = \frac{\tau-1}{\sigma\nu z} + 1$, $\mathcal{F}_s$ and $\mathcal{F}_t$ are universal scaling functions and h and r are proportional to $H - H_c$ and $R - R_c$ respectively.

In addition to scaling in pulse distributions, universal behavior is observed over a wide range of measurable quantities. Universal scaling is also found in the power spectrum of the ztneRFIM. For frequencies above $\omega_c \sim \frac{1}{T^*}$, where T^* is the cutoff in the scaling behavior of the duration distribution, the power spectrum of the voltage[1] as a function of time scales as $P(\omega) \sim \omega^{\frac{-1}{\sigma\nu z}}$. The exponent value for the ztneRFIM [36] is $\frac{1}{\sigma\nu z} = 1.77(3)$. This exponent also relates the size of the avalanche to the duration as follows: $T \sim S^{\sigma\nu z}$. The connection between the exponent $\frac{1}{\sigma\nu z}$ and the size-duration scaling appears to be a general feature of BN [6].

Avalanche shapes in the ztneRFIM also exhibit scaling. Although individual avalanches are rather jagged, taking averages of many avalanches of the same duration $\sum_i v_i(t|T) \equiv V(t|T)$ obeys [37] the scaling form $V(t|T) \sim T^{\frac{1}{\sigma\nu z}-1} f(t/T)$. Collapsing data from a range of durations results in a scaling function $f(x)$ that is symmetric about the $x = 0.5$ line and approximately parabolic in shape (exactly parabolic in the mean field limit) [38].

3.2 The ABBM model

The ABBM model was published [30] in 1990 to explain the basic phenomenology of Barkhausen noise in conductors. The model is a synthesis of two properties of domain

[1]The voltage is proportional to the time rate of change of the magnetization

wall motion discovered some 40 years earlier: The role that eddy current damping plays in determining domain wall velocity [39] and the random nature of the domain wall pinning field.

Eddy current damping gives rise to a coupling of the domain wall velocity, ν, to a difference between the external field, H, and the coercive field, H_p, required to depin the domain wall given as

$$k\nu = H - H_p, \tag{3.3}$$

where k is derivable from Maxwell's equation for a particular sample geometry.

The pinning field, H_p, is treated as a random function of position with some finite correlation length ξ that obeys the following Langvin equation

$$\frac{dH_p}{d\Phi} + \frac{H_p - \langle H_p \rangle}{\xi} = \frac{dW}{d\Phi}, \tag{3.4}$$

where Φ is the flux through the pickup coil (Chapter 2) and $W(\Phi)$ is a weiner-levy process with zero mean and finite variance. Decoupling the field, H, into the contribution from the applied field and the demagnetization field, yields the following equation for the measured voltage, V,

$$\frac{dV}{dM} = \frac{c}{V} - k + \eta(M),$$

where c is proportional to the external field sweeprate and k is a measure of the demagnetization effects.

The equation above (e.q. 3.2) is equivalent to a random walk in a logarithmic "potential" $U(V) = kV - c\,log(V)$, with a step at each position in space. Consequently, the avalanche size and duration distributions can be determined by first return time statistics of this random walk and are given by;

$$D(S) \sim S^{-\frac{3}{2}+\frac{c}{2}} f_S(Sk^2) \tag{3.5}$$

for the distribution of areas under Barkhausen pulses (*i.e.*, the "size"); and

$$D(T) \sim T^{-2+c} f_T(Tk) \tag{3.6}$$

for the distribution of durations of pulses. I note this particular result (out of many) because in chapter 6 we derive this in a completely different way.

Overall the ABBM model has been highly successful in capturing basic phenomenology of BN: Intermittence in the response to external driving; scaling in the high frequency regime of the power spectrum taken of the measured voltage; scaling in the pulse size and duration distributions, and the dependence this scaling has on sweeprate. There are, however, a number of results that lie beyond this beautifully simple model: While some materials obey the scaling exponents some have notably different exponents that show no sweeprate dependence; irreproducibility of Barkhausen signals in singular samples with identical field loops [40, 41], as well as detailed studies on the pinning field deconstructed from the voltage signal [42] show that the pinning field is "a collective effect of a flexible wall, not a direct measure of the spatial dependence of the pinning in the material "; Asymmetry in the average pulse shapes seen in experiments is inconsistent with the average symmetric sinusoidal pulse shape of a random walk. [2]

3.3 The flexible domain wall model

The price for the elegance of the ABBM model was knowingly paid by its creators: All degrees of freedom associated with the domain wall itself have been somehow folded into the pinning potential. One can deconstruct this effective treatment by considering the domain wall, more realistically, as an extended object [43] (*i.e.*, with many degrees of freedom rather than just one "mean" position). Assuming a single over-damped domain wall with no overhangs the equation of motion is given by

$$\Gamma \frac{\partial h(\mathbf{r},t)}{\partial t} = -\frac{\delta E(\{h(\mathbf{r},t)\})}{\delta h(\mathbf{r},t)},$$

[2] Recently an explanation for the asymmetry has been suggested by Zapperi *et al.* [19].

where, $h(\mathbf{r},t)$ is the "height" of the domain wall (*i.e.*, its distance from one reference line in two dimensions) at a given position $\mathbf{r}$ and time t, $E(\{h(\mathbf{r},t)\})$ is the total energy functional for a given configuration of the domain wall and Γ is an effective viscosity.

The energy of the domain wall can be represented as a sum of contributions from magnetostatic and dipolar fields, ferromagnetic and magnetocrystalline interactions and disorder. The resulting equation of motion is

$$\frac{\partial h(\vec{r},t)}{\partial t} = \overbrace{H - \gamma \langle h \rangle} + \overbrace{\nu_o \nabla^2 h(\mathbf{r},t)} + \overbrace{\int d^2r' K(\mathbf{r}-\mathbf{r}')[h(\mathbf{r}') - h(\mathbf{r})]} + \overbrace{\eta(\mathbf{r},h)}. \quad (3.7)$$

The terms under the first brace represent the force from the external field H and the restoring force due to the demagnetizing field (a macroscopic consequence of the dipolar interactions). The demagnetizing field is a complicated function of the geometry of the sample and is absorbed into the value γ and $\langle h \rangle$ is the average height of the domain wall. The second term is a force proportional to the surface tension, ν_o of the wall and serves to keep the wall flatish (*i.e.*, the force is negative when the curvature is concave down and positive when the curvature is concave up). The third term results from the local dipolar interactions inducing a magnetic "charge" density when there is a local curvature of the surface. If one allows only small gradients in the wall shape the kernel is given by $K(\mathbf{r}-\mathbf{r}') = \frac{\mu_o M_s^2}{2\pi|\mathbf{r}-\mathbf{r}'|^3}\left(1 - \frac{3(x-x')^2}{|\mathbf{r}-\mathbf{r}'|^2}\right)$ where M_s is the saturation magnetization and $\mathbf{x}$ is normal to the domain wall . The last term in eq. 3.7 is the local pinning field. Random impurities typically have a range comparable to the domain wall thickness. Consequently, the random pinning field can, under coarse graining, be represented by a gaussian noise characterized by delta function correlations in space and rapidly decaying function of domain wall position.

In the limit of zero sweeprate ($H(t) = H_o$) and no demagnetization effects ($\gamma = 0$), equation 3.7 can be expanded around the mean field solution using the Martin-Siggia-Rose (MSR) formalism [44, 45, 46]. In this limit the equation yields a depinning

transition with an upper critical dimension that depends on the general form of the interaction kernel (*i.e.*, the range of the interaction is important). This model has shed light on two observed distinct universality classes in Barkhausen noise [18] based on expected contributions of dipolar fields; namely, $FeSi$ polycrystalline alloys and $Fe_xCo_{85-x}B_{15}$ amorphous alloys under stress. In polycrystals the results suggest that the dipolar interactions are much stronger than the surface tension contributions and in amorphous alloys under stress the surface tension terms dominate the physics on long length scales.

It has also been shown that with $H(t) = \Omega t$ and $\gamma > 0$ in the infinite range interaction limit (*i.e.*, mean-field) the domain wall model can be mapped to the ABBM model above, where the effective pinning field used in the ABBM model is interpreted as a a sum over all points of the random pinning potential $\eta(\mathbf{r}, h)$. Hence, the mean field exponents of the model in eq. 3.7 show a linear change with Ω as in eq. 3.6.

The large universality class of this model, derived by use of the renormalization group, makes the study of this and similar works on depinning transitions relevant for a large class of experimental systems. However, when investigating the experimentally important effects of sweeprate on the critical exponents it has, thus far, been standard practice to rely on numerical results or mappings to other problems. In this thesis I shall provide an alternate explanation for the mean field scaling w.r.t. sweeprate and explain why this type of scaling is not found outside of mean field treatments; in doing so, I provide broadly applicable model-independent predictions for sweeprate effects on 3 different sets of universality classes of crackling noise.

Chapter 4

Simulation and numerical tools

The various numerical results in this thesis were obtained using three types of code. The first code was developed to investigate the effects of finite sweeprate on the properties of the disorder induced critical point in the ztneRFIM [13]. The base code [34] was provided by Sethna's group and is also available online. In the remainder of this thesis I shall refer to this code as the Kuntz-Sethna code (or KS code). The second code was developed to investigate the effects of finite sweeprate *and* thermal fluctuations on the properties of the disorder induced critical point. Failed efforts to augment the KS to include thermal fluctuations resulted in the development of this new code (by Alex Travesset and myself) based on a Monte Carlo update scheme with Glauber dynamics (henceforth referred to as the Glauber code). The third code, the forced superposition tool (FST), was developed by me as a tool to investigate non-trivial aspects of superimposing power-law distributed avalanches.

In this chapter I introduce the basic algorithms employed and other issues regarding the numerics that I think are important and would be good to know for future generations but might be distracting when discussing the science in later chapters.

4.1 Kuntz-Sethna code

Kuntz, *et al.*, developed three different algorithms to study the ztneRFIM based on the dynamic rule—flip when local field changes sign. The common element among these algorithms, made possible by the absence of thermal fluctuations and the inherent sequential nature of the dynamics, is the basic algorithmic loop (scan-propagate) shown in figure 4.1. The three algorithms in order of increasing complexity are; brute-force, sorted-list and bits [34].

- The brute-force searches through the entire lattice with N sites to find each nucleation site (A nucleation site is the next unstable spin in the external driving field is raised adiabatically slowly). Since there are $O(N)$ avalanches in a saturation hysteresis loop, the runtime scaling for the brute-force algorithm is $O(N^2)$.

- The sorted-list algorithm uses a clever pointer construct (discussed in the next section) to find nucleation events that diminishes the number of operations each spin is involved in from $O(N)$ to $O(1)$ during the simulation. As a result, the asymptotic run-time scaling of the sorted-list algorithm is due to the sorting of the list (*i.e.*, $O(NlogN)$).

- The bits algorithm was developed to minimize the amount of memory required in the simulation. It achieves this by taking advantage of the fact that, in the saturation loop, it is not necessary to store the random fields of the spins. Instead they can be generated, when needed, at the interface of propagating fronts. The asymptotic runtime scaling for the bits algorithm is fixed by the search for nucleation events and is bounded below by $O(NlogN)$. Despite being comparable in asymptotic scaling to the sorted-list algorithm the bits algorithm is, in practice, significantly slower than the sorted list algorithm but allows for

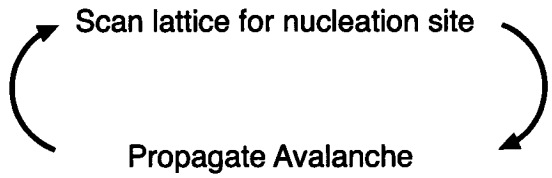

Figure 4.1: Algorithmic loop common to algorithms by Kuntz and Sethna (KS). KS developed and published 3 algorithms to study the zero temperature nonequilibrium RFIM [34] that, at the most coarse grained level, consisted of scanning the lattice for nucleation sites and then propagating an avalanche.

roughly $8X$ larger system sizes.

4.1.1 Zero sweeprate ($\Omega = 0$) algorithm

Efficiency in the simulation of the ztneRFIM (discussed in chapter 3) is borne out of the nearest neighbor only interaction and the correspondingly local relaxations to metastable states. In being far from equilibrium the system is freed from the time consuming search for global minima in the free energy landscape. Consequently, for monotonic field histories a spin, once flipped, need never be flipped again. This property has been taken advantage of by Kuntz, *et al.*, in the so called sorted-list algorithm [34].

Beginning the simulation of the saturation loop with all spins pointing down the algorithm consists of the following:

1. Initialize an array of N double variables representing the local random field of the $N = L^d$ spins on the cubic lattice. Sort the array by increasing random field.

2. Create an array of $z+1$ pointers, where z is the number of nearest neighbors of a spin in a d-dimensional cubic lattice. The pointers point to the location of the next spin that would flip if it had $n_\uparrow = 0, 1, 2, ..., z$ neighbors in the up position. (For the so-called saturation history of an increasing external field starting at

$H = -\infty$ the simulation begins with all $z+1$ pointers pointing to the spin with the largest random field.)

3. Query all $z+1$ spins pointed to and chose the one with the largest total local field (includes contribution from external field, the random field, and the interaction with the nearest neighbors. See equation 3.2). The total local field will be negative because the external field has not been increased since step 2.

4. Move the pointer selected in step 3 to the next spin on the sorted list.

5. If that spin actually has $n_\uparrow$ up neighbors, increment the field to just flip that spin, push the spin onto a first in first out (FIFO) queue, and hence nucleate an avalanche. If not, to go back to step 3. It is important to note here that this step is the only step in which the external field H changes.

6. Pop spin off the FIFO queue.

7. If the spin has not been flipped, flip it and push all unflipped neighbors with positive local fields onto the queue.

8. As long as the size of the FIFO queue is greater than zero, loop back to step 6.

9. Repeat from step 2 until all spins in the lattice are flipped.

To ensure that the temporal flip order is maintained, an end of shell (EOS) marker is pushed onto the FIFO queue to keep track of the order in which the spins are flipped. For example, suppose that the nucleating spin occurs at t_n. The spins it causes to flip at t_{n+1} are pushed onto the queue followed by an EOS marker m_1. After the spins that flip at t_{n+1} are popped off the queue and potentially cause other spins to flip, m_1 is popped of the queue and m_2 is pushed on. The spins now in the queue represent the spins that flipped due to shell 2.

Surprisingly the asymptotic scaling derives from the first step of the algorithm. Sorting the list of N random fields takes $O(NlogN)$ time steps while all other aspects of the algorithm scale, at most, with the system size, $O(N)$. The multiplier on the $O(N)$ operations, however, is large enough to drown out all $logN$ contributions in the system sizes we were able to achieve. (On a computer with at least 2G of RAM we could simulate systems up to 500^3 spins using this algorithm.)

4.1.2 Finite sweeprate ($\Omega > 0$) algorithm

When the external field is allowed to increase during the propagation of an avalanche the basic algorithmic loop has to be modified (fig. 4.2). The purely sequential and local dynamics forced by the nearest neighbor interaction and adiabatic increase in the external field are replaced by a hybrid dynamics in which the external field can nucleate other avalanches throughout the lattice as causally related avalanches propagate. Fortunately the sorted-list algorithm was easily augmented to allow for this change.

The modified algorithm for the finite sweeprate, sorted-list algorithm is as follows:

1. Initialize an array of N double variables representing the local random field of the $N = L^d$ spins on the cubic lattice. Sort the array by increasing random field.

2. Create an array of $z+1$ pointers, where z is the number of nearest neighbors of a spin. The pointers point to the location of the next spin that would flip if it had n neighbors in the up position ($n_\uparrow$). (The simulation begins with all $z+1$ pointers pointing to the spin with the largest random field.)

3. Query all $z+1$ spins pointed to and chose the one with the largest total local field.

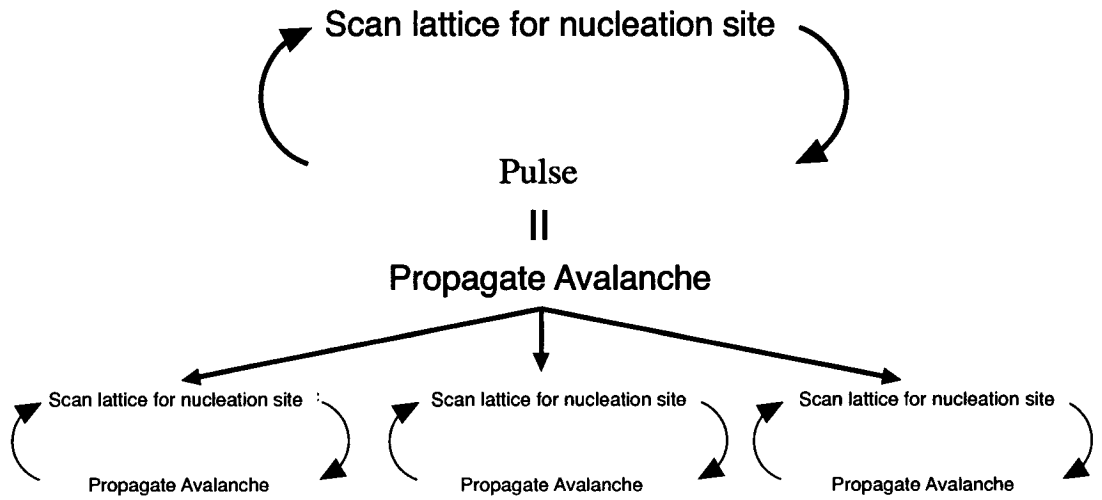

Figure 4.2: Algorithmic loop at finite sweeprate $\Omega > 0$. If swept slow enough, the driven dynamics can still consist of marked bursts of activity (pulses) separated by long periods of inactivity. These bursts, however, are different from the collective avalanche events. The external field at finte sweeprate can nucleate other, spatially separated, during the propagation of previously nucleated avalanches. Consequently, the algorithmic loop must allow for simultaneously propagating avalanches.

4. Move the pointer selected in step 3 to the next spin on the sorted list.

5. If that spin actually has $n_\uparrow$up neighbors and the spin flip queue is empty, increment the field to just flip that spin, push the spin onto a FIFO queue (nucleate a pulse), and push an EOS marker on the queue. If not, to go back to step 3. If that spin actually has $n_\uparrow$up neighbors and the spin flip queue is not empty; if the field required to flip that spin is less than the current field, push the spin on the FIFO queue (nucleate an avalanche) and go back to step 3; If the field required to flip that spin is greater than the current field, do not push the spin on the FIFO queue but do push a EOS marker on the queue and continue.

6. Pop shell off the FIFO queue spin by spin. Increment the external field by $\Omega\delta t$, where the field sweeprate is again $\Omega = \frac{dH}{dt}$.

7. If the spins in the shell have not been flipped, flip them and push all unflipped

neighbors with positive local fields onto the queue.

8. As long as the size of the FIFO queue is greater than zero, loop back to step 2.

9. Repeat from step 2 until all spins in the lattice are flipped.

Inside a pulse, the time proceeds in unit increments ($\delta t = 1$). The time between pulses, however, is obtained by taking the difference between the field at the conclusion of a pulse and the field at the nucleation of the next (determined in the same manner as the sorted list algorithm) and dividing by the sweeprate. The potential time shift in the "clock" of the simulation between avalanches has no effect on the pulse size and duration distributions.

This augmentation maintains all of the benefits of the ztneRFIM KS code in the adiabatic limit. The asymptotic scaling is unchanged and the difference between the actual run-times of the adiabatic and the finite sweeprate code was negligible.

4.2 Finite temperature non-equilibrium RFIM

The system sizes obtainable with the KS code are addictive. It would be nice to take advantage of the efficiency and the highly developed infrastructure of the KS code when investigating the effects of small temperatures far from equilibrium. However, despite the apparent benefits, I was unable to do this[1]. Instead, we relied on a tried-and-true method used to study systems in contact with a thermal bath: A kinetic

[1]I had conceived of a method of randomizing the pointer list that could be coupled to a "temperature" but based on preliminary calculations the run-time scaling would be $O\left(\frac{\Delta H \theta a}{\Omega \delta t}\right)$, where θ is the temperature, a is the number of spins over an energy range ($O(N)$) , ΔH is the total change in external field over the saturation loop ($O(1)$) and δt is the microscopic time step ($\delta t = 1$). To sweep slow enough to observe signatures of the serial dynamics in the power spectra, $\Omega \sim \frac{1}{N}$ (see chapter 6). Hence, unless we limited ourselves to *very* small temperatures (*i.e.*, $\theta = O\left(\frac{1}{N}\right)$) the run-time scaling would approach $O\left(N^2\right)$. This is not much of an improvement over conventional methods.

Monte Carlo (MC) algorithm [47] based on single spin-flip Glauber dynamics [48].

The base algorithm is straight forward: For each spin s_i = "*down*" $= -1$ *or* "*up*" $= +1$ in the lattice, select a uniformly distributed random number, r, between 0 and 1. If

$$r < \frac{1}{1 + exp(\frac{2H_i^{loc}s_i}{\theta})},$$

flip the spin. Here $\theta \equiv k_B T$ where T is the temperature and k_B is Boltzmann's constant. The minimal goal in constructing the code was to meet two criteria:

- Obtain the equilibrium state of the system in the adiabatic finite temperature regime (*i.e.*, for $\theta > 0$ and sweeprate $\Omega \to 0$).
- Match the non-equilibrium dynamics at zero temperature and finite sweeprate of the KS code.

Since Glauber dynamics satisfy detailed balance when spins are updated sequentially (by construction) the relaxation to the equilibrium state is guaranteed. Matching the non-equilibrium dynamics at zero temperature, however, required more thought.

The first issue to be addressed was a proper assignment of a Glauber code time increment to match that of the KS code. There are two standard time steps used in kinetic MC: one time step per spin update; and one time step per N spins updated, where N is the number of spins in the lattice. By contrast, the KS time step corresponds to the flipping of a shell. There is an obvious question to ask: Which of the kinetic MC time steps corresponds to the KS time step, if any, and does it matter? There is a short answer: One time step per N spins updated corresponds to the KS time step and, yes, it does matter. The two time assignments are fundamentally different and differ by more than a multiplicative constant in the regime in which we are interested.

To understand why the one time step per spin update will not reduce to the dynamics of the KS code, consider the following: In the KS code for the ztneRFIM

near the disorder induced critical point, the relationship between the avalanche size, S, and its duration, T, is given by $S \sim T^{\frac{1}{\sigma\nu z}}$ (Chapter 3). If the one time step per spin update were used, it would take S time steps to propagate an avalanche of size S, forcing the exponent equality $\frac{1}{\sigma\nu z} = 1$. The fact that the KS code [37, 36] and most known materials exhibiting BN [6] yield values of $\frac{1}{\sigma\nu z}$ well above 1 is sufficient to discard the one time step per spin update as a viable for our current purposes. However, even *without* known counter examples, an exponent equality determined by a time assignment scheme is anathema to the study of critical phenomena.

The more natural assignment is the one time step per N spins updated as this is what the KS code is doing. At every time step the KS algorithm *does* update every spin in the lattice. However, it takes advantage of the fact that most of the spins will not be participating in the avalanche and does not bother to look at them. Consequently, the one time step per N spins updated is a necessary condition in achieving our minimal goals.

Another issue central to matching the dynamics of the Glauber code to the KS code is the importance of the update order and how it effects the dynamics. The update order in the KS code is dynamically determined by the causal relationships between spin flips. That is, the lattice is scanned for a nucleation event, subsequent spins that flip are connected to that spin, and the update propagates outward from the nucleation site. Monte Carlo update methods are fundamentally different. In traditional MC methods, the control of the update order is determined in the construction of the code and not emergent from the model under investigation. Even if the update is randomized, a certain aspect of the dynamics are coded into the simulation and it is unclear, *a priori*, what effect the update scheme will have on the dynamics observed. As a result, to ensure our minimal goals were met, our use of MC methods to introduce thermal fluctuations had to be accompanied by a detailed knowledge of how the causal dynamics were affected by the update scheme.

Comparing various sequential update schemes quoted in the literature (such as random-sequential where update sites are chosen at random throughout the sample [49] or deterministic sequential, where one updates through the lattice, site by site, in a deterministic way) we found significant deviations (see fig. 4.3) from the KS code in the scaling regime of the power spectra at high frequencies [36]. By employing an old trick used to parallelize the sequential dynamics on a cubic lattice, without violating detailed balance, we were able to alleviate these deviations. The old trick is called the "checkerboard" update and it is very easy to understand: In two dimensions the "red squares" of a checkerboard patterned lattice (order does not matter) are sequentially updated, followed by the "black squares". (This is easy to explain in two dimensions and easily generalized to three and higher). Why does this reduce to the KS algorithm at low temperature? Because the nearest neighbor interaction forces shells in the KS code to alternate between black and red sub-lattices! This trick works so perfectly only because the interactions are nearest neighbor only. With long range interactions the effect of the update on the dynamics becomes problematic again.

4.3 The forced superposition tool (FST)

Over the course of my sweeprate investigations, it became clear (Chapter 6) that a primary, and fairly odd, result of a sweeprate dependent exponent could be understood as a superposition of power law distributed avalanches. The scaling arguments presented in chapter 6, although satisfying, offered little in the way of qualitative understanding of the effects of sweeprate on experimentally common distributions with limited scaling regions (sometimes only 1 decade of scaling in the duration distributions). In order to numerically test the consequences of the assumptions listed in sec. 5, I constructed a little tool that would take the assumptions as input and produce pulse statistics as output (Fig. 4.4). For reference it is called the forced superposition

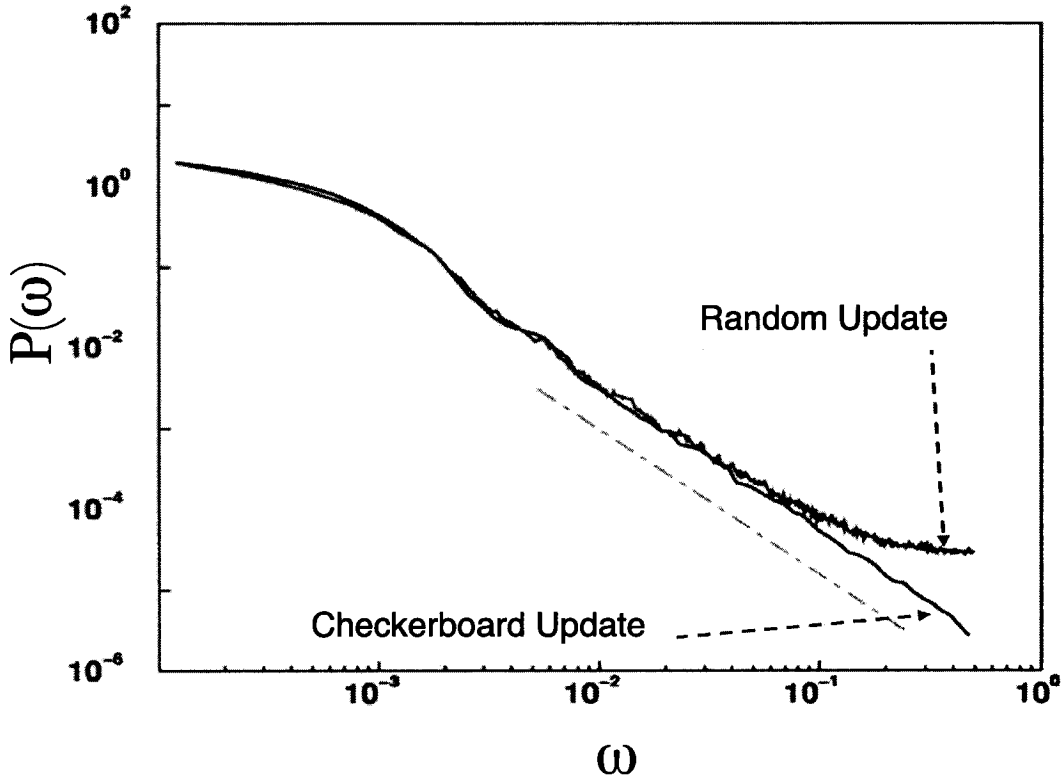

Figure 4.3: Power spectra illustrating importance of update order. Shown here are power spectra for a system updated by random as well as checkerboard updates at zero temperature. Actual parameters are $R = 2.3$ and $L = 50$ (total size L^3). Each power spectrum is averaged over 30 disorder realizations. The dash-dotted line is the exact result from eq. 7.2 [36]. The discrepancy at larger frequencies for the random update is quite apparent in the high frequency regime.

tool (FST).

The forced superposition tool takes the avalanche distributions and, in principle, an arbitrary distribution of nucleation fields and generates pulse distributions. For results reported here we generate avalanches nucleated at H_i with a symmetric shape given by

$$V(t,T) \equiv \left\{ \begin{array}{cc} AT^{\frac{1}{\sigma\nu z}-1}(1-4(\frac{t}{T}-\frac{1}{2})^2) & 0<t<T \\ 0 & otherwise \end{array} \right\},$$

where A gives the relationship between the max avalanche size measured in Wb/s and the max avalanche duration measured in seconds, T is selected from a power law distribution with a hard cutoff at T^* (to speed up the random number generation [2]) and the nucleation fields, H_i, are Poissonian distributed in the internal field yielding an exponential distribution of times τ_{ni} between nucleation seeds given by $D_{\tau_n} = \lambda e^{\lambda\tau_n}$ where $\lambda = a\Omega$. We ran the simulations for the mean avalanche shapes from the ztneRFIM and the ABBM with indistinguishable results. (The ztneRFIM yields an inverted parabola [37] and the ABBM yields a sinusoid [50].

Pulses obtained with a zero threshold are defined as follows: An avalanche is created with duration T_0 randomly picked from a distribution $D(T)$ of our choice (here we used a power law distribution with tunable exponents). In the next time step we increment the effective field by $(\Omega - \gamma V(1,T))\,\delta t$, where $\delta t \equiv 1$. If the effective field is larger than the nucleation fields of N avalanches of sizes $S_1, ..., S_N$, obtained by selecting from the exponential distribution, we create N avalanches, as above, with shape functions that originate at the nucleation time. The process is continued until no more avalanches are nucleated. The pulse size is increased by $\sum_{i=1}^{N} S_i$ and the pulse duration T_p is set to equal $Max\left\{T_i + \tau_i, T_p\right\}_{i=1,...,N}$ where $T_p = T_0$ in the first

[2]The details of how to generate the power law distributed random numbers can be found in any textbook that discusses random number generation of arbitrary distributions from a uniform distribution. I used the class notes from Klaus Schulten's non-equilibrium statistical mechanics course.

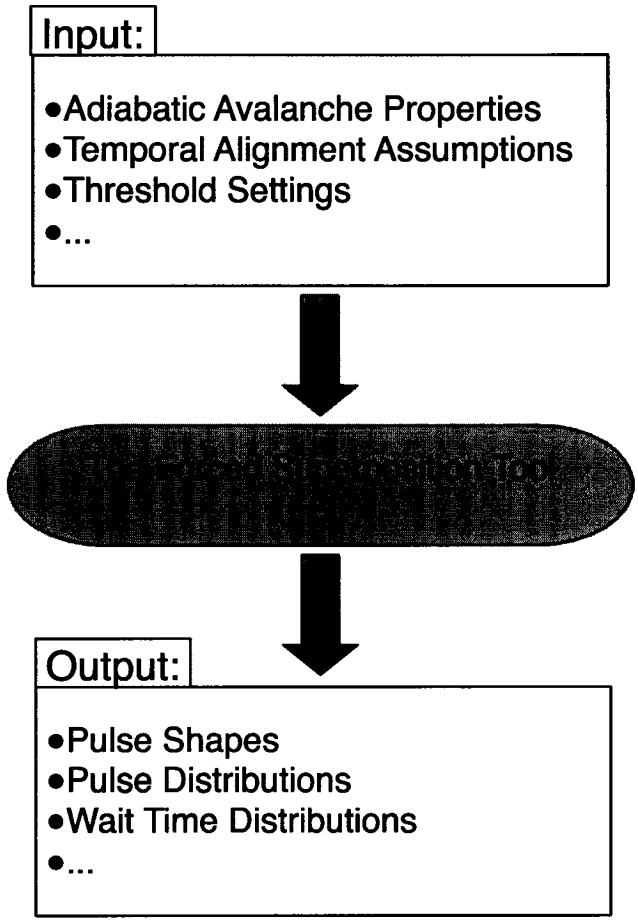

Figure 4.4: Inputs and outputs of the forced superposition tool (FST). The FST is used to numerically implement the assumptions in chapter 5 to obtain pulse distributions at finite sweeprate from the avalanche characteristics in the zero sweeprate limit. Avalanche size and duration distributions, average avalanche shapes, as well as conditional distributions of size *given* duration can be arbitrarily chosen to generate avalanches that match the system or model under consideration. These avalanches are then placed on the time axis with the temporal alignment assumption (see section 5.2). The threshold for pulse determination can be adjusted to mimic experimental conditions or to study the effect that the threshold choice has on resulting pulse statistics. The output is then the pulse shapes, the pulse size and duration distributions, and wait time distributions.

iteration and τ_i is the nucleation time of the ith avalanche. This algorithm iterates until there are no more nucleations during the propagation of the pulse. The pulse is then recorded and a new pulse is started.

The FST could be useful as an experimental data analysis tool as well. Instead of fixing a function to generate avalanches, data could be fed directly into a database of real pulse profiles for a given material. One could then use this database as the generator of the avalanches to be sprinkled on the time axis according to the assumptions in chapter 5. Differences between actual results obtained by increasing the sweeprate and FST obtained results would indicate interesting features to investigate and potential breakdowns of the null assumptions. This would also allow for the measurement of meaningful power spectra of the intra-avalanche correlations not available for artificially generated avalanches. In the future this can be incorporated into an easy-to-use package and help distill interesting new physics. Work for a future student perhaps.

Chapter 5

Null assumptions for spatio-temporal overlap in crackling response

In this chapter I provide a set of assumptions that will be used throughout the remainder of the thesis. I call these the null assumptions because they apply to a large number of crackling systems as well as a majority of models of CN. These assumptions, I believe, should be the starting point for analysis of CN in a finite sweeprate regime. The violation of these assumptions will usually indicate interesting physics.

The arguments throughout this dissertation are predicated on the null assumptions listed in this chapter that have been generalized from earlier work [51] to explicitly include the effects of long ranger interactions which we call here a long range restoring force (LRRF). In BN observed in soft magnets the LRRF is the so-called demagnetizing field (DF) that arises out of bulk magnetic dipole interactions. This inclusion is motivated by the fact that DF have been shown [52, 18] to have a profound effect on the characteristics of BN, and may also have qualitative relevance to earthquakes and other crackling phenomena. The range of the restoring force will be considered

infinite and present as a coupling to the total magnetization through the local field (this is justified in Barkhausen studies by use of renormalization group arguments [31]). As a matter of convenience, we refer to systems with LRRF as $LRRF^{+}$ and systems without LRRF as $LRRF^{-}$. Assumptions 5.2 through 5.4 below are consistent with all systems known to us in which assumption 5.1 below holds.

5.1 System is near a non-equilibrium critical point

We take as given the system's proximity to a non-equilibrium critical point and the associated presence of power law distributed avalanches on long length scales in the limit of zero driving rate, $\frac{dH_{ext}}{dt} \equiv \Omega = 0$. The size S of the avalanche, proportional to the number of elements involved in the relaxation, obeys a distribution given by $D(S, L, \gamma, ...) \sim S^{-\tau}\mathcal{F}_S(S/\xi^{d_f}, L/\xi, \gamma^{-\nu_\gamma}/\xi, ...)$ where d_f is the fractal dimension of the avalanche, L is the system size, γ represents the system's dependence on an infinite range restoring field (DF in the case of BN) and is proportional to L^{-d}, ν_γ controls the divergence of the correlation length with diminishing LRRF, and ξ is the correlation length of the system. The duration T of the avalanche, proportional to the time it takes an avalanche to propagate, obeys a distribution given by $D(T, L, \gamma, ...) \sim T^{-\alpha}\mathcal{F}_T(T/\xi^z, L/\xi, \gamma^{-\nu_\gamma}/\xi, ...)$. To assure normalization independent of cutoff at long length scales we consider only $\alpha > 1$ and $\tau > 1$.

We also assume that the duration and size of a particular avalanche are related by $T \sim l^z$ where l is the linear extent of the avalanche. Since $l^{d_f} \sim S$ and $d_f = \frac{1}{\sigma\nu}$ we have the equivalent and more familiar $T \sim S^{\frac{1}{\sigma\nu z}}$. Furthermore, we assume that the average shape, $\langle V(t,T)\rangle$, of avalanches of duration T is given by

$$\langle V(t,T)\rangle \sim T^{\frac{1}{\sigma\nu z}-1} f(\frac{t}{T}). \tag{5.1}$$

For BN the average shape $\langle V(t,T)\rangle$ is defined [37] as the average voltage as a function of time obtained by averaging the voltage trains of all avalanches of a fixed duration.

The important characteristic of $f(x)$, for our purposes, is that it is smooth and that $f(0) = f(1) = 0$.

Expected universal features include the exponents τ, α, z, d_f and ν_γ as well as the scaling functions $\mathcal{F}_S(x_1, x_2, ...)$, $\mathcal{F}_T(x_1, x_2, ...)$, and $f(\frac{t}{T})$ where the x_i are system/model specific, unitless combinations of scaling variables. The values ξ^{d_f} (ξ^z) correspond to the largest avalanche size (duration) when $\xi < L$. If $\xi = L$ the values of the largest avalanche size and duration are given by L^{d_f} and L^z respectively. In SOC systems, where there is no tuning parameter, the correlation length is constrained only by the system size, $\xi \sim L$. In "plain old critical" systems, the correlation length diverges as the system approaches the critical point. The proximity to the critical point is measured with a unit-less tuning parameter such as $r = \frac{R-R_c}{R_c}$ in the disorder induced critical point in the ztneRFIM where R_c is the critical disorder [13]. As $r \to 0$, $\xi \sim r^{-\nu}$.

5.2 Nucleation events are uniformly distributed on the nucleation manifold and over the internal field

We consider systems that have, in the adiabatic limit, a number of avalanches nucleated per unit of internal field increase that is a smooth function of the internal field H denoted by $a(H)$. The internal field H is a combination of the applied field H_{ext} and the field associated with the LRRFs. Following BN studies [30, 52] we take the simplest, non-trivial means of modeling the LRRF and that is to increase the range of interaction from "long range" to "infinite range" (justified in [43]). This simplification reduces the LRRF to a coupling to the bulk magnetization M and yields the

following expression for the internal field:

$$H = \Omega t - \gamma M. \tag{5.2}$$

Contributions of LRRFs smoothed out over time can be absorbed into an effective sweeprate $\widetilde{\Omega}$ derived as follows: Over multiple avalanches in the stationary region, the change in magnetization is

$$\Delta M \sim 2\frac{n}{N}\langle S\rangle, \tag{5.3}$$

where n is the number of avalanches that have been nucleated, N is the total number of spins in the systems and $\langle S\rangle$ is the average number of spins that flip in each avalanche. The number of avalanches nucleated, n is related to the change in the internal field and the density of nucleation $a(H)$. Combining $n = \Delta H\, a(H)$ with equations 5.2 and 5.3 yields $\Delta H = \widetilde{\Omega}\,\Delta t$ where

$$\widetilde{\Omega} \equiv \frac{\Omega}{1 + a\gamma\langle S\rangle}. \tag{5.4}$$

(*N.B.* We will suppress the functional relation on H and express $a(H)$ as a for the remainder of this dissertation since, by the stationarity assumption below (5.3), $a(H)$ will be approximately constant over the intervals in H we are interested in.)

We assume that in the adiabatic, zero temperature limit the nucleation events of avalanches adjacent in time are uncorrelated in space. This corresponds to the so-called weak pinning limit where there are a large number of spins on the nucleation manifold at any particular effective field value available to nucleate depinning. In this limit $a \propto L^d$ in the case of avalanche nucleation events allowed in the bulk, and $a \propto L^{d-1}$ when nucleations occur only on a domain wall.

5.3 Stationary region exists

Stationarity of the signal is crucial to obtaining reliable scaling characteristics. If statistics are obtained by integrating over some parameter that controls the cutoff

in the scaling, results can be considerably dependent upon the integration range. Take, for example, the disorder tuned critical point in the ztneRFIM. The avalanche size distribution at the critical value of disorder is given by $D(S,h) \sim S^{-\tau}\mathcal{F}(Sh^{\sigma\beta\delta})$. At the critical point in h the scaling will be $D(S) \sim S^{-\tau}$ but if the distribution is integrated over h the distribution will be $D_{int}(S) = \int D(S,h)\,dh \sim S^{-(\tau+\sigma\beta\delta)}$. In the 3-d ztneRFIM the exponent for the size distribution integrated over h is $\tau + \sigma\beta\delta \sim 2.03$. Compare this to the exponent of $\tau \simeq 1.6$ at the critical point and the importance of clearly defining the stationary region is obvious.

We consider systems for which it is possible to chose an interval of forcing fields small enough to ensure the distributions $D(S)$ and $D(T)$ are fixed, and large enough to obtain many avalanches. This applies to SOC models since, by definition, such models are self-tuned to sit at the critical point for all external conditions. Although magnets are not stationary over the whole saturation loop, soft magnets with LRRF have a large region around the coercive field in which the magnetization as a function of external field is virtually linear and the distributions are stationary.

In "'plain old critical" systems, such as the ztneRFIM in which the external field (equal to the internal field H since there are no $LRRF$) is a tuning parameter with a critical point at H_c with $\xi \sim |H - H_c|^{-\nu_H}$, one has to choose a smaller and smaller external field interval, δH, as one approaches the critical point from $R > R_c$ to ensure approximate stationarity for a given system size. This is due to the diverging slope in the magnetization curve $M(H)$. What follows is an argument for the criterion on ν_H to guarantee this stationary region exists in known "plain old critical" crackling systems.

Any field interval that shrinks slower than L^{-d} upon increasing the system size will have an arbitrarily large number of nucleations obtainable by increasing the system size. We need to show that within this interval the distribution will be fixed. Although not rigorously a sufficient condition (to our knowledge) we consider the

necessary condition of vanishing fractional difference in the correlation length over this interval to be compelling evidence of stationarity over this region and set out to prove it as follows:

Consider the field interval that we want to measure to be $H_2 - H_1 = \Delta H \sim L^{-b}$ where $H_1 < H_2 \leq H_c$. Values of b that are consistent with the stationarity assumption will be determined. We focus on the "stiffness" of the correlation length over this interval to get a handle on the an acceptably narrow field interval over which we can assume stationarity. The difference in correlation length over ΔH is

$$\begin{aligned} \Delta\xi &\sim (H_c - H_1 - \Delta H)^{-\nu_H} - (H_c - H_1)^{-\nu_H} \\ &\sim (H_c - H_1)^{-\nu_H - 1}\Delta H + O((\Delta H)^2). \end{aligned} \tag{5.5}$$

Suppose that the system is just close enough to the critical point that $\xi = L$ thus limiting $H_c - H_1 \geq L^{-\frac{1}{\nu_H}}$. (*N.B.* we can get arbitrarily close to the critical point using this criteria by increasing L). Thus, to lowest order in ΔH, $\Delta\xi \sim L^{1+\frac{1}{\nu_H}}\Delta H$. There is no interval ΔH, *fixed* w.r.t. L, that can guarantee stationarity for arbitrarily large values of L arbitrarily close to the critical point. However, with $\Delta H \sim L^{-b}$, $\frac{\Delta\xi}{\xi}$ will vanish for increasing system sizes as long as $b > \frac{1}{\nu_H}$. From assumption 5.2 we observe that to obtain large numbers of nucleations in the interval, $b < d$ where d is the dimension of the system. For a stationary interval in H to be possible both relations, $b > \frac{1}{\nu_H}$ and $b < d$, must be satisfied. The exponent relation $\nu_H > \frac{1}{d}$ guarantees that such a "stationary" interval exists. This holds for the "plain old critical" ztneRFIM. Since $LRRF^+$ are "self organized" to sit at the critical field, one only has to make sure to be in the linear regime of the "hysteresis" curve for the stationarity assumption to hold.

5.4 Avalanche sizes are uncorrelated

The sizes and durations of avalanches adjacent in time are uncorrelated. Assumption 5.2 can produce intriguing effects on the time series as the coupling between the size of an avalanche and the field at which subsequent avalanches are nucleated will cause islands of avalanches to precede other large avalanches. These might be interpreted as "precursors" and perhaps imply some correlation between avalanche sizes where non exists.

Chapter 6

The effects of spatio-temporal overlap on crackling noise

In most models for systems with avalanches, the first step is to study the system in the adiabatic limit (*i.e.*, for an infinitely slowly increasing driving force or field). This is achieved by increasing the field until it triggers one avalanche and keeping the field fixed until that avalanche is finished. Afterwards the field is increased until it triggers the next avalanche and so on. In this limit one avalanche propagates at a time. The field only serves to nucleate each avalanche and has no effect on the avalanche dynamics.

Real systems may or may not be in this limit. The driving rate could, in fact, be beyond experimental control as in the case of earthquakes and solar flares. Even with the ability to experimentally tune the sweeprate, lack of spatial resolution of the avalanches themselves necessitate bulk measurements. A macroscopic view of the system makes it difficult to rule out the possibility that individual pulses are composed of simultaneous, but otherwise independent, collective events (avalanches). What is lacking is a general framework for understanding the effects of temporal overlap to determine how misleading the macroscopic view can be. In this chapter we study

these effects in crackling noise in a general, model independent way.

We show that various adiabatic universality classes can be grouped into three overarching groups based on how the pulse scaling changes with sweeprate. We also show, through the forced superposition tool (FST chapter 4), how results on pulse statistics can be misinterpreted due to small scaling regimes. Explanations of hitherto mysterious behavior in the low frequency of the power spectra with sweeprate are presented as well as the qualitative behavior of large avalanche shapes.

Even though the calculations in this chapter are system and model independent we felt that it is useful, for the sake of expositional clarity, to phrase our results in the language of one example system and one well characterized model for crackling noise. We chose Barkhausen noise in magnets as an exemplar system since it has been studied in great depth theoretically as well as experimentally and is unmatched as a controllable instance of crackling response (see chapter 2). The model is the random field Ising model at zero temperature driven far from equilibrium (ztneRFIM presented in chapter 3) and was chosen because it has a wealth of well-studied scaling forms and nicely illustrates the characteristics of crackling response.

6.1 Slow forcing and the loss of a clean avalanche picture

In the picture of the adiabatic dynamics that emerges from the ztneRFIM (chapter 3), the change in the dynamics upon increasing the external sweeprate is transparent: For $\Omega \to 0$ the external field is kept fixed during the propagation of an avalanche; with non-zero sweeprates, $\Omega > 0$, the field increases while the avalanche grows. This allows for the nucleation and subsequent propagation of avalanches before the others have had time to finish. It is not clear, a priori, how this overlap will affect the pulse statistics. What is clear is that a meaningful comparison of experiment with theory

requires a detailed understanding of these effects.

The elucidation of these effects requires the following distinction between "avalanche" and "pulse".

- **Avalanche**: An avalanche is the collective relaxation that occurs in the theoretical limit in which the external field is changed infinitesimally slowly at zero temperature.

- **Pulse**: A pulse is obtained *experimentally* by setting a threshold below which the system is considered quiescent. A pulse would then be the sequence of signals temporally between two neighboring quiescent regimes.

In the adiabatic limit, a pulse is an avalanche. However, as the sweeprate is increased, pulses can be composed of several, simultaneously propagating avalanches.

In what follows we shall show that this distinction can be more than a matter of language. In fact, pulses can have rich behavior due only to the properties of the underlying avalanches. We need to be able to distinguish between the consequences of potentially interesting physics, and the consequences of possibly rich behavior of overlapping avalanches to fully appreciate the physics underlying the measurements made in crackling systems. Under what conditions are the pulse statistics obscured by sweeprate effects; and are they obscured in such a way that we will know that we are looking at sweeprate effects? To unravel some of these issues we begin with a study of the time scales that arise from the assumptions detailed in chapter 5. This will allow us to carefully expand the parameter regime from the narrow adiabatic limit to include temporal overlap of avalanches.

6.2 Critical sweeprates

In this section we present scaling arguments for critical sweeprates. We represent all dynamics occurring at the atomic level by one microscopic timescale ($\delta\tau = 1$): In the ztneRFIM [13] this is the time it takes for one spin to flip once its local field changes sign; and in domain wall (DW) motion this is the time it takes for the DW to depin locally. It is assumed here that this time is independent of the magnitude of the local effective field h_i^{eff} that has just changed sign. This is an approximation; we do not know of any experimental evidence that suggests strong dependence of the time to flip a single "spin", or element of a domain wall on the magnitude of the local field at zero temperature. All other time scales emerge from collective serial dynamics in the adiabatic case with the potential addition of parallel dynamics as the sweeprate is increased.

We focus on two critical sweeprates, Ω_t and Ω_s: Ω_t is the sweeprate at which the overlap in time of the adiabatic avalanches results in a total loss of distinct pulses; and Ω_s is characterized by the onset of spatial overlap of simultaneously propagating avalanches. It is obvious that temporal overlap is a prerequisite for spatial overlap. What must be determined, however, is the extent to which spatial overlap begins in the regime that temporal overlap occurs without wiping out the existence of separate pulses.

6.2.1 Full temporal overlap in systems without long range restoring forces

The sweeprate needed to have a significant fraction of the avalanches overlap in time (see fig. 6.1) is central to the discussion of pulse statistics. We shall call Ω_t the upper bound of the regime in which pulse statistics can be measured at all (*i.e.*, the so called "slow" sweeprate regime). To define Ω_t we find under what conditions the

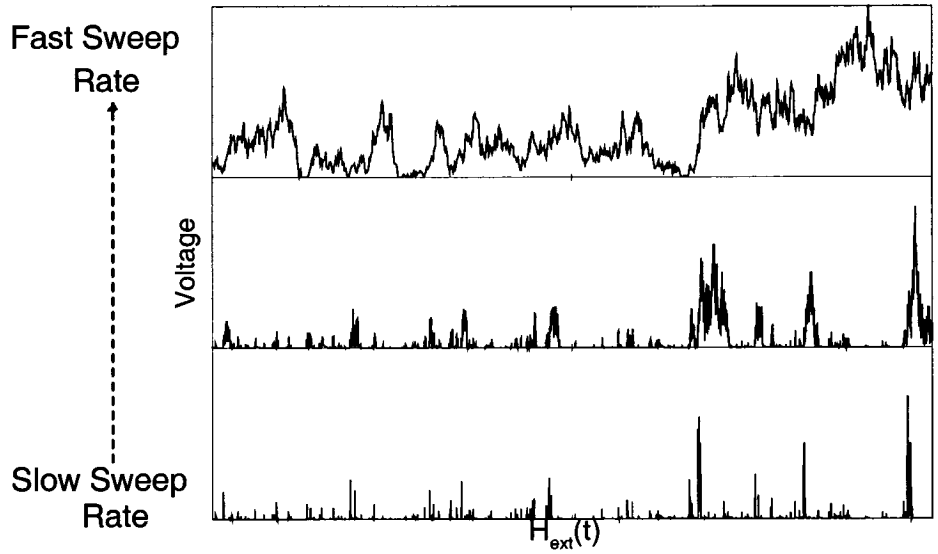

Figure 6.1: Sample voltage profile for increasing sweeprate in the ztneRFIM. This example obtained from simulations for increasing field sweep rates in ztneRFIM near the critical disorder ($R_c = 2.16$) and external field ($H_c = 1.43$). At the bottom one can observe separate pulses. As sweeprate in increased the pulses merge and become bigger until no pulses can be observed. In this regime the trace is a superposition of the adiabatic avalanches.

probability of finding quiescent time between avalanches approaches zero. We define the quiescent, or "dead", time τ_d, between the nucleation of an avalanche and the end of its n^{th} predecessor as-

$$\tau_d = \tau_n - T_n, \tag{6.1}$$

where $\tau_n = \frac{\Delta H_n}{\Omega}$ is the time separating the current and the n^{th} previous nucleation events and T_n is the duration of the n^{th} previous avalanche. For $LRRF^-$, assumptions 5.2 and 5.4 imply that τ_n and T_n are uncorrelated random variables with gamma and power law distributions respectively.[1]

Let $D_{\tau_d}(\tau_d, n)$ be the distribution of dead times defined in eq. 6.1 (we omit the explicit functional dependence on α, $a\Omega$ and T^* for clarity). The probability, P_n, that the nucleation seed will be temporally overtaken by the n^{th} previous avalanche

[1]The results from this chapter can likely be presented in a more formal way through detailed analysis of the distribution of τ_d.

is given by $P_n = \int_{x<0} D_{\tau_n}(x,n)dx$. The probability that it will not be overtaken by the n^{th} previous avalanche is $\tilde{P}_n = 1 - P_n$. It follows that the probability that an avalanche will not be absorbed by *any* of the previous avalanches is

$$\tilde{P} = \prod_{n=1}^{\infty} \tilde{P}_n. \tag{6.2}$$

On average, the number of pulses, N_p, in terms of the number of avalanches, N, is simply $N_p = \tilde{P}N$. Neglecting fluctuations in the nucleation times (*i.e.*, considering an avalanche nucleation every $\frac{1}{a\Omega}$ time units) enables a simple solution of $P_n = \int_{T>\frac{n}{a\Omega}} T^{-\alpha}\mathcal{F}_T(\frac{T}{T^*})$ which yields

$$\tilde{P}(a\Omega, T^*, \alpha) = \prod_{n=1}^{\infty} \left(1 - (T^*)^{1-\alpha}\, h\left(\frac{n}{a\Omega T^*}\right)\right), \tag{6.3}$$

where $h(x)$ is related to $\mathcal{F}_T$ (relationship obtained in appendix A) and has the following limiting behavior: $h(x) \to 1$ as $x \to 0$ and $h(x) \to 0$ as $x \to 1$.

Analysis of eq. 6.3 leads to a characteristic scale that describes the decay of N_p with increasing Ω as a function of T^* and α (see appendix A). We use this scale to define Ω_t. The sweeprate at which N avalanches, where $N \to \infty$, overlap to form one big pulse, or similarly the characteristic sweeprate at which $\frac{N_p}{N} \to 0$ is

$$\Omega_t \equiv \frac{1}{ka\ \langle T \rangle}, \tag{6.4}$$

where k is dependent upon the threshold used to define pulses and details of the cutoff function.

Given eq. 6.4 consider the role that the coupling of the nucleation density in space has on Ω_t. We define

$$a \equiv \widetilde{a}\, L^{d_{nm}},$$

where $\widetilde{a}$ is independent of the size of the nucleation manifold and d_{nm} is the dimension of the nucleation manifold, we obtain

$$\Omega_t = (\langle T \rangle\ \widetilde{a}\,)^{-1} \frac{1}{L^{d_{nm}}}.$$

It is important to note that the external field must be increased at a rate inversely proportional to the size of the nucleation manifold (or slower) to get separate pulses in the time series. In general, it is expected that this rate will be proportional to $\frac{1}{N}$ where N is the number of spins in principle available to nucleate an avalanche. N is proportional to the system size if avalanches can nucleate anywhere in the sample, whereas in single front propagation N would be proportional to the size of the front (*i.e.*, scale as L^{d-1}). From this arises the result that in the thermodynamic limit any finite sweeprate Ω results in the loss of distinct pulses since all avalanches merge into one big pulse.

We note further that by fixing the sweeprate at any arbitrary value coupled to the nucleation manifold size and allowing the cutoff of the duration distribution to diverge (by allowing the system to get arbitrarily close to the critical point in the thermodynamic limit $L \to \infty$), there would be no distinct pulses in systems with $\alpha \leq 2$. (*N.B.* From this perspective, the observance of pulses at all is a consequence of the finite cutoff in the duration distribution.) For $\alpha = 2$, the mean avalanche size diverges logarithmically since $\langle T \rangle = \int_1^\infty T^{-\alpha+1} \mathcal{F}_T(\frac{T}{T^*})$. For $\alpha < 2$, the divergence of the mean with T^* is more dramatic. For $\alpha > 2$, $\langle T \rangle$ is independant of T^* and it is possible to observe distinct pulses for a nonzero sweeprate even if the system is at the critical point approaching the thermodynamic limit.

6.2.2 Spatial overlap $LRRF^-$

The sweeprate associated with the overlap of nucleated avalanches in space *and* time, Ω_s sets an upper bound in Ω for the range of Ω in which our assumptions are justified. To determine Ω_s we investigate the expected number of spins flipped as a result of the finite sweeprate within the volume of a large avalanche of size S and duration T. When this number is a finite fraction of the avalanche size we will begin to see the effects of spatial overlap in the time series. This relationship is

$$SeedsInside * \langle S \rangle \sim S.$$

The number of seeds inside the avalanche is just the total number of avalanches nucleated in time T multiplied by the fraction of spins that are flipped in the avalanche. If $\tau < 2$, the relationship is

$$a\,\Omega T \cdot \frac{S}{L^{d_{nm}}} \cdot \langle S \rangle \sim S.$$

Since $\tau < 2$, the mean avalanche size $\langle S \rangle$ is determined by the cutoff in the avalanche size distribution that scales as ξ^{d_f} yielding $\langle S \rangle \sim \xi^{d_f(2-\tau)}$. (*N.B.* For $\tau > 2$, the relationship reduces to $\frac{a\Omega T}{L^{d_{nm}}} \sim 1$ and spatial overlap does not occur in the $\Omega < \Omega_t$ regime.) As Ω is increased, the effect of spatial overlap is observed first on the larger avalanches. With $T^* \sim \xi^z = \xi^{d_f \sigma \nu z}$ the critical sweeprate required for spatial overlap of simultaneous avalanches is-

$$\Omega_s \sim \frac{\xi^{d_f(\tau-2)}}{T^*} \sim \xi^{d_f(\tau-2-\sigma\nu z)}. \tag{6.5}$$

If $\tau - 2 - \sigma\nu z > -1$, as it is in the 3-d ztneRFIM where $\tau = 1.6$ and $\sigma\nu z = 0.57$, then, even if avalanches are compact (*i.e.*, $d_f = d$), the onset of sweeprate induced spatial overlap occurs at a field sweeprate much faster than the maximum allowed to observe pulses (since Ω_t is proportional to $\frac{1}{L^d}$). Therefore, in the frequency region $\Omega_t \leq \Omega \ll \Omega_s$, where we expect the temporal overlap to merge all pulses, we expect no significant change in the flip order of the spins within individual avalanches. As a result, the time series in the "slow" sweeprate region $\Omega < \Omega_t$ is simply a superposition of the adiabatic avalanches.

If $3 - 2(\tau + \sigma\nu z) \leq \frac{d_{nm}}{d_f}$ spatial overlap will occur at $\Omega_s \leq \Omega_t$. Consequently, the assumptions will break down at Ω_s but will still be valid up to Ω_s. The effect of this will be most prominent in the low frequency regime of the PS as correlated, large avalanches will be prematurely cut-off.

6.2.3 Critical sweeprates in systems with long range restoring forces

One must assume the presence of LRRFs can have a significant impact on the determination of Ω_t and Ω_s calculated above. With eq. 5.2 we define the manner in which the internal field is directly tied to the response of the system and, in principle, the propagation of an individual avalanche. To address the impact of LRRF on the determination of Ω_t and Ω_s and to set the stage for further discussions of LRRFs we begin at time scales comparable to the propagation of one single avalanche. Clearly, on this time scale in the adiabatic limit, the internal field is determined by a trivial combination of the applied field and the contribution to the internal field of any propagating avalanches. The temporal structure of the field during the propagation of one avalanche nucleated at $t = 0$ as a function of time is

$$H_{eff} - H_0 = \Omega t - \gamma T^{\frac{1}{\sigma\nu z}} g_i(\frac{t}{T}), \tag{6.6}$$

where γ represents the coupling to the long range restoring force, $g_i(\frac{t}{T}) = \int_o^{t/T} f_i(y)\, dy$ with the voltage profile of the i^{th} avalanche represented by $f_i(t)$. Averaging over many avalanches of duration T, and replacing $g_i(t/T)$ with $\langle g(t/T) \rangle$ we plot (fig. 6.2) the temporal structure of the internal field as the sweeprate is increased for an average symmetric avalanche shape.

The internal field (shown as solid lines in fig. 6.2) is the sum of the applied field and the restoring field. The randomly distributed dots on the y-axis represent the values of internal field at which an avalanche will nucleate. The qualitative behavior of internal field extrema in the positive range of the internal field as the sweeprate is increased from zero can be summarized as follows: At zero sweeprate the internal field is negative and no other avalanches nucleate during the propagation (we neglect the rare possibility of already flipped spins flipping back due to the restoring force).

As the sweeprate is increased, a maximum in the effective field appears near the origin and allows for the nucleation of avalanches up to time $\leftarrow T_1$ and $H_{eff} = H_1$ (where the $\leftarrow T_i$ times are indicated on the figure). Nucleation will not occur beyond this time. Further increasing the sweeprate shifts the maximum to later times in the avalanche to $\leftarrow T_2$. For still higher sweeprates the internal field is always positive but still with a local maximum at $\leftarrow T_3$. Nucleations will occur up to $\leftarrow T_3$ and when the internal field surpasses the previous maxima nucleations will occur again (*i.e.*, beyond $T_3 \rightarrow$). Finally, at a critical sweeprate Ω_I, the maximum is replaced by an inflection point and nucleations can occur throughout the propagation of the avalanche.

The sweeprate Ω_I sets the scale for sweeprates that yield a structure of the internal field: For $\Omega > \Omega_I$ the internal field is effectively equal to that in $LRRF^-$, namely linear. we find $\Omega_I \sim \gamma T^{\frac{1}{\sigma\nu z}-1}$ by locating the extrema in eq. 6.6 and associating Ω_I with the highest value of Ω that allows for an extrema to exist. In other words, for a given sweeprate Ω, avalanches with duration smaller than $\left(\frac{\Omega}{\gamma}\right)^{\frac{\sigma\nu z}{1-\sigma\nu z}}$ will have an internal structure of the same character as $LRRF^-$. If $\left(\frac{\Omega}{\gamma}\right)^{\frac{\sigma\nu z}{1-\sigma\nu z}} > T^*$ the internal structure of the effective field is negligible in all avalanches. Consequently, as long as $\Omega > \Omega_I$ (with $\Omega_I \sim \gamma T^{\frac{1}{\sigma\nu z}-1}$) we may use $LRRF^-$ results (with a shifted effective Ω). Recalling $\gamma \propto L^{-d}$, we observe that when the dimension of the nucleation domain is less than the dimension of the system (as in domain wall propagation in soft magnets) we have $\Omega_I \ll \Omega_t$. As a result, when $d_{nm} < d$, LRRF will not effect the structure of the internal field in the sweeprate interval $[\Omega_I, \Omega_t]$ (*i.e.*, over the majority of the interval where pulses can be observed $[0, \Omega_t]$).

Over time scales large enough to involve many avalanche nucleations (which is appropriate for the determination of Ω_t and Ω_s), all differences between observations in $LRRF^+$ and those in $LRRF^-$ can be captured in an effective sweeprate. Recalling assumption 5.2 we note the smoothed out internal field will be globally linear in time

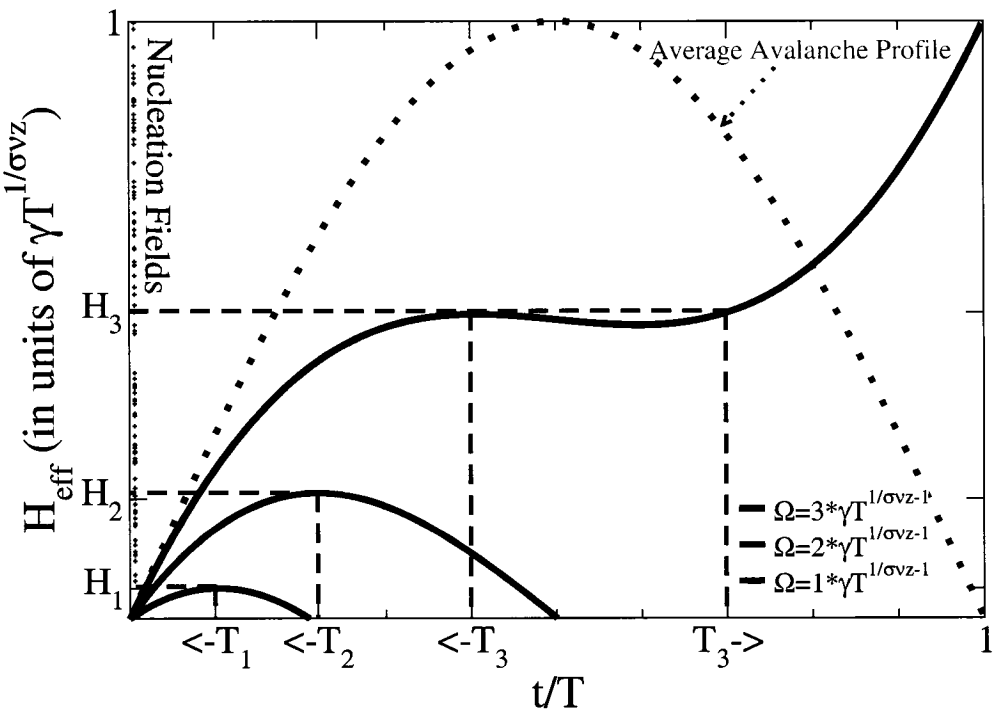

Figure 6.2: Effective internal field due to LRRF. Plot of the effective field inside a hypothetical avalanche with a sinusoidal [6] shape with strong LRRFs. An example of a realization of uniformly distributed nucleations events are pictured on the left axis (see text for details).

and have the form $H = \widetilde{\Omega}t$ where $\widetilde{\Omega} \equiv \frac{\Omega}{1+a\gamma\langle S\rangle}$ (see derivation leading to eq. 5.4). The number of avalanches, $N_{\mathcal{T}}$, nucleated during duration $\mathcal{T}$ is then given by $N_{\mathcal{T}} = \widetilde{\Omega}\mathcal{T}a$. Similar to the derivation of eq. 6.4 we obtain the sweeprate required for total temporal overlap by setting $N_{\mathcal{T}}\langle T\rangle \sim \mathcal{T}$, which yields $\Omega_t \sim \frac{1+a\gamma\langle S\rangle}{a\langle T\rangle}$. We note that $a\gamma \propto L^{-1}$ for DW motion and $a\gamma \propto 1$ for nucleation allowed through the bulk. So, in the limit of infinite system size and $\xi < L$, $\Omega_t \to \frac{1}{a\langle T\rangle}$ for DW systems and $\Omega_t \to \frac{\gamma\langle S\rangle}{\langle T\rangle}$ for systems with nucleation allowed throughout the bulk. Similar arguments carry over to the determination of Ω_s, so both $LRRF^-$ and $LRRF^+$ require a faster sweeprate to cause avalanches to overlap in space than in time and the ability to treat the pulse statistics as temporal superposition of adiabatic avalanches holds.

It is important to note that with the introduction of long range restoring forces, the adiabatic avalanches can be affected in another way: Temporal overlap can lead to the premature termination of avalanches. Consider an avalanche nucleated at t_o at the critical H field (*n.b.* in $LRRF^+$ the system is globally self tuned to sit at the critical field but fluctuations can move the system away from the critical field locally). If the avalanches that temporally overlap cause enough spins to flip to decrease the effective H field, moving the system appreciably away from the critical field, it is conceivable that the distribution of the avalanches that compose the pulses could change. This effect is neglected in this dissertation.

6.3 Pulse statistics: Theory

The fact that in the slow sweeprate regime ($\Omega < \Omega_t$) a finite sweeprate $\Omega > 0$ leads only to simple superposition of the adiabatic avalanches in the time domain allows us to estimate the sweeprate dependence of the pulse distributions $D(T, R, H, \Omega)$ and $D(S, R, H, \Omega)$. We treat the resulting effects on the pulse duration and size distributions as arising from two related processes: Absorption and swelling.

Absorption occurs when an avalanche A nucleates "during" the propagation of another avalanche B. By "during" we mean A(B) propagates simultaneously with avalanche B(A) respectively measured on a temporal scale set by the maximum between the durations of avalanche A or B. If the temporal scales of A and B are scale separated, say $T_A \gg T_B$, then the scale is set by avalanche A (*i.e.*, avalanche B is absorbed and the duration of avalanche A is unscathed).

Swelling occurs when this scale separation does not exist so that avalanche B starts while avalanche A propagates and $T_A \simeq T_B$. In this case, the resulting signal is a pulse of possible duration range from $Max\,(T_A, T_B)$ to $T_A + T_B$. Where there are many avalanches of similar scale overlapping the result is one-dimensional percolation phenomena where pulses of much larger duration than individual avalanches can emerge upon increasing temporal avalanche nucleation density (*i.e.*, faster sweeprate).

As a consequence of these two mechanisms, the scaling of the pulse duration and size distributions may change continuously as a function of sweeprate or scaling might be lost completely. We have shown [51] that absorption is the controlling mechanism responsible for the exponent changes observed in crackling noise data and swelling has the less insidious effect of destroying the adiabatic scaling completely. By decoupling these effects (see fig. 6.3) we elaborate on each of these mechanisms for change, in turn, and discover the role adiabatic scaling plays upon introducing finite sweeprate.

6.3.1 Absorption

For an avalanche to contribute to the distribution it must not be absorbed into an avalanche of a larger scale duration. The probability $D(T, \Omega)$ that a certain avalanche of duration T remains a pulse of duration T as Ω is increased is given by

$$D(T, \Omega) = D(T, \Omega = 0) \prod_{T' > T} (1 - P^{-}(T')), \tag{6.7}$$

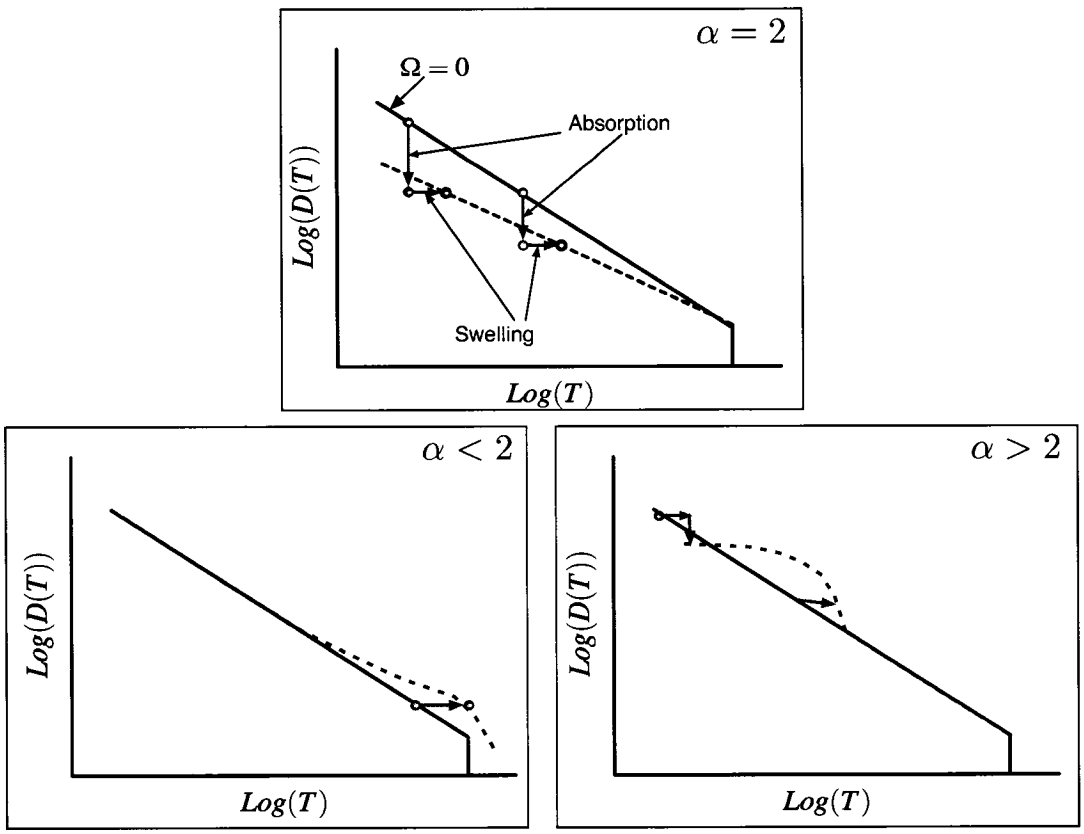

Figure 6.3: Schematic plot of the effects of temporal swelling and absorption. Systematic effects of absorption dominate for $\alpha = 2$. As the sweeprate increases systems with adiabatic exponent $\alpha < 2$ exhibit loss of scaling caused by swelling beginning near the T^* end of the distribution. In systems with $\alpha > 2$ swelling destroys the adiabatic scaling at the small avalanche side.

where

$$D(T, \Omega = 0) = T^{-\alpha} \mathcal{F}_t(\frac{T}{T^*}, \frac{h}{r^{\beta\delta}}),$$

and $P^-(T')$ is the probability that the avalanche of duration T is absorbed in a larger avalanche of duration T'. $P^-(T')$ is obtained by discretizing the observation time interval of duration Θ into $\frac{\Theta}{T'}$ time unites of duration T'. We presume simple superposition of the adiabatic avalanches. There are a total of $a\Omega\Theta$ avalanches nucleated in the observation time Θ. The number of time units of size T' occupied by avalanches of duration T' is then proportional to $T'^{-\alpha} \mathcal{F}_t(\frac{T'}{T^*}, \frac{h}{r^{\beta\delta}}) * a\Omega\Theta$; by multiplying this by $\frac{T'}{\Theta}$, we obtain

$$P^-(T') = a\Omega \cdot (T')^{1-\alpha} \mathcal{F}_t(\frac{T'}{T^*}, \frac{h}{r^{\beta\delta}}). \tag{6.8}$$

For large durations,

$$Log(D(T, \Omega)) = Log(T^{-\alpha} \mathcal{F}_t(\frac{T}{T^*}, \frac{h}{r^{\beta\delta}})) - a\Omega \int_T^\infty T'^{1-\alpha} \mathcal{F}_t(\frac{T'}{T^*}, \frac{h}{r^{\beta\delta}}) dT. \tag{6.9}$$

We are faced again with the importance of the adiabatic scaling exponents:

- If $\alpha > 2$ the second term on the RHS of eq. 6.9 is negligible for large T and

$$D_A(T, R, H, \Omega) \sim T^{-\alpha} \mathcal{F}_t(\frac{T}{T^*}, \frac{h}{r^{\beta\delta}}) = D(T, R, H).$$

- If $\alpha = 2$ and we consider the essential contribution from the integral to be from the domain $\frac{T}{T^*} \leq 1$ where the scaling function is roughly constant, the distribution is approximately

$$D(T, \Omega) \sim T^{(-\alpha + a\Omega \mathcal{F}_t(\frac{T}{T^*}, \frac{h}{r^{\beta\delta}}))} \mathcal{F}(\frac{T}{T^*}, \frac{h}{r^{\beta\delta}}).$$

From this we read off a linear dependence of the scaling exponent α on the sweeprate Ω.

- If $\alpha < 2$ the integral in the second term diverges as the mean avalanche duration. In the slow sweeprate regime, $\Omega < \Omega_t$, the integral term is controlled by the small Ω multiplier which is bounded from above by the inverse of the mean duration. Consequently, as long as there are pulse statistics in the $\alpha < 2$ case there will be $T^{-\alpha}$ scaling in the duration distributions.

Considering absorption alone, the only systematic change in the distribution functions occurs at $\alpha = 2$. Although it will take the next section on swelling to convince the reader of this, absorption is the predominant process in sweeprate effects on scaling when there are many decades of scaling available.

6.3.2 Swelling

In the approach to Ω_t, avalanches that occur during a timescale comparable to each other must cluster and form pulses greater than the avalanches that compose them.

To investigate the clustering of avalanches, we discretize the time axis in chunks of time $\delta\tau \equiv 1$ (the microscopic time scale associated with flipping). The number of time intervals $\delta\tau$ between successive avalanches is determined by the sweeprate Ω because the avalanches are nucleated at a particular value of external field H_{n_i}. We use again that the number of nucleations in ΔH is $a\,\Delta H$. In a slightly different definition of absorption suggested in the previous section, we now consider an avalanche to be absorbed into another one when the time of nucleation of the absorbed avalanche occurs during the propagation of the absorbing avalanche. From this we estimate the average number N of avalanches absorbed into an avalanche of duration T:

$$N = a\Delta H = a\,T\,\Omega.$$

What is the largest of the N avalanches absorbed having duration T_{max}? We know the distribution from which these N avalanches were selected, namely-

$$D(T,H,R) \sim T^{-\alpha}\mathcal{F}_t(\frac{T}{T^*},\frac{h}{r^{\beta\delta}}),$$

with the duration cutoff $T^* = \xi^z$ where ξ is the correlation length of the system (in the ztneRFIM at $R = R_c$ we have $T^* = |h|^{-\frac{\nu z}{\beta\delta}}$). We find $T_{max}(N)$ using a standard extreme value statistics technique [53] as follows:

Following the simplification of the duration scaling form by replacing the scaling function with a hard cutoff we set the weight of the tail, defined by $T > T_{max}$, to be equal to $\frac{1}{N}$:

$$\frac{1}{N} = \int_{T_{max}}^{T^*} T^{-\alpha}\mathcal{F}_t(\frac{h}{r^{\beta\delta}})\,dT.$$

Letting $T^* \to \infty$ we have

$$T_{max} \sim \left(N\mathcal{F}_t\left(\frac{h}{r^{\beta\delta}}\right)\right)^{\frac{1}{\alpha-1}}.$$

Since $N = a\,T\,\Omega$, the maximum avalanche duration absorbed in an avalanche of duration T at $h = 0$ has a duration maximum

$$T_{max} \sim (a\,T\,\Omega)^{\frac{1}{\alpha-1}}.$$

As with absorption, the effects of swelling are broken into three categories based on the adiabatic exponent α.

- For $\alpha > 2$, even if the avalanche of duration T_{max} was nucleated as the last spin of the initial avalanche of duration T was flipping, the resulting pulse duration would be $T_p \sim T + T^{\frac{1}{\alpha-1}} \sim T$. Hence, if $\alpha > 2$, the large avalanches will not swell appreciably and swelling will not appreciably effect the distribution. In

particular, for $\alpha > 2$, swelling will not change the scaling exponent α compared to the adiabatic case.

Qualitatively, the scaling is destroyed at the small avalanche end of the distribution. This destruction occurs due to the crossover to 1-d percolation of the time axis. The 1-d percolation regime shows a flat distribution up to a cutoff controlled by the density of primary clusters (*i.e.*, the sweeprate Ω).

- If $\alpha = 2$ an avalanche of duration $T_{max} \propto T$ will be seeded inside the initial avalanche; hence, there will be an overhang past the end of the initial avalanche proportional to T. This allows for more avalanches to be seeded during the, now elongated, pulse and the process continues on ("recursive swelling"). To calculate the mean swelling of an avalanche of duration T_o (*i.e.*, the duration of the pulse) we consider the absorbed avalanche with maximum duration is seeded halfway through the propagation of the absorbing avalanche. If the absorbed avalanche lasts longer than $\frac{T_o}{2}$, then there will be some overhang past the end of the T_o avalanche. We can now find the largest avalanche in the overhang and assume that falls in the middle of the overhang and so on. We end up with the following recursion relationship for successive temporal overhangs (Δ_i) which will allow us to estimate how the adiabatic avalanche swells due to the increase of sweeprate:

$$\Delta_i = (a\Omega\Delta_{i-1})^{\frac{1}{\alpha-1}} - \frac{\Delta_{i-1}}{2}. \tag{6.10}$$

For $\alpha = 2$ we can solve for the new duration of the pulse arising from an avalanche of duration T_o-

$$T(\Omega > 0) = T_o \sum_i \Delta_i = \frac{T_o}{1 - a\Omega}.$$

If $a\Omega < 1$, the swollen duration is proportional to T_o; however, as $a\Omega \rightarrow 1$ the pulse duration diverges or "runs away" forming a pulse of macroscopic duration due to temporal superpostion of independant avalanches. The effect on the distribution is then a shift along the T axis.

- If $\alpha < 2$, growth of Δ from eq. 6.10 will be most pronounced at the large T end of the distribution. Although this will not present a systematic change in the scaling, it does tell us that we should expect the destruction of scaling to occur at the cutoff of the adiabatic scaling and progress to smaller avalanches as $\Omega \rightarrow \Omega_t$.

To summarize, we have two crucial parameters contributing to the mode of failure of the scaling distributions by temporal "run away": The value of the adiabatic exponent ($\alpha < 2$) and, as expected, the value of the sweeprate Ω. There is no systematic contribution from swelling to scaling functions with scaling over many decades aside from a shift in the marginal $\alpha = 2$ case. Hence, systematic contributions to exponents arise solely out of the absorption arguments in the previous section.

Of course, as one approaches Ω_t, scaling must eventually fail. We believe this occurs at the small T end of the distribution for $\alpha > 2$ and near the large avalanche cutoff for $\alpha < 2$. While this may appear to be a change in the exponent measured over the distribution near the cutoff (as pictured in figure 6.8 and recently reported [54]) we believe this is simply how the distribution begins to fail and does not belie interesting scaling behavior.

6.4 Spectral analysis: Theory

The ability to view the time series at slow but nonzero field driving rate as a superposition of pulses formed in the adiabatic limit also allows us to cleanly determine the effect of field sweeprate on the power spectrum (PS) of the voltage time series.

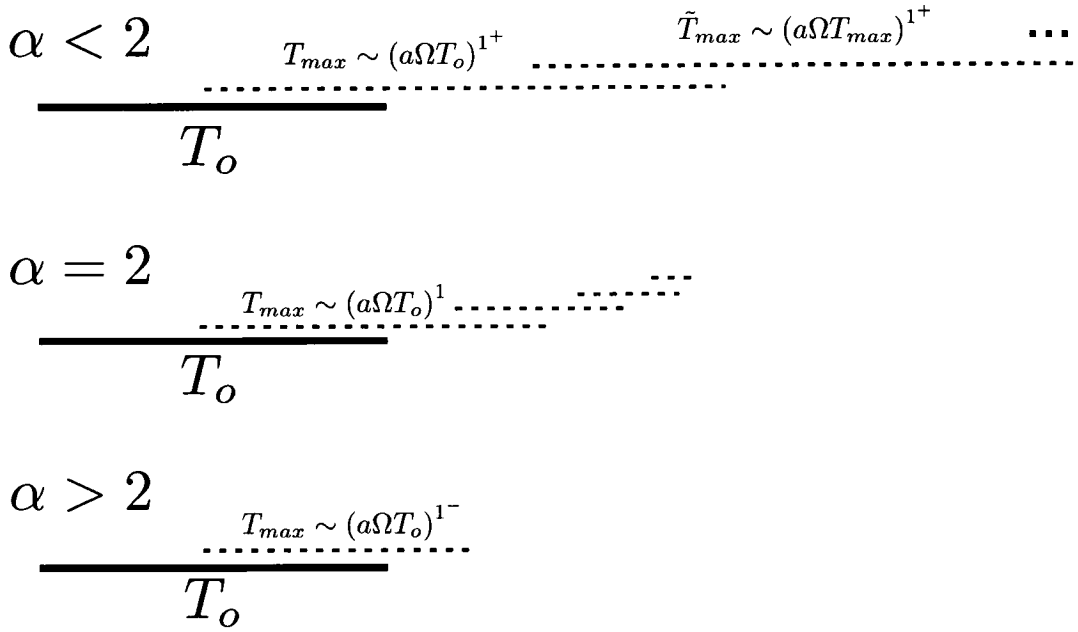

Figure 6.4: Schematic figure of swelling argument. For $\alpha < 2$ the avalanches temporally absorbed by an avalanche of duration T_o scale with T_o to a power greater than 1; hence, large avalanches cluster as $\Omega \rightarrow \Omega_t$. For $\alpha = 2$ the absorbed avalanches scale with T_o, which implies that avalanches throughout the distribution swell by a constant multiplier as $\Omega \rightarrow \Omega_t$. For $\alpha > 2$ swelling is controlled by the high density of smaller avalanches as they cluster to percolate the time axis as $\Omega \rightarrow \Omega_t$.

In appendix B we derive the following PS for $LRRF^-$ at a sweeprate $\Omega < \Omega_s$:

$$P(\omega) = a(H)\Theta\,\Omega\,\left\langle |V(\omega)|^2 \right\rangle + 2\,|\langle V(\omega)\rangle|^2\, Re\left(\int_0^\infty D(\tau)e^{i\omega\tau}d\tau \frac{1-\left(\int_0^\infty D(\tau)e^{i\omega\tau}d\tau\right)^{a(H)\Theta\Omega}}{1-\int_0^\infty D(\tau)e^{i\omega\tau}d\tau}\right), \tag{6.11}$$

where Θ is the duration of the BN train, $V_i(\omega)$ is the Fourier transform of each individual pulse and the angled brackets are averages over all of the pulses. $D(\tau_i)$ is the distribution of times τ_i separating the seeds of subsequent avalanches.

If $D(\tau)$ is Poissonian in the applied field, as it is for the ztneRFIM [36] and, by assumption, for general $LRRF^-$, eq. 6.11 reduces to a special case of Campbell's theorem [55]: $P_{total}(\omega) = a\Theta\Omega\,\langle P(\omega)\rangle$.

The calculation of the high frequency behavior of the average PS, *i.e.*, the first term on the RHS of eq. 6.11, has recently been done [37] by Kuntz and Sethna (KS) that corrected errors associated with assuming a smooth shape for each individual avalanche. What KS found was that high frequency fluctuations in the individual avalanches were the dominant contribution to the PS when $\tau < 2$. For $LRRF^-$ there is no interesting behavior in the low frequency regime due to the lack of correlations between avalanches in contrast to experimentally observed low frequency structure in $LRRF^+$. In this section we review the arguments of KS and expand on arguments briefly presented earlier [36] regarding the effects of long range forces in the low frequency regime of the PS.

Given the spectrum of an individual avalanche, $P(\omega|S)$ the average power spectrum for all avalanches is calculated simply by integrating over the weights $P(\omega) = \int_1^{S^*} P(\omega|S)D(S)dS$. The scaling form for high frequencies of the conditional spectrum of avalanches of size S is given by $P(\omega|S) \sim S\omega^{-\frac{1}{\sigma\nu z}}$. For frequencies below the low frequency cutoff, $\omega_c(S) \sim \frac{1}{T} \sim S^{-\sigma\nu z}$ the PS approaches a constant value proportional to the square of the total number of spins flipped in the avalanche. Simplifying $P(\omega|S)$ to a piecewise function in the case where no inter-avalanche correlations exist

we have approximately

$$P(\omega|S) \sim \begin{cases} S^2 & \omega < S^{-\sigma\nu z} \\ S\omega^{-\frac{1}{\sigma\nu z}} & \omega > S^{-\sigma\nu z} \end{cases} . \tag{6.12}$$

The scaling features of the average PS are then given by (with $D(S) \sim S^{-\tau}$):

$$P(\omega) \sim \int_1^{\omega^{-\frac{1}{\sigma\nu z}}} S^{-\tau+2} dS + \omega^{-\frac{1}{\sigma\nu z}} \int_{\omega^{-\frac{1}{\sigma\nu z}}}^{S^*} S^{-\tau+1} dS.$$

$$P(\omega > \frac{1}{T^*}) \sim \begin{cases} \omega^{-\frac{1}{\sigma\nu z}} & \tau < 2 \\ \omega^{\frac{\tau-3}{\sigma\nu z}} & \tau > 2 \end{cases} . \tag{6.13}$$

Below $\omega < \frac{1}{T^*}$, $P(\omega) \sim N \langle S^2 \rangle$, where N is the number of avalanches in the measured time. The shape of the PS is unaffected by sweeprate until the Ω is increased into the so-called hydrodynamic limit [56], *i.e.*, $\Omega > \Omega_s$, where avalanches overlap in space. This allows for a determination of the exponents associated with the adiabatic avalanches (z,νz,$\sigma\nu z$,$\frac{3-\tau}{\sigma\nu z}$,$\frac{2-\tau}{\sigma\nu z}$) even in the intermediate sweeprate regime where no separate "pulses" exist [36]. This fact allows for a check of exponents obtained by pulse statistics in experiment and offers a substantial advantage in computational time when studying large scale simulations of crackling systems.

In the approach to the hydrodynamic regime, the spatial overlap introduces a sweeprate induced cutoff to the avalanche size, $S^* \sim \Omega^{-b}$, and a corresponding sweeprate induced shift in the low frequency cutoff of the PS given by $\omega_c \sim \Omega^{b\sigma\nu z}$. From eq. 6.5 we read off $b = \frac{1}{2+\sigma\nu z-\tau}$ and obtain $\omega_c \sim \Omega^{\frac{\sigma\nu z}{2+\sigma\nu z-\tau}}$ which matches with the scaling behavior in the low frequency maximum with sweeprate for BN in conductors. Measuring the spectrum over a fixed total number of spins flipped ΔM such that $N = \frac{\Delta M}{\langle S \rangle}$ the total PS in the low frequency limit will be $P(0) \sim \frac{\langle S^2 \rangle}{\langle S \rangle}$. For $\tau < 2$ all moments are determined by the cutoff giving $P(\omega < \omega_c(\Omega)) \sim \Omega^{-b}$. For $2 < \tau < 3$ second and higher moments are controlled by the cutoff giving $P(\omega < \omega_c(\Omega)) \sim \Omega^{b(\tau-3)}$.

In $LRRF^+$ the correlations between the size of the avalanche and the nucleation

time of the next avalanche introduces structure in the low frequency regime of the PS. We give the PS for $LRRF^{+}$ in the adiabatic limit (derived in appendix B):

$$P(\omega) = a(H)\Theta\,\tilde{\Omega}\,\left\langle|\phi(\omega)|^2\right\rangle + 2Re\left(\left\langle V^*(\omega)\right\rangle\left(\int_1^{S^*} S^{-\tau}e^{i\omega\tilde{\gamma}S}V(\omega|S)\,dS\frac{1-\left(\int_1^{S^*} S^{-\tau}e^{i\omega\tilde{\gamma}S}\,dS\right)^N}{1-\int_1^{S^*} S^{-\tau}e^{i\omega\tilde{\gamma}S}\,dS}\right)\right). \tag{6.14}$$

The precise behavior of eq. 6.14 has not been worked out, but we hypothesize that the generic behavior of the PS can be understood by the following argument: First consider only the largest avalanches as they form the scaling behavior of the PS. Since the time separation between the largest avalanches is linearly coupled to the size of these avalanches, there will be a characteristic frequency in the PS around $\omega_m = \frac{\Omega}{\gamma S^*}$. In the slow sweeprate regime we thus expect there to be a broad peak in the PS which scales with the sweeprate as $P(\omega_m) \sim \Omega$. As the sweeprate is increased from the adiabatic regime into the hydrodynamic regime this scaling is lost due to the spatial overlap of avalanches. In this regime we hypothesize that the broad peak will no longer be controlled by the temporal separation of the avalanches but from the change in the low frequency cutoff in the PS derived above for $LRRF^{-}$. Consequently we expect a crossover from $P(\omega_m) \sim \Omega$ to $P(\omega_m) \sim \omega_c \sim \Omega^{\frac{\sigma\nu z}{2+\sigma\nu z-\tau}}$ as the sweeprate is increased.

6.5 Wait-time distributions: Theory

The wait time distribution (WTD) is defined in various ways throughout the literature and usually depends on the crackling system of interest. We shall define two types of wait time distributions: dead time distributions, $(D_{dead}(\tau_d))$; and adjacent nucleation time distributions, $(D_{an}(\tau_n))$. (*N.B.*: We suppress the subscripts on the

distributions as the arguments unambiguously define the distribution.) One should further distinguish between WTD of pulses and those of avalanches (if fine spatial and temporal resolution is available). In bulk measurements $\tilde{\tau}_d$ is the quiescent time between adjacent pulses and $\tilde{\tau}_n$ is the time between the nucleation of adjacent pulses where the tilde denotes WTD from the pulses in contrast to the the WTD for the avalanches (see fig. 6.5).

Without long range forces the WTD are easy to conceptualize since they follow directly from the assumptions. In the adiabatic limit where there is no temporal overlap $D(\tau_n)$ is simply a Poisson distribution. Since the random variable τ_d is the sum of two independent (by assumption) random variables, *i.e.*, $\tau_d = \tau_n - T$, where T is the duration of avalanche A and τ_n is the time between nucleations of successive avalanches A and B (A is nucleated first), $D(\tau_d)$ is generally derivable from experimentally obtained $D(T, \Omega = 0)$ and $D(\tau_n)$. As Ω increases $\tilde{\tau}_d = \tilde{\tau}_n - \tilde{T}$ where $\tilde{T}$ is the pulse duration. Generically we note that as $\Omega \to 0$, $D(\tilde{\tau}_d) \to D(\tilde{\tau}_n)$ and as $\Omega \to \Omega_t$, $D(\tilde{\tau}_n) \to D(\tilde{T})$.

In $LRRF^+$, the effect of the avalanche size itself on the effective field induces a WTD that is coupled to the avalanche size. As a result, as $\Omega \to 0$, $D(\tau_n) \sim D(\tau_d) \sim D_S(bS)$ where b is simply a multiplier to get the units right and $D_S(S)$ is the distribution of avalanche sizes. And, similar to $LRRF^-$as $\Omega \to \Omega_t$, $D(\tilde{\tau}_n) \to D(\tilde{T})$.

6.6 Summary of theoretical predictions

The null assumptions in chapter 5 have a number of interesting consequences. First, they imply a criterion for sweeprate dependence on the pulse distribution exponents. For both $LRRF^+$ and $LRRF^-$ we summarize this criterion as follows:

- For the case with $\alpha < 2$ the pulse perspective is lost for very small sweeprates since total overlap takes over at Ω_t. In the regime where there is finite sweeprate

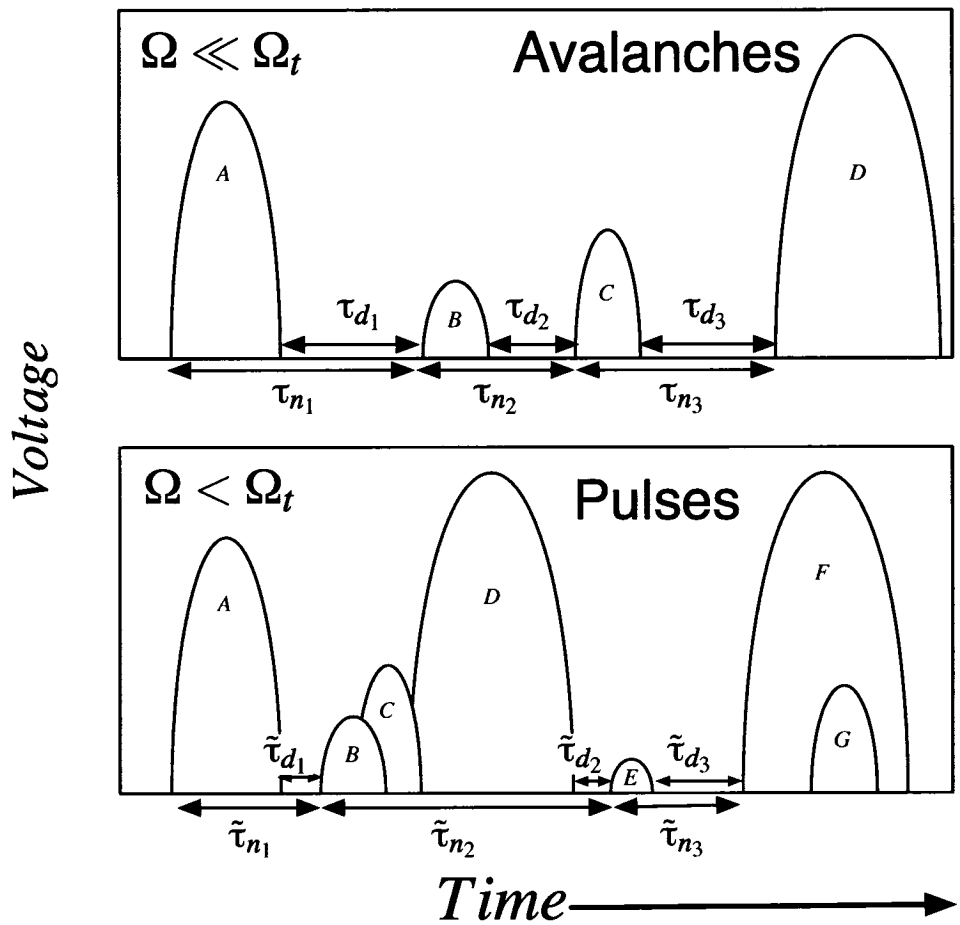

Figure 6.5: Schematic figure to outline wait time distribution definitions. Wait time distributions of both the nucleation times and the dead times in the adiabatic regime (top) are directly related to avalanche nucleation and duration distributions while, in the temporal overlap regime (bottom), wait time distributions have a more complex dependance upon temporal overlap details.

but still slow enough to discern distinct jumps, the jumps are so sparse on the time axis that we expect no changes in the avalanche statistics. For these systems we conclude that; if you can discern jumps and significant scaling, you will measure the zero sweeprate scaling exponents and functions in the large system limit. Qualitatively as $\Omega \rightarrow \Omega_t$ scaling will begin to be lost at the large pulse limit as large pulses cluster and begin to percolate the time axis.

- For the intermediate case of $\alpha = 2$ the avalanche size and duration distributions exhibit a linear frequency dependency in the exponent. In the slow sweeprate regime the exponents α and τ are given by -

$$\alpha(\Omega) = 2 - c\Omega \qquad \tau(\Omega) = \frac{3}{2} - \frac{c\Omega}{2}$$

where c is a non-universal constant. This is solely a consequence of smaller avalanches being absorbed into scales set by larger avalanches.

- When $\alpha > 2$ we expect no change in the exponents in the slow sweeprate regime for the large avalanche limit. In contrast to the $\alpha < 2$ case, as $\Omega \rightarrow \Omega_t$ scaling will begin to be lost at the *small* pulse limit as the much more numerous small avalanches cluster and begin to percolate the time axis.

It is important to emphasize that in each of these cases for $\Omega < \Omega_s$ the dynamics of the system are still determined by collective relaxations. That is, the adiabatic scaling is still present but it is not observable from pulse statistics. Consequently, the interpretation of avalanche scaling behavior from pulse statistics as $\Omega \rightarrow \Omega_t$ is difficult and likely incorrect for systems with adiabatic avalanche exponents $\alpha \neq 2$ and perhaps easier but definitely incorrect if the adiabatic avalanche exponent is $\alpha = 2$.

The consequences of our assumptions in measured power spectra are less dramatic. We have shown that at high frequencies ($\omega > \frac{1}{T^*}$) the power spectrum is invariant in the sweeprate regime $\Omega = [0, \Omega_s]$ for both $LRRF^+$ and $LRRF^-$. As a result, the

spectrum is simply the sum of all the spectra from the avalanches in the time series. It has previously been shown [37] that this sum scales as $P(\omega) \sim \omega^{\frac{-1}{\sigma\nu z}}$ (in the high frequency limit for systems with adiabatic scaling exponent $\tau < 2$) and arises out of intra-avalanche fluctuations.

For $\omega < \frac{1}{T^*}$ spectra from $LRRF^-$ are also invariant w.r.t. sweeprate and flat since there are no inter-avalanche correlations. Sweeprate will begin to have an effect on the PS when $\Omega > \Omega_s$. As the sweeprate is increased into the fast regime the low frequency cutoff will scale as $\Omega^{\frac{\sigma\nu z}{\sigma\nu z+2-\tau}}$. For $LRRF^+$ the low frequency regime exhibits a broad peak due to the characteristic frequency imposed by the coupling between the size and the temporal displacement of the nucleation of the next avalanche. In the slow sweeprate regime we expect the frequency at which the peak is observed to scale with the sweeprate. If $\Omega > \Omega_s$ we argue that the scaling of the peak frequency is controlled by the same low frequency cutoff as predicted in $LRRF^-$ namely that $\omega_m \sim \Omega^{\frac{\sigma\nu z}{2+\sigma\nu z-1}}$.

Generally, spectral measurements are more robust to changes in the sweeprate than are pulse statistics. Indeed, we have used the PS in a study [36] deliberately in the regime where no pulses exist to obtain the adiabatic exponents from data collapses in the ztneRFIM. From the scaling in the low frequency cutoff we can, perhaps paradoxically, learn the adiabatic exponents by driving the system *faster* as follows: From scaling in the high frequency regime in the PS one can determine $\frac{1}{\sigma\nu z}$. By driving the system beyond Ω_s to obtain the scaling of the low frequency cutoff with sweeprate one can determine $\frac{\sigma\nu z}{\sigma\nu z+2-\tau}$. Since $\alpha = \frac{\tau-1}{\sigma\nu z} + 1$, these two measurements will yield the adiabatic τ and α free from problems associated with temporal overlap of the pulses in the interpretation of pulse statistics.

6.7 Comparison to experimental results

Adiabatic exponents or scaling functions in any particular model are associated with that model alone. In order to independently test the consequences of our assumptions beyond the scaling arguments just presented, we wrote a routine which allowed us to numerically determine the consequences of our assumptions and to isolate the effects of superposition of pulses with distributions of choice rather than being determined by the dynamics of the model at hand. Furthermore, though the scaling arguments above are illustrative to explain general trends, the ability to actually generate distributions given our assumptions allows for a more rich comparison to experiment.

We call the numerical procedure the forced superposition tool (FST). In the FST we create, by choice, independent avalanches of any chosen shape with power law distributions of size and duration and place them on the time axis as per the assumptions in chapter 5. (details discussed in chapter 4.)

The FST allows us to look at sweeprate effects on both the size and duration distributions of the pulses as well as investigate results obtained in experiments and simulations [57] , examples include; The linear change in exponents in materials that have adiabatic exponents τ =1.5 and α =2 (fig. 6.6); the constance of exponents w.r.t. sweeprate in materials with other exponents; the sweeprate induced "bump" near the cutoff and beyond in the pulse distributions distributions observed over limited scaling regimes for $\alpha \leq 2$; the cross over between $T \sim S^{\sigma\nu z}$ and $T \sim S$ behavior (fig. 6.9); and the flattening of the average pulse shape for large pulses.

We compare the numerics with BN data obtained on two different soft magnetic materials: Fe-Si 7.8 wt% strip and amorphous samples $Fe_{21}Co_{64}B_{15}$ under tensile stress [18]. These materials were chosen because they represent two distinct universality classes of CN. The Fe-Si sample dominated by dipolar (long range) forces and has adiabatic exponents $\tau = 1.5 \pm 0.05$ and $\alpha = 2 \pm 0.2$. The amorphous alloy be-

havior is dominated by surface tension effects and has adiabatic exponents given by $\tau = 1.27 \pm 0.03$ and $\alpha = 1.5 \pm 0.1$. Experimental pulse size and duration distributions were obtained by choosing a voltage threshold value that produced distributions that were robust to changes in the threshold level.

6.7.1 Pulse size and duration distributions

Materials with adiabatic exponents $\alpha = 2$ and $\tau = 1.5$ show the following linear dependence in the exponents with increasing sweeprate: $\alpha(\Omega) = 2 - \frac{\Omega}{\Omega_t}$ and $\tau(\Omega) = \frac{3}{2} - \frac{\Omega}{2\Omega_t}$. Experiments, at best, give 4-5 decades of scaling in pulse sizes. Since $T \sim S^{\frac{1}{\sigma\nu z}}$, where $\frac{1}{\sigma\nu z}$ ranges from $\sim 1.5 - 2$, the broadest regions of scaling in duration distributions tend to be 2-3 decades. As a result, interpreting exponents from experimentally obtained duration distributions is difficult. Results obtained by numerical means in the FST can obtain twice the number of decades in scaling with little computational effort which illustrate nicely the linear dependence of the exponent (fig. 6.6).

An illustration more typical of experiments with only a couple of decades of scaling is shown in figure 6.7. The linear change in the exponent is apparent at the low sweeprate limit but is not so clear as $\Omega \rightarrow \Omega_t$. When determining whether observed sweeprate effects on the distributions are a consequence of adiabatic models coupled with the temporal superposition arguments or actually represent unmodeled physics we believe the qualitative features obtained by the FST over similar, limited scaling ranges offers more insight into sweeprate effects than measurement of exponents.

Materials with adiabatic exponents $\alpha < 2$ and $\tau < 1.5$ should show no sweeprate dependence in the exponents. The Si-Fe polycrystals are members of this category. The side by side comparison between the FST results and experiment shown in figure 6.8 illustrates this. The growth in the distribution in the regime near the cutoff shows good qualitative agreement suggesting the observed distributions are a result

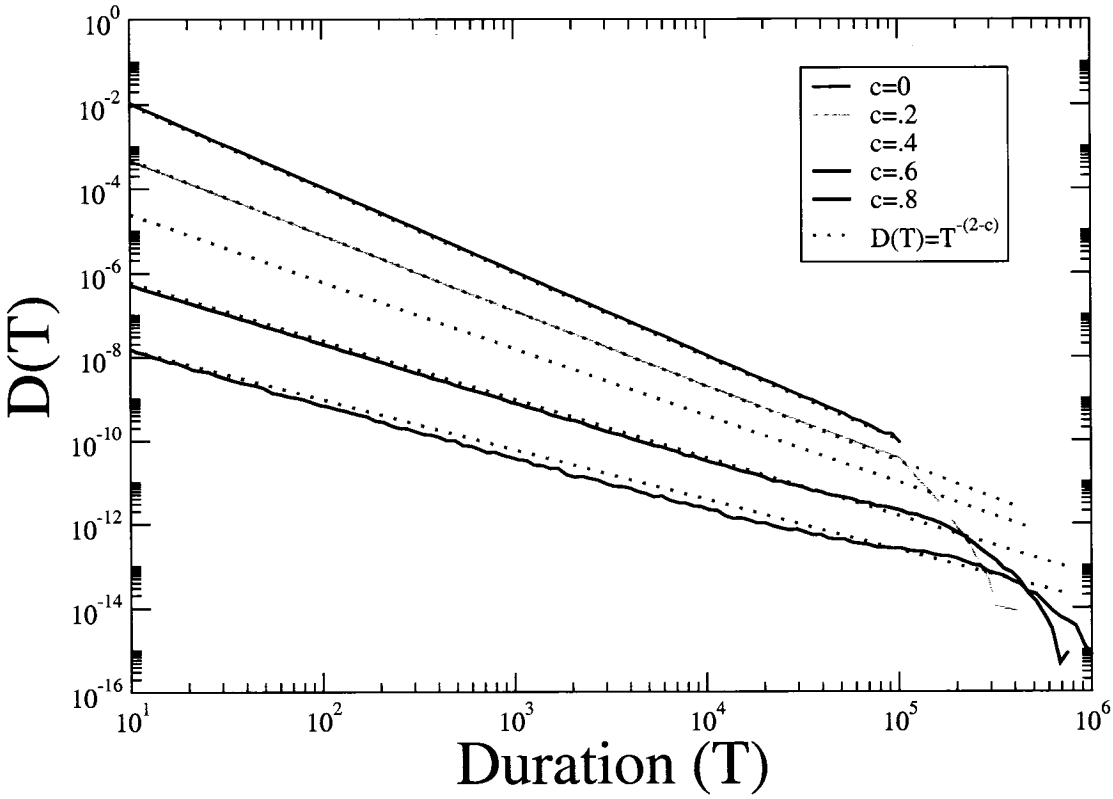

Figure 6.6: Linear change in exponent for $\alpha = 2$ obtained from the FST. We show the pulse duration distribution for increasing sweeprate without LRRF in the FST. In the legend, c is the probability of "nucleating" and avalanche at a given time interval and corresponds to the sweeprate. The dotted lines are not fits but plots of the function $D(T) = T^{c-\alpha}$. The plots have been vertically shifted for clarity.

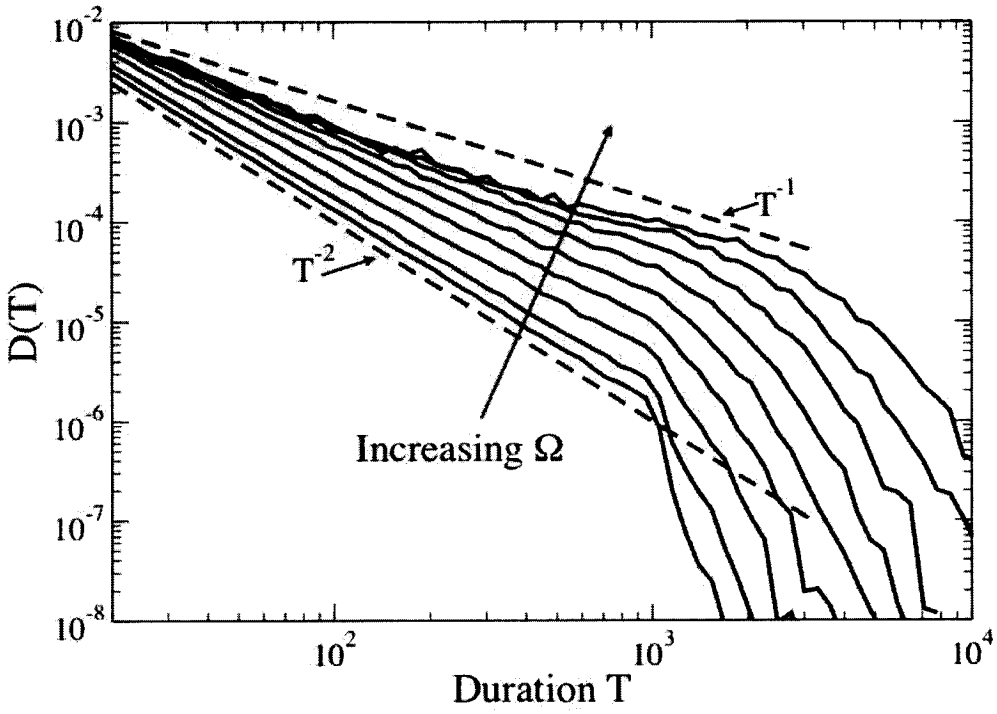

Figure 6.7: Experimentally realistic scaling regime duration distribution from FST. We show the duration distribution plot generated by FST with $\alpha = 2$ and $\tau = 1.5$ for sweeprates from $0.1\,\Omega_t$ to $0.9\,\Omega_t$. The limited range of scaling is imposed in FST to mimic typical (small) experimental scaling ranges.

of temporal superposition.

6.7.2 Spectra

Spectra found in the BN literature for different materials have the following unexplained features [6]: A low frequency bump, $P_{max}(\omega_{max})$ that shows $P(\omega_{max}) \sim C$ where C is a constant for $\Omega < \Omega_t$ and $P(\omega_{max})$ diminishing for $\Omega > \Omega_t$ with the frequency of the maximum having a scaling behavior of $\omega_{max} \sim \Omega^{\frac{1}{2}}$; An apparent cross-over in the high frequency scaling regime from $\omega^{-\frac{1}{\sigma\nu z}}$ behavior for high frequencies to ω^{-a} for lower ω where $a \simeq 1$; A low frequency scaling region (on the low frequency side of the maximum) that scales as $P(\omega) \sim \omega^{\psi}$ where $\psi \sim 0.6$ or ~ 1.

The first feature is a consequence of the redistribution of weights as avalanches overlap in space. As the sweeprate is increased into the fast regime, where avalanches overlap in space, the cutoff of the avalanche duration diminishes (but not until then) due to "parallel processing". Since the spectrum is controlled by the cutoff in this regime, the amplitude of the maxima will diminish. From eq. 6.5, above Ω_s, we find that the low frequency cutoff scales like $\omega_c \sim \Omega^{\frac{\sigma\nu z}{\sigma\nu z+2-\tau}}$. For mean field ztneRFIM and ABBM model exponents $\omega_c \sim \Omega^{\frac{1}{2}}$ which is consistent with experimental results reported in [58, 59] for materials in the same universality class. Numerical comparisons to non mean field exponents lie within experimental error.

The second feature is discussed in chapter 7. The third feature, *i.e.*, scaling at frequencies less than ω_{max}, is not addressed in this dissertation but we speculate explanations will follow from these arguments. This will most likely require a detailed study of eq. 6.14.

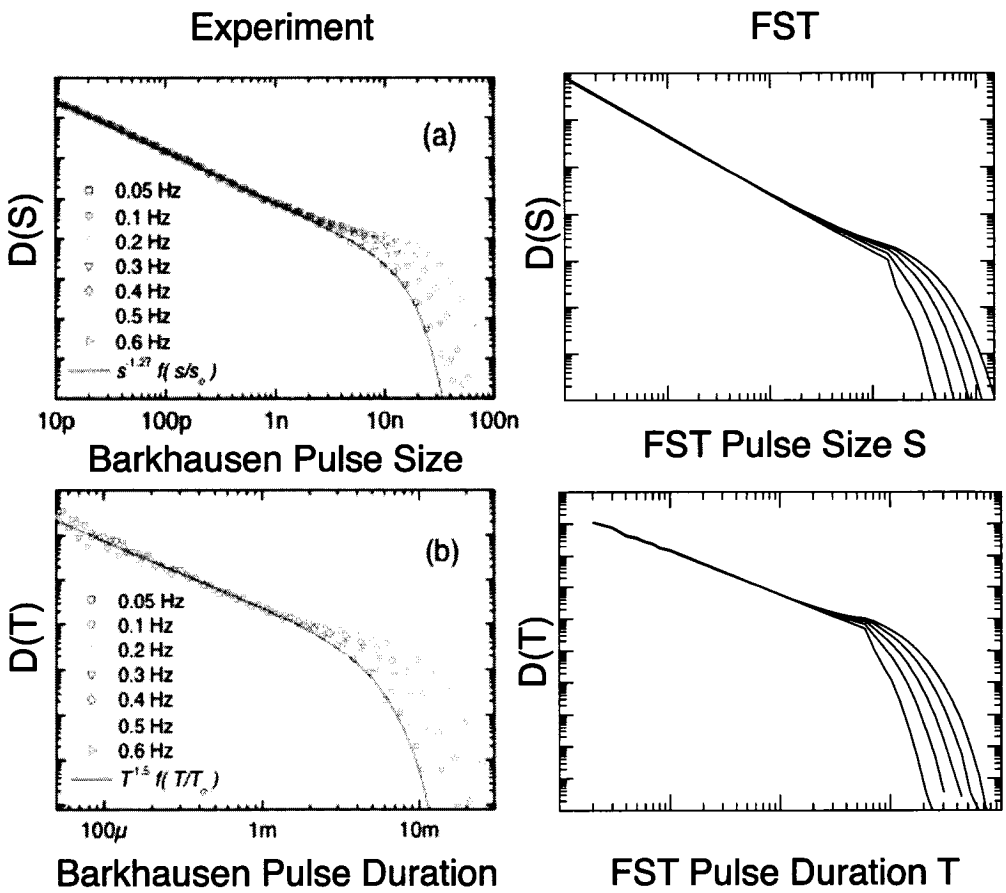

Figure 6.8: Size and duration distribution comparison: FST and $Fe_{21}Co_{64}B_{15}$. We show a side by side comparison of numerically obtained FST results and size and duration distributions for $Fe_{21}Co_{64}B_{15}$ under tensile stress with increasing sweeprates. In this material, the adiabatic exponents are $\tau = 1.27$ and $\alpha = 1.5$. We fix the number of decades of scaling in the FST to mimic that found in experiment (units are arbitrary). Increasing sweeprate leaves the pulse exponents unchanged but increases the cutoff.

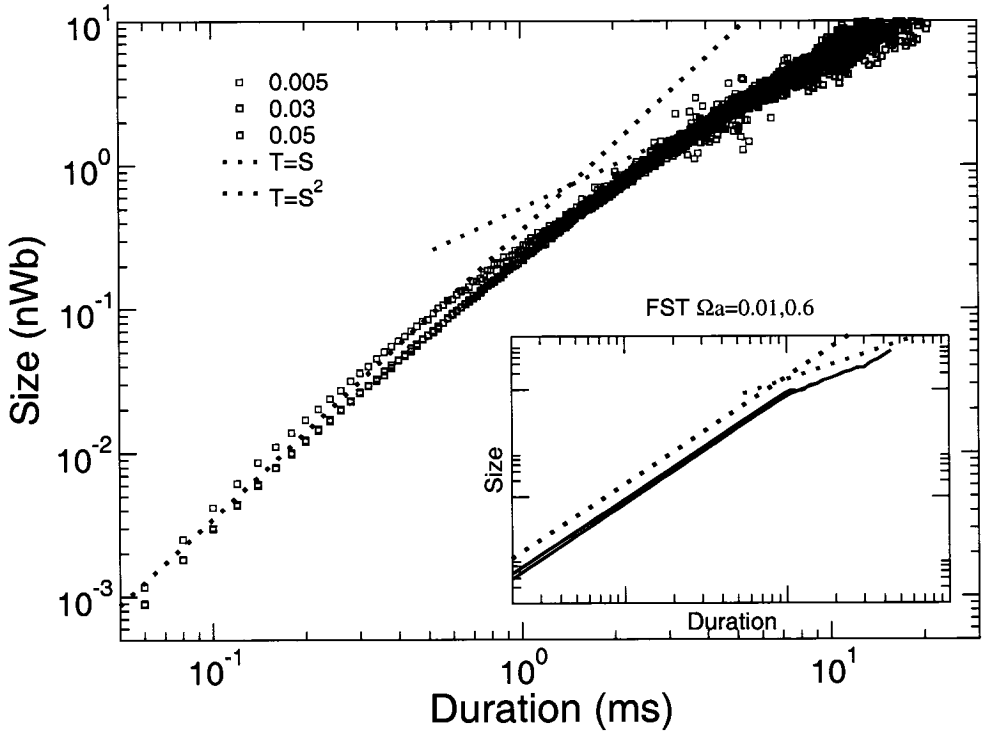

Figure 6.9: Size vs. duration scaling in Si-Fe polycrystals compared to FST. Data on Si-Fe polycrystals shows a crossover between $T \sim S^{\sigma\nu z}$ and $T \sim S$. Insert is the same plot derived from the FST exhibiting the same type of crossover.

6.7.3 Wait-time distributions

Although there does not seem to be many experimental studies on WTD in BN, Gianfranco Durin has provided us with some preliminary data on $FeSi$. The coupling of the WTD to the pulse size distribution is apparent by overlaying the size distribution with the WTD (This result is seen clearly in figure 6.10.). Further measurements that could investigate the slaving of the WTD to the size distribution in $LRRF^{+}$ would be to measure the conditional WTD. That is, the distribution of wait times following a pulse of size S. If this distribution has a peak as a function of S that is linear in S the origin of the WTD would be fairly clear as being due to the LRRF.

6.8 Discussion

In early studies of BN, "pulses" were thought to be a result of superimposed, likely coupled, local relaxations whose distributions directly mirrored the quenched disorder in the system [60, 61, 62]. Subsequent studies have shown that the power law scaling of the pulses does not directly mirror the quenched disorder in the system but arises out of collective behavior of domains traversing a disorder strewn landscape. More recent theoretical treatments [6] focused on how this can arise. Consequently and understandably the consequences and language of superposition were abandoned for the more interesting origin of the scaling behavior.

In this chapter we have revisited the idea of superposition, not to provide insight about the distribution of avalanches, but to take them as given and examine how their formation of pulses through temporal overlap can effect data that is commonly collected from these systems. As a concrete example we have found that our results provide insight to hitherto unexplained and interesting features of BN exhibiting power-law scaling. The generic nature of the arguments should apply beyond BN however and aid in interpreting data in other crackling systems. It is our hope that a

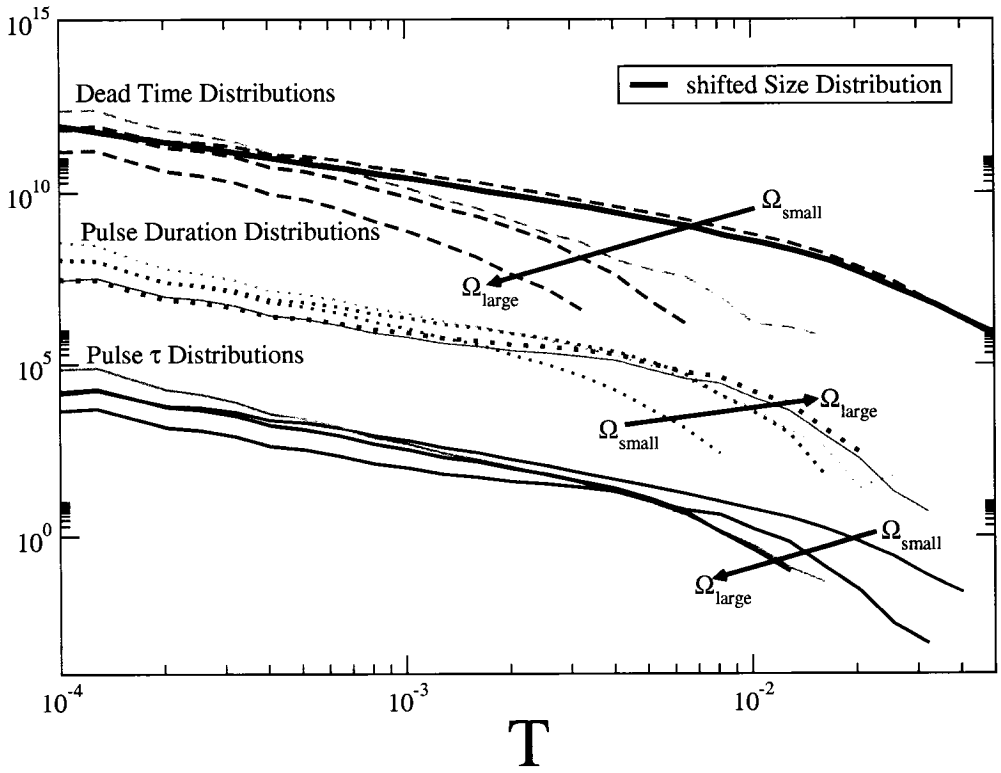

Figure 6.10: Wait time distributions from experiment displaying effects of LRRF. We show the wait time and duration distributions obtained from FeSi polycrystalline sample for increasing sweeprates. Top set are dead time distributions with a size distribution solid line horizontally and vertically shifted to lie on top of the low sweeprate dead time distribution , middle set are pulse distributions and the bottom set are nucleation time distributions. The superimposed size distribution (shifted) illustrates the slaving of the wait time distribution to the size distribution for slow sweeprates. As sweeprate is increased $D(\tilde{\tau}) \rightarrow D(\tilde{T})$.

more clear understanding of the effects of temporal overlap in power-law distributed pulses will aid in extracting proper models for crackling phenomena and perhaps lead to uncovering more interesting physics.

Chapter 7

Thermal effects on crackling noise

Thermal fluctuations (TF) are largely dismissed from the modeling of crackling response. The justifications for this are sometimes difficult to discern, even though many crackling systems—such as disordered magnets—are typically studied at room temperature. In some large scale crackling systems (*e.g.*, earthquakes and solar flares) the driving mechanisms are not fully understood so the neglect of thermal effects, or more generally, local dynamic fluctuations in the driving mechanisms[1] is done out of necessity. It seems that at least a qualitative picture of these effects is required to proceed with the modeling of many crackling systems.

In this chapter, we provide a look at CN at finite temperature and investigate the effects that TF have on coercive fields and spectral measurements. As with the previous chapter on sweeprate effects, we use the RFIM to frame our discussion and scaling arguments. Numerical results are obtained by judicious inclusion of TF to the ztneRFIM in the saturation history by a Monte Carlo method with glauber dynamics and checkerboard update. Discussion of the important reasons behind this particular choice is presented in chapter 4.

[1] or any additive stochastic process

7.1 Preliminaries

To review: The Hamiltonian for the RFIM is

$$\mathcal{H} = -J\sum_{\langle i,j\rangle} s_i s_j - \sum_i (H_{ext}(t) + h_i)s_i \tag{7.1}$$

where the first term represents the ferromagnetically coupled nearest neighbors (with nearest neighbor coupling $J > 0$), $H_{ext}(t)$ is the external applied field, and h_i is the quenched local random magnetic field with Gaussian distribution having standard deviation R-

$$\rho(h_i) = \frac{1}{R\sqrt{2\pi}} \exp(-\frac{h_i^2}{2R^2}) \; .$$

Far from equilibrium, the state of the system is dependent upon the history of the external field. In this chapter we follow the saturation loop history whereby the external field is initialized with $H_{ext}(0) = -\infty$ and increased linearly with time (*i.e.*, $\frac{dH_{ext}}{dt} = \Omega$) up to $H_{ext} = +\infty$.

We focus on the power spectrum (PS), defined by

$$P(\omega) = \left| \sum_{t=t_o}^{t=t_1} e^{i\omega t} V(t) \right|^2 ,$$

where $V(t) = \frac{dM(t)}{dt}$ is the time derivative of the magnetization of the system (which is proportional to the voltage measured in Barkhausen noise induction experiments). The PS contains much of the same information as can be obtained from the study of avalanche statistics (*e.g.*, size and duration distributions) but it avoids the difficulties [36] associated with defining distinct avalanches in the time series of the voltage.

At zero temperature, Ω does not have a significant effect on the power spectrum as long as $\Omega < \Omega_s$, where Ω_s denotes the sweeprate at which avalanches overlap in space (see chapter 6). This might lead one to treat the inclusion of TF in the sweeprate regime defined by $\Omega < \Omega_s$ as an independent direction in the parameter space. This is, of course, not the case. Temperature and sweeprate are intimately coupled to

each other. We will point out, in detail, our understanding of this coupling in the crackling regime throughout this chapter. In the extreme case of $\Omega = 0$, however, this coupling is obvious: Driven adiabatically through the saturation history at finite temperature, the RFIM is in equilibrium and exhibits critical behavior controlled by a zero temperature fixed point (ZTFP).

Near the ZTFP of the equilibrium RFIM, divergence of the free energy barriers to equilibration cause [63, 64] the system to fall out of equilibrium if the system is driven faster than the characteristic relaxation rates. For the ZTFP, as in the disorder induced critical point (DICP), the external field value is a relevant parameter. In the ZTFP the critical field is at $H_c = 0$ while in the DICP $H_c > 0$. If the field at which the system falls out of equilibrium, H_{neq}, is small, scaling in H_{neq} with temperature and sweeprate is controlled by the ZTFP. In appendix C we make the following conjecture: The hysteresis loops observed near the ZTFP are described by the disorder induced critical point found in the ztneRFIM. We investigate testable consequences of this conjecture through scaling arguments. In *this* chapter, however, we operate in the temperature and sweeprate regime such that the system falls out of equilibrium at $H_{neq} = O(1)$. In other words, even though we operate in a non-zero temperature regime we expect no signature from the ZTFP of the equilibrium RFIM. As such, we believe this regime is most relevant to CN.

Details of the numerical results reported in this chapter are as follows: Our simulations were performed on a 100^3 cubic lattice with periodic boundary conditions. Roughly 10^3 hours of dedicated simulation time on a P4 2.8GHz processor were used. In the 3-d ztneRFIM, for $L = 100$ and $\theta = \Omega = 0$, critical scaling is observed at $R = 2.3$ and $H_c = 1.41$ (both in units of $J = 1$). To ensure stationarity of the signal we measure the PS in a small window, $\Delta H < 0.05$ around a slightly temperature dependent H_c (see figure 7.1) and fixed disorder $R = 2.3$.

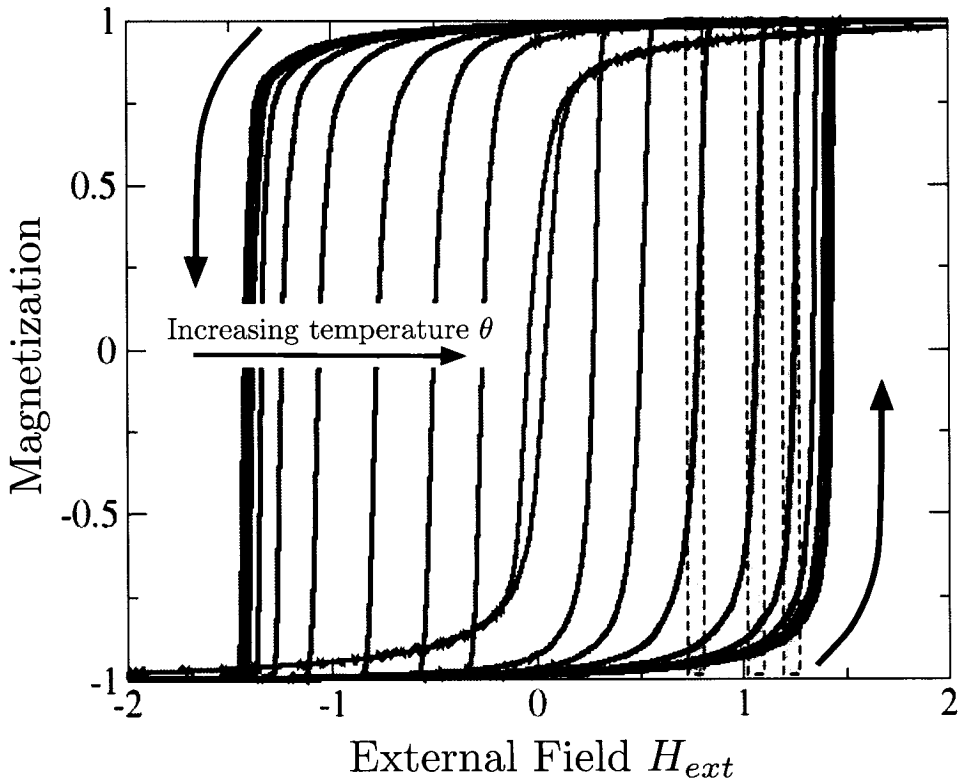

Figure 7.1: Saturation Loops in the RFIM for increasing temperatures. We show the magnetization as a function of external field with $L = 100$, $R = 2.3$ and $\Omega = 1/L^d$. The long boxes illustrate the temperature dependance of the field at which the PS was measured. To insure stationarity, the window selected was $\Delta H < 0.05$ (shown in figure exaggerated). From the inner (hotter) loop outward the temperatures for this figure were $\theta/J = 12.8, 6.4, 3.2, 1.6, 0.8, 0.4, 0.2, 0.1, 0$. We report upon PS for temperatures up to $\theta/J = 0.64$.

7.2 The power spectrum

To place the discussion in context we begin with the numerical results on the spectrum in the ztneRFIM. The scaling arguments for the various regimes found that are apparently mirrored in BN at room temperature, will follow.

In the ztneRFIM, for R very close to the critical disorder R_c, the power spectrum is given by [37]

$$P_{ztne}(\omega) \sim \omega^{-1/\sigma\nu z}. \tag{7.2}$$

If the system size L is not large enough, or the disorder or the external field are not close enough to their critical values a more general formula exists [36]. As an example, in fig. 4.3 the effect of the finite size L in the PS is apparent in the low frequency regime. We typically simulate large systems to emulate typical BN studies, hence the zero temperature PS is well described by the expression above.

We investigate the spectrum in the slow sweeprate regime, defined by the presence of distinct pulses in the avalanche dynamics at $\theta = 0$. In this regime there are no effects from spatial overlap of the adiabatic zero temperature avalanches [51]. As shown in fig. 7.2, the PS splits into three regimes

$$P(\omega) = \begin{cases} \omega^{-\phi} & \omega_L(\theta) > \omega \\ \omega^{-1/\sigma\nu z} & \omega_H(\theta) > \omega > \omega_L(\theta) \\ \omega^{a} & \omega > \omega_H(\theta) \end{cases} . \tag{7.3}$$

Two additional critical exponents, ϕ and a have been introduced, along with two corner frequencies—ω_H and ω_L—separating the different regimes. Both corner frequencies have a strong temperature dependence with ω_H decreasing with increasing temperature, and ω_L increasing as the temperature increases.

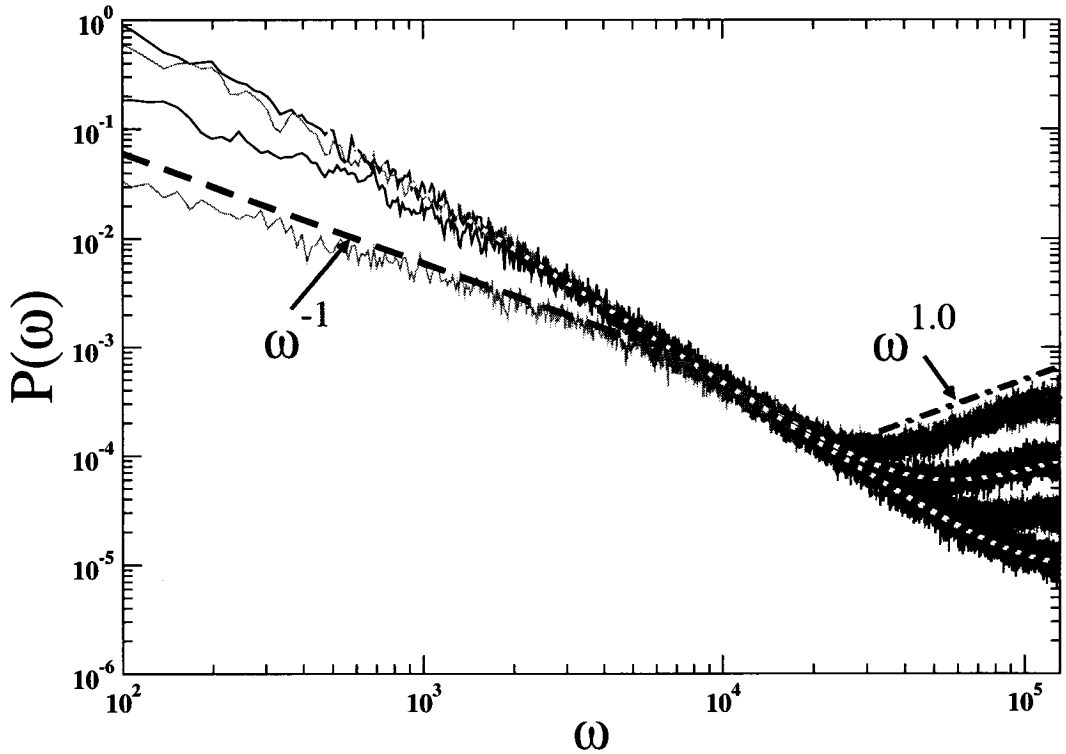

Figure 7.2: Power spectrum in the RFIM for increasing temperature in the far from equilibrium regime. We measure the power spectrum of $\frac{dM}{dt}$ where M is the magnetization in the RFIM near the non-equilibrium disorder induced critical point ($R = 2.3$, $\Delta H < 0.05$). Simulation of 3d system with 100^3 total spins averaged over 60 disorder realization system. Black and grey spectrum starting from the bottom at the high frequency end are increasing temperatures $\theta = 0.01, 0.04, 0.16, 0.64$. Dashed line is low frequency scaling discussed in the text. Dash-dotted line is expected scaling for independent two-state switchers. Dotted line overlapped with spectrum is a fit from the spectruml form shown in eq. 7.5.

7.3 The high frequency crossover: ω_H

Of all the structure in the PS this crossover is the least intriguing. The high frequency crossover, ω_H is the rough demarcation frequency between the spectral signature of the large avalanches, $P_{ztne}(\omega)$ and the thermal fluctuations. As $\theta \to 0$, the avalanche size distribution follows a power law, $D(S) \sim S^{-\tau}$ where $\tau > 0$ ensures there will be many small avalanches. At $\theta > 0$ the small avalanches will be thermally active as they have small energy barriers to flipping. This population of thermally active spins will have a contribution to the power spectrum. The contribution of these spins to the spectrum can be understood from Arrhenius transition rates of independent switchers over a relatively smooth energy distribution. The spectrum of the magnetization takes on the form [65] familiar from studies of $1/f$ noise.

$$P_M(\omega) \sim \left| \int e^{i\omega t} M(T) dt \right|^2 \propto \frac{\theta}{\omega}. \tag{7.4}$$

The PS of the time derivative of the magnetization (*i.e.*, the voltage) becomes $P_{temp}(\omega) \propto \theta\,\omega$. (Although the exponent a in eq. 7.3 is $a = 1$, it is well known that small deviations from 1 are common in generic $1/f$ noise [66]). The total power spectrum is obtained by simply adding the PS from Eqs. 7.2 and 7.4,

$$P(\omega) \sim P_{ztne}(\omega) + \theta\omega. \tag{7.5}$$

In fig. 7.2 we show with dotted lines that the fit of the above expression to the data give excellent results. Equation 7.5 provides an explicit expression for the corner frequency ω_H obtained when both contributions on the RHS become of the same order of magnitude yielding

$$\omega_H \sim \theta^{\frac{-\sigma\nu z}{1+\sigma\nu z}}. \tag{7.6}$$

The fit of the corner frequency scaling data compared to ω_H scaling is again in excellent agreement (see fig. 7.5). The contribution from the thermally active spins

vis-à-vis measurements of pulse statistics in BN will be that of an increased background noise and subsequent need to increase the voltage threshold required to define pulses in experiments [6]. If this contribution to the noise is below the background experimental noise, thermal effects at the high frequencies will not be observed. These spins should have no other significant effect on the CN measurements.

7.4 The low frequency crossover: ω_L

The structure in the PS at low frequencies results from avalanches being thermally nucleated at a field less than the field they would have been nucleated in the absence of thermal fluctuations. The low frequency scaling regime, $P(\omega) \sim \omega^{-\phi}$ (and corresponding corner frequency, ω_L) is reminiscent of low frequency crossovers apparent in the PS of Barkhausen pulses at room temperature [58, 6] as well as sandpile automata with increasing deposition rates [56]. In modeling of the Barkhausen noise experiments, thermal fluctuations were neglected and the cross-over unexplained. In the sandpile model the temperature was not a parameter although the random deposition in the sandpile model may induce fluctuations analogous to thermal fluctuations[2].

We will now argue that the low frequency behavior of the PS can be understood by introducing an effective nucleation field—depending both on temperature and sweeprate—that is shifted in relation to the applied external field. This effective nucleation field pushes the system away from the critical external field, and the $\theta = 0$ scaling of the PS is modified at low frequencies.

To better understand the origin of the effective nucleation field, we recall the study of magnetic viscosity (MV) [67]. The experimental setup for measuring MV is as follows: The external field is fixed and the magnet is initialized in some meta-stable

[2]At large Ω and $\theta = 0$, large avalanches are interrupted by field triggered spins within their bulk. In our argument, this process occurs, at $\theta > 0$, due to the parsing of the $\Omega = \theta = 0$ avalanche into smaller domains by virtue of being nucleated away from the real critical field.

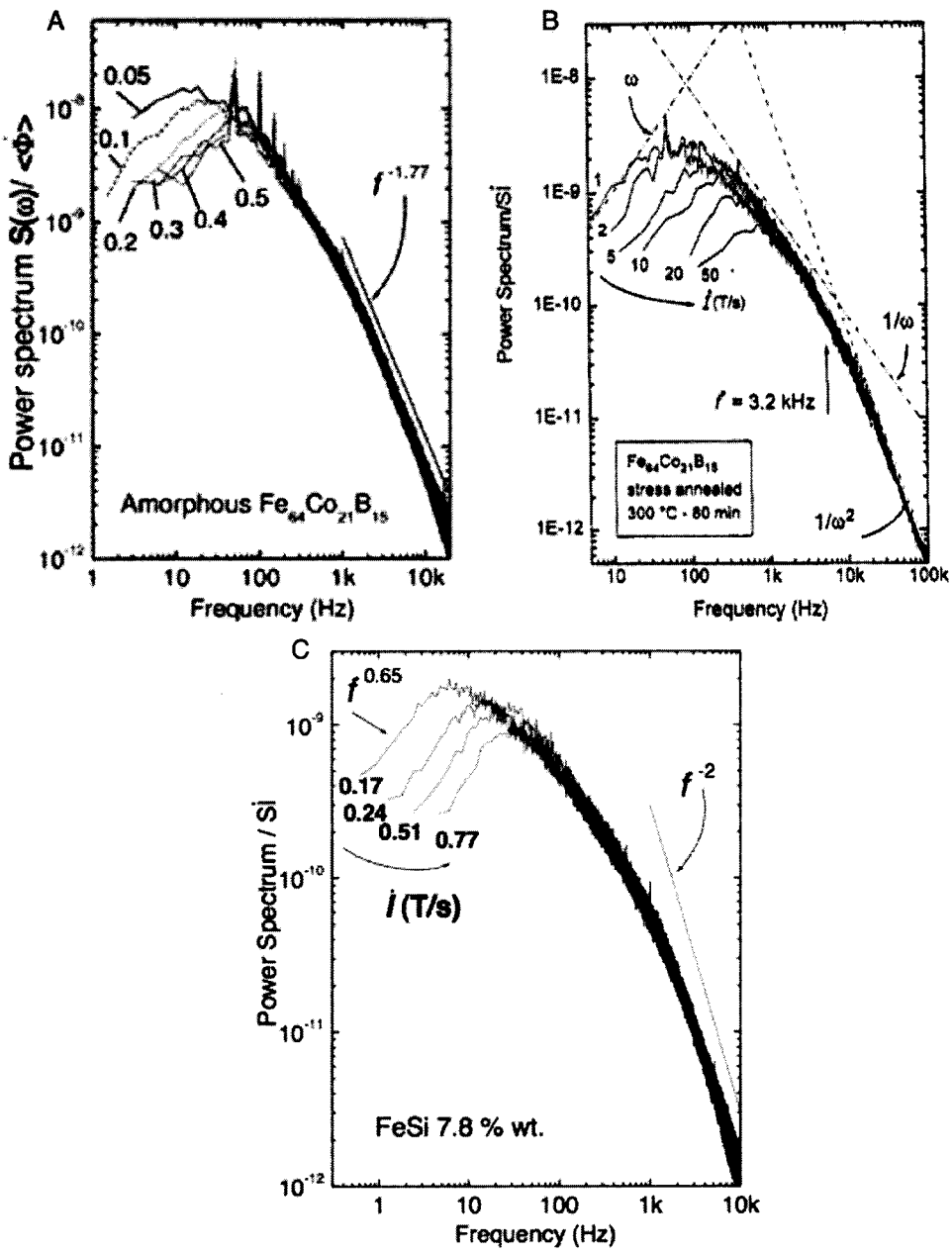

Figure 7.3: Barkhausen voltage power spectra measured at room temperature for various materials. We show spectra as a function of sweeprate for 3 materials: A.) Amorphous $Fe_{64}Co_{21}B_{15}$. B.) Partially crystallized (16%) sample induced by annealing and C.) Polycrystalline 7.8% $SeFe$ ribbon (reproduced from [6]). These materials were all measured at room temperature and all exhibit a crossover regime from $P(\omega) \sim \omega^{\frac{-1}{\sigma\nu z}}$ at higher ω to $\sim \omega^{-1}$ at lower ω.

state. The magnet slowly relaxes to an equilibrium state by a process assumed to be independent domain flipping. It is further assumed that these domains have a flat random distribution of energy barriers to flipping and that for simplicity, the domains flip irreversibly. Over time, after the spins with energy close to zero have flipped, one has to wait longer and longer to flip the next domain. The effective nucleation field is the field that would be required at zero temperature to flip a spin that has been thermally pushed over the barrier. This field grows as the logarithm of the waiting time.

When equilibration times are long compared to the driving rates, the difference (h_s) between the effective field and the real field can be obtained by equating the rate of effective field change over time to the real field driving rate yielding $h_s \sim \theta ln(\frac{\theta}{\Omega})$. (Figure 7.4 sketches the idea of the effective nucleation field whose value is mathematically derived in appendix D).

At finite temperature, when the field is increased from $H_{ext} = -\infty$ to the critical field H_c, thermally induced spins will prematurely trigger zero temperature avalanches. If we assume that the scaling of these avalanches will come from the real field proximity to the critical field, avalanches that would be nucleated at the critical field and have an infinite cutoff in the infinite system size limit will be nucleated instead when $H_{ext} + h_s = H_c$. The duration distribution cutoff will then be $T^*_{\theta>0} \sim h_s^{\frac{-\nu z}{\beta\delta}}$, where the 3-d exponents are obtained from numerics [68, 91]. Large $\theta = 0$ avalanches will thus be parsed into smaller chunks at $\theta > 0$. Consequently, the system never reaches the critical field H_c at the ztneRFIM R_c when $\theta > 0$.

The contribution to the power spectrum of all avalanches with duration less than the temperature induced cutoff, $T^*_{\theta>0}$, will remain unchanged while scaling for frequencies below $\omega < 1/T^*_{\theta>0}$ will be cut-off. This yields the scaling with temperature and sweeprate of ω_L to be

$$\omega_L \sim (\theta \ln(\theta/\Omega))^{\frac{\nu z}{\beta\delta}} . \tag{7.7}$$

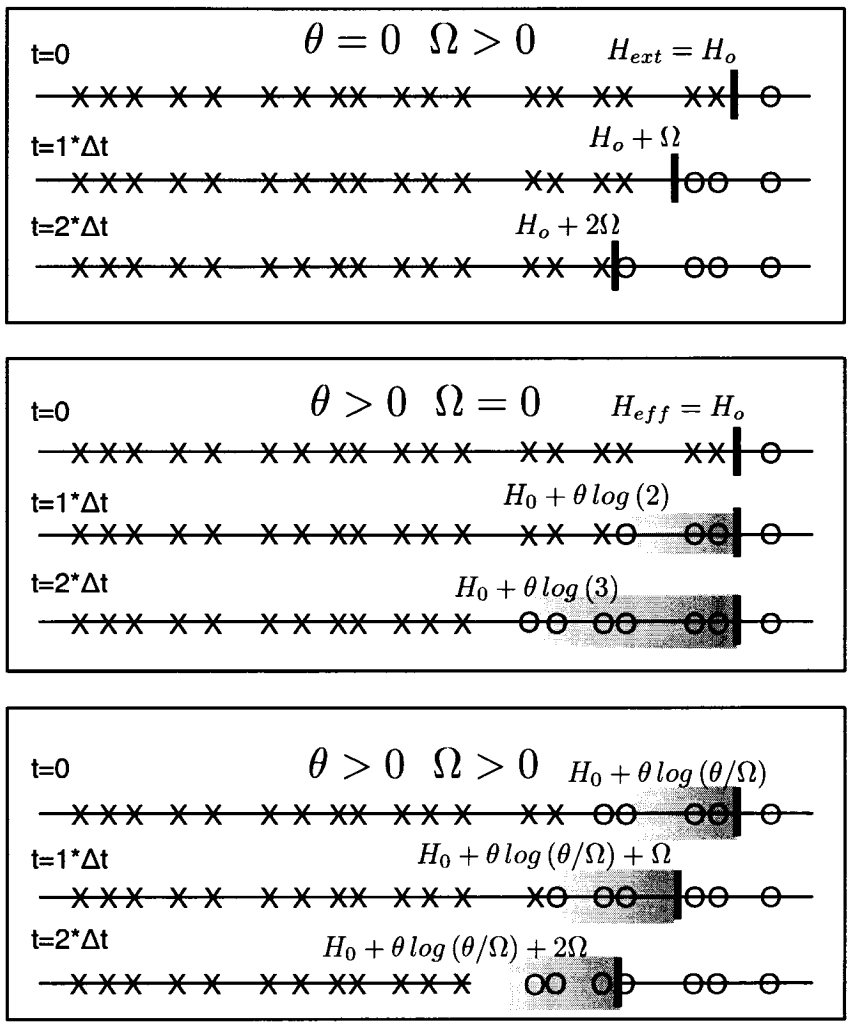

Figure 7.4: Illustration of effective nucleation field. In this figure, "X" and "O" represent the zero temperature field required to flip an avalanche. The bold vertical line represents the external field at a given time measured in units of $\Delta t = 1$. For $\theta = 0$ the line has no horizontal "width" and avalanches to the right of the line have been nucleated, "O", and avalanches to the left have not, "X". As the field is increased (*i.e.*, moved to the left in the diagram) nucleation events cross the line and are nucleated. At $\theta > 0$ and $\Omega = 0$ the line gets smeared out and allows for the thermal nucleation of avalanches that would require larger external fields at $\theta = 0$. The avalanches that result from *these* nucleations will not be the same at those that would have been nucleated at $\theta = 0$ (discussed in the text). The length in H covered by the smear grows in time t as $\theta \log\left(1 + \frac{t}{t_o}\right)$. At $\theta > 0$ and $\Omega > 0$ the length of the smear, h_s reaches a constant value if the rate at which the external field is increasing is greater than the rate at which the thermal smear is advancing. The effective nucleation field is then $H_{ext} + h_s$.

The fact that scaling persists for $\omega < \omega_L$ with a different exponent suggests that critical correlation still exist at low frequencies. We suggest that this is the result of the propagation, albeit interrupted, of large zero temperature avalanches. A zero temperature avalanche, at finite temperature, flips in fast chunks (consisting of as many MC time steps as shells) with a typical size given by $(T^*_{\theta>0})^{\frac{1}{\sigma\nu z}}$. The zero temperature avalanche of size S at $\theta = 0$ will then break up into roughly N of these chunks for $\theta > 0$, where $N \sim S(T^*_{\theta>0})^{\frac{-1}{\sigma\nu z}}$. If the typical amount of time between these chunks is some interval, t_o independent of both the size of the zero temperature avalanche and the chunks, the time it takes to propagate the entire zero temperature avalanche, *i.e.*, the stretched duration T_s, scales roughly like $T_s \sim \theta^{\frac{1}{\sigma\beta\delta}} S\, t_o$. The $T_s \sim S$ scaling behavior is in contrast to the zero temperature size-duration scaling of $S \sim T^{\frac{1}{\sigma\nu z}}$. At $\theta = 0$ the power spectrum scales like $P(\omega) \sim \omega^{\frac{-1}{\sigma\nu z}}$, where $\frac{1}{\sigma\nu z}$ is derived from the size vs. duration scaling. We assume the connection between size vs. duration scaling and scaling in the spectrum holds for finite temperature below ω_L. Consequently, we suggest that the crossover in frequency space of the power spectrum mirrors a crossover in size-duration scaling of the avalanches. This is consistent with our numerical results shown in fig. 7.2.

7.5 Discussion

In this chapter we have developed a scaling theory for thermal fluctuations in crackling noise. The PS at high frequency departs from the zero temperature case at a characteristic frequency crossover (ω_H) which exists due to the contribution of independent two-state switchers consisting of thermally active small avalanches. This contribution may not be seen in experiments as this noise may be below the threshold of other, experimental sources of background noise.

Below a characteristic crossover frequency ω_L, the PS differs from the PS at $\theta = 0$

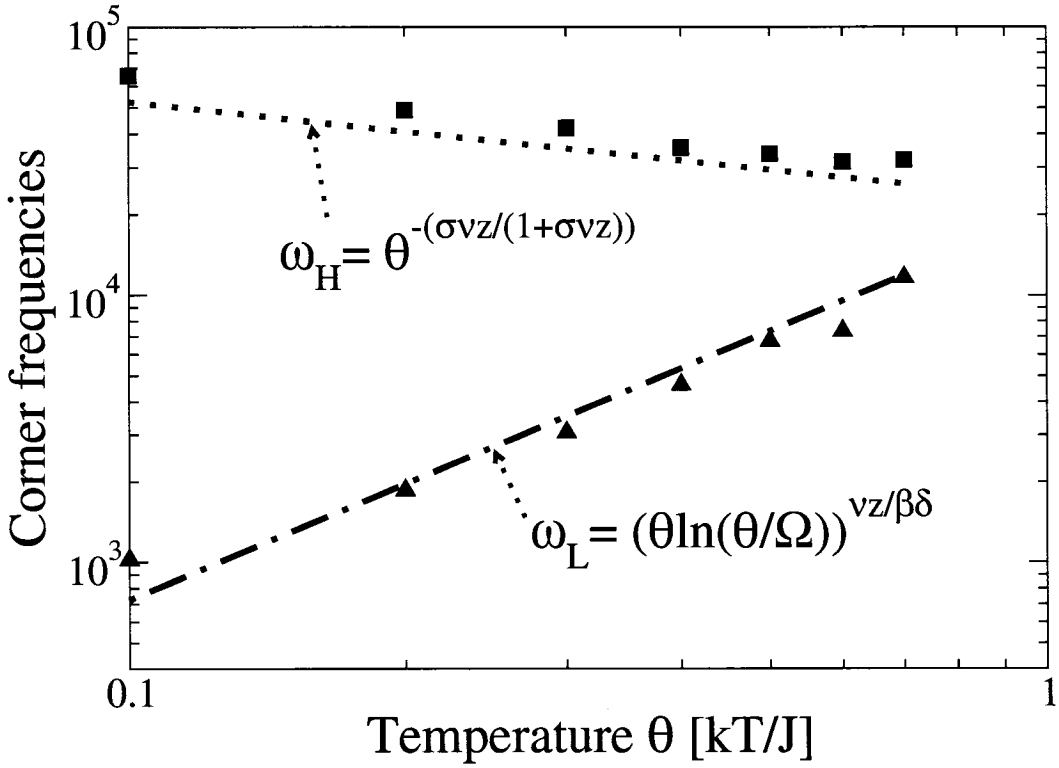

Figure 7.5: Corner frequencies from simulation compared to theory. We show a Log-Log plot of corner frequencies, ω_L(triangles) and ω_H(squares) as a function of temperature obtained from simulations (same parameters as fig. 7.2). Dotted and dash-dotted line represent the scaling argument for Eqs. 7.6 and 7.7 for ω_L and ω_H with values $\frac{\nu z}{\beta\delta} = 1.32$ and $\frac{\sigma\nu z}{1+\sigma\nu z} = 0.36$ obtained from ztneRFIM in 3d [14].

due to a temperature/sweeprate induced cutoff resulting from the nucleation of large, zero temperature avalanches away from the critical field. To my knowledge, this has not been experimentally investigated. The scaling of this crossover frequency with temperature can be experimentally tested in Barkhausen systems. For systems that are near to a non-equilibrium critical point, exemplified by SOC systems as well as the disorder induced critical point in the ztneRFIM, proximity to the critical field is of utmost importance. If validated by experiment the temperature induced shift of the effective nucleation field may have significant impact on the propensity to neglect temperature in future studies.

We have also discovered an apparent scaling regime below a temperature dependent corner frequency ω_L analogous to a crossover found in BN experiments at room temperature [6]. The heuristic argument for the exponent in this scaling regime is not ultimately satisfactory as we would expect this scaling to have some relationship to the adiabatic exponents. Future studies in this regime would, no doubt, be illuminating.

One interesting aspect, from the point of view of the ztneRFIM that was neglected from our study is whether or not the low frequency scaling regime denotes significant departure from the scaling found near the disorder induced critical point. Perhaps the scaling we found is simply a manifestation of a changing of the non-universal parameters that define the critical point, such as the critical disorder? That is, we might be able to recover the zero temperature scaling by tuning the disorder. The long computational time required for the simulations we performed precluded such a study in my time in Illinois but it would be interesting to work this out in more detail in the future.

Chapter 8

Summary and possible extensions

In this dissertation I have presented results obtained by considering the effects of widening the parameter regime over which CN is typically studied, namely the $\Omega = 0$ and $\theta = 0$ regime. In chapter 6 we introduced finite sweeprate, and revisited the ideas of temporal superposition. We illustrated how experimental results on pulse size and duration distributions on various materials exhibiting BN could be understood by generic features determined from analysis in the adiabatic scaling.

The overall message of the slow sweeprate investigations is that analysis of the pulse statistics at finite sweeprate does not, in principle, tell you any more about the system than does a study in the adiabatic regime. This is true even when interesting sweeprate behavior, such as scaling exponents with sweeprate dependence, is present. This knowledge should aid in the interpretation of sweeprate results obtained in the future and perhaps yield additional means of measuring adiabatic exponents even at finite sweeprates. For example, the scaling argument for spatial overlap of simultaneously propagating avalanches allows one to measure adiabatic exponents by driving the system faster than Ω_t and measuring the sweeprate dependence of the low frequency maximum in the power spectrum.

In chapter 7 we investigated the effects that thermal fluctuations, in addition to a finite sweeprate, would have on the crackling response. Out of this study we have

obtained an experimentally verifiable relationship between temperature, sweeprate, and the crossover to typically observed low frequency scaling behavior in Barkhausen spectra beyond the trivial scaling due to independent, thermally-active spins.

In appendix C we present arguments for a speculative expanded phase diagram and a scaling theory connecting the equilibrium RFIM with the disorder induced critical behavior found in the ztneRFIM. Dispite the speculative nature of this appendix it suggests a number of features that can be verified (or not) by numerics, analysis and/or experiments in the future; for example, numerical investigations could be used to detect the presence of ztneRFIM universality at all temperatures below the critical temperature in the equilibrium model investigated at sweeprates that would barely allow for equilibration at θ_c^{eq}.

8.1 Future projects

Of course, the work presented in this dissertation has not wrapped up all that is of potential interest in crackling systems. Below I provide a sketch of five issues that would be interesting to pursue in the future. They are listed in order of increasing foreseen difficulty.

8.1.1 Develop FST into a widely available application

For experimentalists investigating sweeprate effects of pulse size and duration distributions, even outside the realm of crackling noise, the FST would be an invaluable tool to distinguish between effects that arise out of temporal superposition and those that are due to other effects.

In our study the FST was initiated with idealized distributions of avalanche sizes and durations but one could equally use experimentally determined distributions, or, build a database of the real avalanches to use as the input. One could decouple

the collective microscopic relaxations from larger scale effects, such as interactions between avalanches not captured in the "uniformly distributed in the internal field" assumption. With the FST it is possible to isolate the "controlled" results by comparing the results "manually" obtained from the FST to the full fledged physics going on inside the real material. With a database of real avalanches as input, one could also go beyond pulse statistics and compare spectral measurements. This analysis could be coupled with higher order spectra [20] to provide a complete and intuitive picture of the mesoscopic dynamics occurring in Barkhausen systems.

8.1.2 Investigate Barkhausen noise irreproducibility

It is known that BN taken over identical field histories does not produce identical pulse trains [69, 40]. It is also known that thermal fluctuations, alone, are not able to account for this irreproducibility. One vague theory for this is that first thermal fluctuations slightly modify the nucleation order of avalanches, the long range restoring forces then amplify these slight modifications into observable differences, these observable differences ultimately change the spatial arrangement of a domain wall which ultimately results in a unique path from sweep to sweep. The FST is unable to attest to any spatial rearrangements, however, it can be used to investigate how the long range restoring forces can amplify slight changes in nucleation order.

For example, take two avalanches A_1 and A_2 that would nucleate in $1, 2$ order at $\theta = 0$. The nucleation fields of these avalanches could be very close to each other in internal field space, yet far separated in time due to the long range forces. Thus, small fluctuations in nucleation order that occur in internal field space could have large consequences in the time domain. Over large timescales the pulse profiles measured for a predetermined set of avalanches with deterministic nucleation fields with thermal fluctuations will have generally the same shape due to the inability of the FST to encode spatial information. However, over short timescales the nucleation order could

be scrambled. By scaling arguments relating timescales of scrambled nucleation order to changes in the spatial configurations of a domain wall one could construct a picture of how thermal instabilities eventually get amplified to irreproducibility of Barkhausen pulses.

8.1.3 Develop $\theta > 0$ hybrid algorithm based on the Kuntz-Sethna method

In appendix C we present a scaling theory with the conjecture that the nonequilibrium, zero temperature, disorder induced critical behavior holds over a range of temperatures and sweeprates. In the regime where the system is deterministically falling over free energy barriers, as in the ztneRFIM, it should be possible in a simulation code to take advantage of the local relaxation dynamics which yield fast simulation times while maintaining the ability of the system to make attempts at global relaxation. This would involve a thermal shuffling procedure of the pointer structure used in the KS algorithm.

The speed-up in run-time scaling might be enough make numerical studies of large systems in the disorder induced critical regime at finite temperature more feasible for completion in a graduate student lifetime. Such studies would enable numerical probes into the proposed disorder induced scaling regime at finite temperature ($\theta > 0$).

8.1.4 Investigate connections between equilibrium phase transition and disorder induced critical point.

The similarity between the equilibrium exponents near the para-ferromagnetic phase transition and the ztneRFIM near the disorder induced critical point is a "coincidence" too sweet to ignore. Unfortunately there does not exist an analytical treat-

ment that has shown the ability to cross the gap between the far from equilibrium regime and the equilibrium partition function methods. I cannot guess how this will be resolved.

However, there is still hope. There are powerful and efficient methods for numerically obtaining ground state configurations at the zero temperature fixed point of the equilibrium RFIM (*i.e.*, min-cut/max-flow algorithms discussed in [70] and references therein). These methods can be extended to find the finite field $H_{ext} > 0$ ground state at zero temperature [71]. One interesting numerical study would be to compare how a system progresses from ground state at a field H_1 to a field H_2 to the the method of traversing metastable states to achieved by avalanching processes. Studies such as this may provide valuable insight into the relationship between the equilibrium scaling and the far from equilibrium scaling. Such studies have been done in the past for very small system sizes in the 2-d RFIM [72] but new methods allowing for large system sizes in the 3-d RFIM coupled with the perspective presented in appendix C would lead to illuminating results.

8.1.5 Investigate possible relationships between disorder induced critical behavior and glassy phenomenology

Slow equilibration times characterizing the so-called glassy dynamics in systems with either quenched disorder (spin glasses), or disorder that is dynamically generated and frozen in (structural glasses), are responsible for some of the most interesting puzzles facing statistical physicists today. There is a rich collection of models used to study glassy behavior (for an overview see [73]) but some of the basic characteristics, such as a non-arrhenius rise of the relaxation time as the glass transition temperature is approached from above, are still not understood [74]. It seems tacitly accepted that whatever is going on, it is a result of co-operative effects. However, the nature of

these effects remains a mystery.

It would be interesting to attempt to characterize glassy behavior in the RFIM from the point of view described in appendix C. The benefit of this perspective is that it straddles the valley formed by the a well studied equilibrium phase phase on one side and the disorder induced critical behavior and corresponding inclusion of field history on the other. Perhaps the lessons learned from the ztneRFIM can be of aid in the grand glassy dynamics endeavor.

Appendix A

Number of pulses as $\Omega \to \infty$: The determination of Ω_t

As discussed in section 6.2.1, the dead time distribution $D_{\tau_d}(\tau_d, n)$ can be determined by considering that τ_d is the sum of two random variables, $\tau_d = \tau_n + (-T_N)$, where τ_n is the nucleation time of the n^{th} previous avalanche, and T_n is the duration of that avalanche. In $LRRF^-$, these variables are independent and the resulting distribution is a convolution of the distributions of τ_n and T are

$$D_{\tau_n}(\tau_n, n, a\Omega) = {\tau_n}^{n-1} (a\Omega)^n \frac{e^{-\tau_n a\Omega}}{\Gamma(n)} \tag{A.1}$$

(see [75]) and

$$D_T(T) = T^{-\alpha} \mathcal{F}_T \left(\frac{T}{T^*} \right) \tag{A.2}$$

(where $\mathcal{F}_T$ is a universal scaling function) respectively.

The gamma distribution is well behaved with mean $\frac{n}{a\Omega}$ and standard deviation $\frac{\sqrt{n}}{a\Omega}$ in contrast to the power law distribution of the durations whose first and higher moments diverge if $\alpha < 2$. To obtain the characteristic sweeprate for $\alpha < 2$ we neglect the fluctuation in τ_n and replace the n^{th} previous nucleation times with their mean values. Consequently, we replace the expression defining dead times, $\tau_n - T$, where both variables have fluctuations, with $\tau = \langle \tau_n \rangle - T$.

With this simplification, the probability that an avalanche is not absorbed by the n^{th} previous avalanche is $1-(T^*)^{1-\alpha}\,h(\frac{\tau_n}{T^*})$, where $h(\frac{\tau_n}{T^*}) = \int_{\frac{\tau_n}{T^*}}^{\infty} \mathcal{F}_T(u)du$. The probability, $\tilde{P}$, that an avalanche is not absorbed into *any* of the previous avalanches is then

$$\tilde{P}(a\Omega, T^*, \alpha) = \prod_{n=1}^{\infty}\left(1-(T^*)^{1-\alpha}\,h\left(\frac{n}{a\Omega T^*}\right)\right), \tag{A.3}$$

or, equivalently,

$$Log\left(\tilde{P}\right) = \sum_{n=1}^{\infty} log\left(1-(T^*)^{1-\alpha}\,h\left(\frac{n}{a\Omega T^*}\right)\right). \tag{A.4}$$

Changing the sum over n to an integral over $u = \frac{n}{a\Omega T^*}$ for large T^* (and consequently large L) we have

$$\log \tilde{P} = a\Omega T^* \int_{\frac{1}{a\Omega T^*}}^{\infty} \log\left(1-(T^*)^{1-\alpha}\,h\left(u\right)\right) du. \tag{A.5}$$

The Taylor expansion for the integral (noting $\log(1-x) = x - O(x^2)$) yields

$$\log \tilde{P} = -a\Omega(T^*)^{2-\alpha} \int_{\frac{1}{a\Omega T^*}}^{\infty} h\left(u\right) - O\left((T^*)^{1-\alpha}\right) h^2(u)du. \tag{A.6}$$

Finally, by considering the formal limit of $T^* \to \infty$ the equation for $\tilde{P}$ is

$$\tilde{P}(a\Omega, T^*, \alpha) = Exp[-a\Omega(T^*)^{2-\alpha} f(a\Omega T^*)], \tag{A.7}$$

where $\lim_{x\to 0} f(x) = 0$. Reading off from eq. A.7 the characteristic sweeprate at which the exponential function goes to zero (*i.e.*, $\frac{N_p}{N}$ goes to zero leaving only one large pulse) we find that $\Omega_t = \frac{1}{(T^*)^{2-\alpha} f(a\Omega T^*)}$.

For $\alpha > 2$, the mean avalanche duration does not diverge and neglect of the fluctuations in the nucleation times is not warranted. However, viewed from the perspective of 1-d percolation theory [76] the characteristic sweeprate is simple to deduce. In 1-d percolation of points on a lattice with spacing ℓ_d the critical density p_c to obtain percolation is $p_c = 1$. Allowing for the points to have a width ℓ the critical density is $p_c^{\ell > \ell_d} \propto \ell^{-1}$. The critical density in our case is $a\Omega_t$ and the width of the

elements on the time axis is $\langle T \rangle$ hence $\Omega_t = \frac{1}{a\langle T \rangle}$. Since $\langle T \rangle$ is constant for $\alpha > 2$ and $\langle T \rangle \sim (T^*)^{2-\alpha}$ for $\alpha < 2$ we obtain the scale of the sweeprate at which total temporal overlap occurs to be

$$\Omega_t \simeq \frac{1}{\langle T \rangle f(a\Omega T^*, \alpha)}, \tag{A.8}$$

where $f(a\Omega T^*, \alpha)$ is a scaling function determined through the relationship given in equation A.6.

Appendix B

Finite sweeprate and spectral superposition

The ability to view the time series at slow but nonzero field driving rate as a superposition of pulses formed in the adiabatic limit also allows us to cleanly determine the effect of field sweeprate on the power spectrum (PS) of the voltage time series. As a starting point in the analysis we first derive the PS in the slow and intermediate sweeprate regime in the ztneRFIM. In this regime avalanche nucleations for a given disorder realization have a deterministic field at which they occur, H_i; The population of these nucleation events are Poissonian distributed in H and time (assuming the external field itself is linear, or approximately so, in time). We begin analysis on the ztneRFIM and discuss how the details will be augmented for different universality classes. Let each avalanche have a voltage time series as follows:

$$V_i(t) = \begin{cases} V_i(t) & if\ 0 < t < T_i \\ 0 & otherwise \end{cases} ,$$

and let the time of the ith nucleation $\tau_i = \Omega\, H_i$. The voltage time series of a train of avalanches is thus

$$V(t) = \sum_{i=1}^{N} V_i(t - \tau_i) .$$

The PS of such a voltage series is

$$P(\omega) = \widetilde{P(\omega)} + 2Re\left(\sum_{j>i}^{N} e^{i\omega(\tau_j - \tau_i)} V_i(\omega) V_j^*(\omega)\right). \tag{B.1}$$

For large numbers of avalanches, the second term on the RHS can be written as

$$2Re\left(\left\langle \sum_{j}^{N} e^{i\omega\Delta_{ij}} V_i(\omega) V_{i+j}(\omega)\right\rangle_i\right), \tag{B.2}$$

where $\Delta_{ij} = \tau_j - \tau_i$. If all avalanches are independent from one another and the nucleation times are fixed in H_{ext} then eq. B.2 simplifies to

$$N\left|\langle V(\omega)\rangle\right|^2 \sum_{j}^{N} \left\langle e^{i\omega\Delta_1}\right\rangle^j.$$

This yields the following PS (result derived differently and reported [60])-

$$\begin{aligned} P(\omega) &= a(H)\Theta\,\Omega\,\left\langle |V(\omega)|^2\right\rangle \\ &+ 2\left|\langle V(\omega)\rangle\right|^2 Re\left(\frac{\int_0^\infty D(\Delta)e^{i\omega\Delta}\left(1-\left(\int_0^\infty D(\Delta)e^{i\omega\Delta}\right)^N\right)}{1-\int_0^\infty D(\Delta)e^{i\omega\Delta}}\right), \end{aligned} \tag{B.3}$$

where Θ the duration of the BN train and $D(\Delta)$ is the distribution of times Δ_i separating seeds of adjacent avalanches. If $D(\Delta)$ is Poissonian eq. 6.11 reduces to a special case of Campbell's theorem [55] and the resultant PS is simply the sum of the spectra for each avalanche. This allows for a determination of the exponents associated with the avalanches (z,νz,$\sigma\nu z$,$\frac{3-\tau}{\sigma\nu z}$,$\frac{2-\tau}{\sigma\nu z}$) even in the intermediate sweeprate regime where no "pulses" exist [36].

In $LRRF^+$ approaching the adiabatic limit $\Delta_{ij} = \tilde{\gamma}\sum_{k=i}^{j-1} S_k$ where $\tilde{\gamma} = \frac{\gamma}{\Omega}$. The resulting correlation between the avalanche size and the temporal displacement of subsequent avalanches leads to the following form of eq. B.2:

$$2Re\left(\left\langle \sum_{j=1}^{N} e^{i\omega\tilde{\gamma}S_i} V_i(\omega)\, e^{i\omega\tilde{\gamma}\sum_{k=i+1}^{j-1} S_k} V_{i+j}^*(\omega)\right\rangle_i\right).$$

Since the sizes are uncorrelated by assumption this reduces to

$$2Re\left(\langle V^*(\omega)\rangle\left\langle e^{i\omega\tilde{\gamma}S} V(\omega|S)\right\rangle \sum_{j=0}^{N}\left\langle e^{i\omega\tilde{\gamma}S}\right\rangle^j\right),$$

where angle brackets are averages over all avalanches. Finally, the full PS in the adiabatic limit for $LRRF^{+}$ is given by

$$P(\omega) = a(H)\Theta\,\tilde{\Omega}\,\left\langle|\phi(\omega)|^2\right\rangle + 2Re\left(\left\langle V^*(\omega)\right\rangle\left(\int_1^{S^*} S^{-\tau}e^{i\omega\tilde{\gamma}S}V(\omega|S)\,dS\frac{1-\left(\int_1^{S^*} S^{-\tau}e^{i\omega\tilde{\gamma}S}\,dS\right)^N}{1-\int_1^{S^*} S^{-\tau}e^{i\omega\tilde{\gamma}S}\,dS}\right)\right). \tag{B.4}$$

At high frequencies the second term goes to zero due to a short period in the oscillatory function. We introduce this equation to illustrate issues to be resolved in the low frequency structure of the PS. We save the detailed analysis of this equation for future work.

In general the analysis of the PS for $LRRF^{*}$ gets complicated by the dependence Δ has upon V. For example, by adiabatically introducing demagnetization fields proportional to the magnetization τ_{i+1} is shifted by an amount τ^s_{i+1} self consistently determined by $\tau^s_{i+1} = \gamma\int V(t,k)dt$, where γ is the demagnetization proportionality constant. In the adiabatic sweeprate limit (*i.e.*, where there are large stretches of time where $V(t,k)$ is zero) the shift is simplified: $\tau^s_{i+1} = \gamma\sum\int_0^{T_i} V_i(t,k)dt$. Despite this complexity, reasonable simplifications can be made that allow for determining the form of $P(\omega)$. With $\gamma = 0$, which can be obtained by suitable geometries of the samples (see [6] and references therein), and applying the assumptions used for the pulse distributions, considerable progress can be made.

Appendix C

Scaling in the RFIM pushed out of equilibrium

As one pushes an extended system further and further away from equilibrium, the task of finding the interdependence between measurable macroscopic variables becomes increasingly difficult. In and near equilibrium, powerful tools from statistical mechanics (which is built to yield a state function description of a system), in principle, allow for as much detail as patience will allow. Far from equilibrium, the questions that must be asked and answered to simply *begin* to study a system can be daunting in themselves. As a trivial illustration, consider the following question: What is the most likely spin configuration of a simple Ising magnet at zero temperature, zero external field and zero magnetization? Potential answer: I most like the state in which the top half is all spin up and the bottom half is all spin down. A perfectly reasonable answer without the context of equilibrium! How one would prepare such a system in the real world and why someone might think that this is the most likely preparation is yet another question. The point is, without the bedrock of equilibrium, these questions whose answers depend on the history of the system become important.

Of course, the zoo of potential ways to prepare a system in a given state may simply

be irrelevant or forced to be so. Equilibration times may be so fast at temperatures of interest that the system is always an equilibrium system as far as us humans are concerned. If, on the other hand, the equilibration times are so long that equilibrium is not approached over time scales of interest, one can proceed by adopting or creating a conventionally accepted preparation and then constructing a dynamic description for the chosen history. In the body of this dissertation I have primarily investigated the latter case. We have compartmentalized Nature into equilibrium systems and far from equilibrium systems. What lies in the gap between? I have introduced a tentative step into this gap in chapter 7 by introducing temperature to the dynamic description. Nature, however, is not so timid.

Materials in which the equilibration times lie over experimentally routine time scales have recently garnered much interest. This slow approach to equilibrium is particularly prevalent in systems that have quenched disorder. The reason for this lies in the fact that the disorder couples to the degrees of freedom in the material and produces large barriers in the free-energy landscape. These "slow" or glassy dynamics can produce technologically and theoretically interesting effects such as aging and memory effects.

Glassy behavior is observed in experimental studies on diluted antiferromagnets in an external field [77, 78, 79, 80] which have been mapped to the RFIM [81], Monte Carlo numerical studies [82, 83] and theoretical studies [84, 63] of the approach to equilibrium near the critical temperature in random field Ising systems. Interestingly, the non-equilibrium critical exponents associated with the universal behavior of the ztneRFIM near the disorder induced critical point in $d = 3$ dimensions [14] seem to match those obtained from 3 dimensional ground state calculations [70] of the equilibrium phase transition point well within the error bars. This is surprising, since the physical starting points of the two systems are very different. Furthermore, a perturbation expansion in $\epsilon = 6 - d$ for non-equilibrium critical exponents can be

mapped onto the expansion for the equilibrium problem to all orders in ϵ [68]. This expansion stems from a dynamical systems description of a deterministic process, which takes into account the history of the system and is designed to single out the correct metastable state, while the calculation for the equilibrium problem involves temperature fluctuations and no history dependence at all. It would be interesting to see if there is actually a deeper connection between the non-equilibrium and equilibrium critical points, and whether the calculation for the non-equilibrium model could be used to resolve long-standing difficulties with the perturbation expansion for the equilibrium model.

In this extended appendix I develop a scaling theory for the effects of temperature in the driven RFIM that have resulted from discussions with Jim Sethna. The idea is to introduce temperature fluctuations in the non-equilibrium calculation and, at the same time, a finite sweeping frequency for the external driving force. The lower the sweeping frequency Ω at fixed temperature, the more equilibrated the system, and the longer the length scale above which non-equilibrium behavior emerges. Tuning Ω allows one to explore the whole crossover region between the two extreme cases that are found in the literature (far from and close to equilibrium). Contrary to previous treatments of relaxation, the history dependence that is so essential in experimental realizations emerges naturally from this approach. At fixed temperature, but for progressively slower sweeprates, one expects to see smaller and smaller hysteresis loops, asymptotically attaining a universal shape at low enough frequencies. The tails of these hysteresis loops will match the equilibrium magnetization curve. In the limit of zero frequency, the hysteresis loop shrinks to a point, and equilibrium is expected at all values of the external magnetic field. On the other hand, taking temperature to zero first, should yield non-equilibrium behavior as seen in recent work on the ztneRFIM.

The critical point in the equilibrium RFIM occurs at zero applied field (*i.e.*, $H_c =$

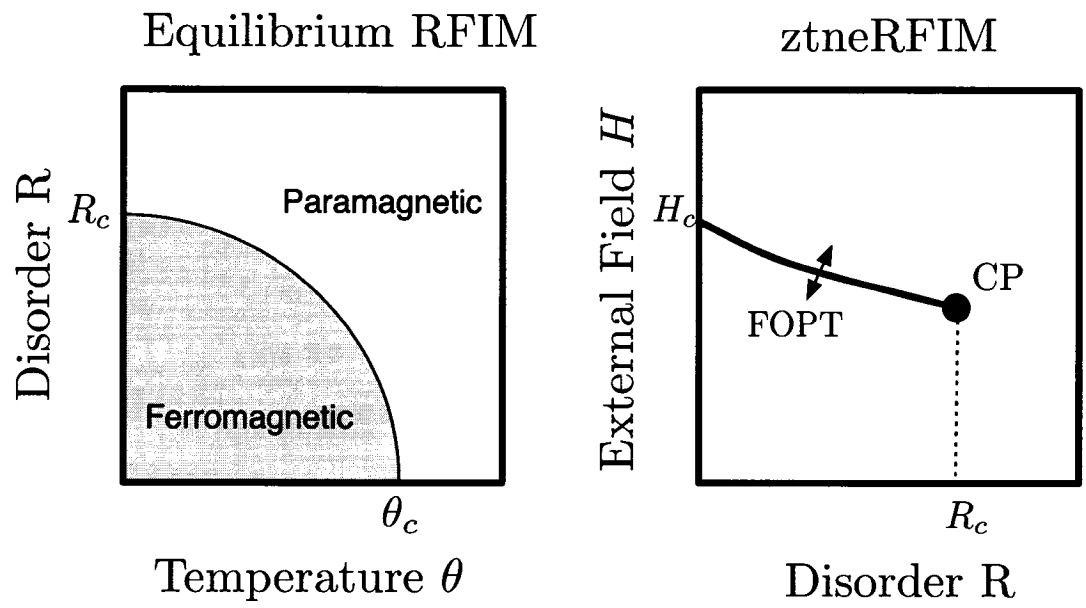

Figure C.1: Phase diagrams for the for the equilibrium RFIM (eRFIM) and the ztneRFIM. In the equilibrium model a critical $R - \theta$ curve separates a paramagnetic phase and a ferromagnetic phase. Near this curve, the critical behavior is controlled by a zero temperature fixed point at R_c^{eq} with a critical external field $H_c = 0$ from symmetry. In the ztneRFIM there is a critical point at R_c^{ne} and H_c which is characterized by power law scaling in, among other things, the avalanche size distributions. Below R_c^{ne} the system undergoes a first order phase transition (FOPT) at $H_c(R)$.

0). Approaching this point from above or below results in diverging correlation lengths and, since the transition is controlled by a zero temperature fixed point, the free energy barriers also diverge [63] resulting in slow relaxation times. In this section I present a scaling theory for the driven dynamics in the hysteresis loop based on the conjecture that, inside the hysteretic regime, the dynamics of the system are described by the disorder induced non-equilibrium critical point in the ztneRFIM.

C.1 Magnetization curves pushed out of equilibrium

Figure C.1 shows a side by side comparison of the phase diagrams in the equilibrium RFIM (eRFIM) and the ztneRFIM. The eRFIM exhibits a ferromagnetic-paramagnetic second order phase transition in 3 dimensions dominated by a zero temperature fixed point (ZTFP) studied extensively in the literature [70, 85, 63, 86, 87, 88]. (A ZTFP is when temperature flows to zero under coarse graining implying that on long length scales the transition is due to a competition between the ferromagnetic bonds and the disorder.) For the remainder of this appendix those exponents without subscripts are understood to be the critical scaling exponents near this equilibrium phase transition.

As θ approaches the ferromagnetic transition temperature $\theta \rightarrow \theta_c(R)$, the correlation length ξ of the equilibrium state grows as

$$\xi \sim (\theta - \theta_c(R))^{-\nu} f(H/(\theta - \theta_c(R))^{\beta\delta}), \tag{C.1}$$

where f is a universal scaling function. The equilibrium critical scaling is determined by a zero temperature fixed point. The energy barriers to equilibrium scale as $E \sim \xi^{\tilde{\theta}}$, where $\tilde{\theta}$ is the violation of hyperscaling exponent [89]. The time τ to get over these energy barriers by thermal activation is given by $\tau \sim \exp(\frac{E}{\theta})$. If the system is driven by an external magnetic field $H(t) \sim \Omega t$ that is increased (decreased) at a fixed rate Ω, then the system falls out of equilibrium when the field sweeprate Ω is faster than the inverse of the equilibration time. The criterion for the onset of nonequilibrium behavior is thus

$$\Omega \sim \exp(-\frac{E}{\theta}). \tag{C.2}$$

At the critical temperature $\theta = \theta_c(R)$, the equilibrium correlation length diverges as the magnetic field H is taken to zero as $\xi \sim H^{-\nu/\beta\delta}$. This implies that the

energy barriers to equilibration and thus the equilibration time scale diverge as $\tau \sim \exp(cH^{-\nu\tilde{\theta}/(\beta\delta)}/\theta)$ as $H \to 0$, with c denoting a constant. Setting $\tau^{-1} \sim \Omega$ yields the following scaling behavior of the field H_{neq} at which the system just falls out of equilibrium for the given Ω:

$$H_{neq} \sim (-\theta \log(\Omega))^{-\beta\delta/(\nu\tilde{\theta})} \tag{C.3}$$

The analysis applies to increasing and decreasing external magnetic field $H \sim \pm\Omega t$, thus the width of the emerging hysteresis loops scales as $2H_{neq}$. Figure 7.1 shows a hysteresis curve obtained using the RFIM from a simulation using Glauber dynamics with finite field sweeprate. Note that here we have implicitely assumed that the sweeprate is chosen slow enough that the fields $\pm H_{neq}$ of hysteresis onset lie within the scaling range of fields around zero, where the equilibrium scaling theory would apply if Ω was slow enough. Numerical simulations in this regime require very slow Ω and thus much computer time due to the glassy behavior of the system. Note also that for $|H| > |H_{neq}|$ the magnetization scales with the field as $M \sim H^{1/\delta}$ – it is the equilibrium magnetization curve at $\theta = \theta_c(R)$.

C.2 Speculative iso-sweeprate (I-Ω) curves in $\theta - H$ space at the critical disorder $R_c(\theta, \Omega)$

Is there any universal dynamic behavior when the system is away from equilibrium yet still subject to thermal fluctuations? Consider a given sweeprate Ω and sawtooth external field history with maximum external field given by $\pm H_{max}$. We chose H_{max} to be large enough to allow the magnetization M to saturate at $\theta = \Omega = 0$. For any Ω and disorder R we can determine the point in $\theta - H$ space where the maximum slope of a continuous magnetization curve in the saturation history occurs. In other

words, we plot the value H_m defined by the value that maximizes the slope

$$\left(\frac{dM(H)}{dH}\right)_{max} = \frac{dM(H_m)}{dH}. \tag{C.4}$$

(*N.B.*: $H_m > 0$ implies nonequilibrium behavior with hysteresis while equilibrium demands $H_m = 0$ from symmetry.) In figure C.2 we plot the external field value corresponding to the maximum slope in the saturation history. We also vary R for each θ to maximize the slope. In the regime in which there is a diverging slope in the saturation history we denote the value of this disorder as $R_c(\theta, \Omega)$. In the regime in which the slope does not diverge, the maximum slope is achieved for the minimal amount of disorder (*i.e.*, the pure $R = 0$ system).

At $\theta = \Omega = 0$ in the 3-d ztneRFIM the critical nonequilibrium disorder is $R_c \simeq 2.16 \pm 0.03$ [91] and the point in $\theta - H$ space is (0,H_c). At $\theta \simeq 0$ and $\Omega = 0$ the equilibrium critical disorder is $R_c \simeq 2.270 \pm 0.004$ [70] and the point in $\theta - H$ space is (0^+,0). For a given sweeprate that is slower than the equilibration rate at a given temperature θ_o, the maximum slope is achieved at a point (θ_o,0) on the equilibrium line (*i.e.*, there is no hysteresis in equilibrium). For this point, if $\theta_o > \theta_c^{eq}$, then the disorder R_m at which the maximum slope is obtained is 0. Otherwise, if the $\theta_o < \theta_c^{eq}$, then the critical disorder is a value determined by following the curve in the equilibrium phase diagram in figure C.1.

The behavior of the RFIM is well defined on the θ-axis (*i.e.*, in equilibrium) and the H-axis (*i.e.*, far from equilibrium) but what happens in the quadrant defined by these axes? In what follows we speculate on the general characteristics, such as curvature and intercepts, of the Iso-Ω curves over a saturation history.

Near the equilibrium line, defined to be the θ-axis, we obtain the local slope and curvature of the $H_c(\theta, \Omega)$ line at fixed Ω from equation C.3 for sweeprate values small enough for the system to reach equilibrium at a temperature less than θ_c^{eq} (for $\theta \gg \theta_c^{eq}$ universal scaling near the equilibrium line is not expected as the equilibrium system

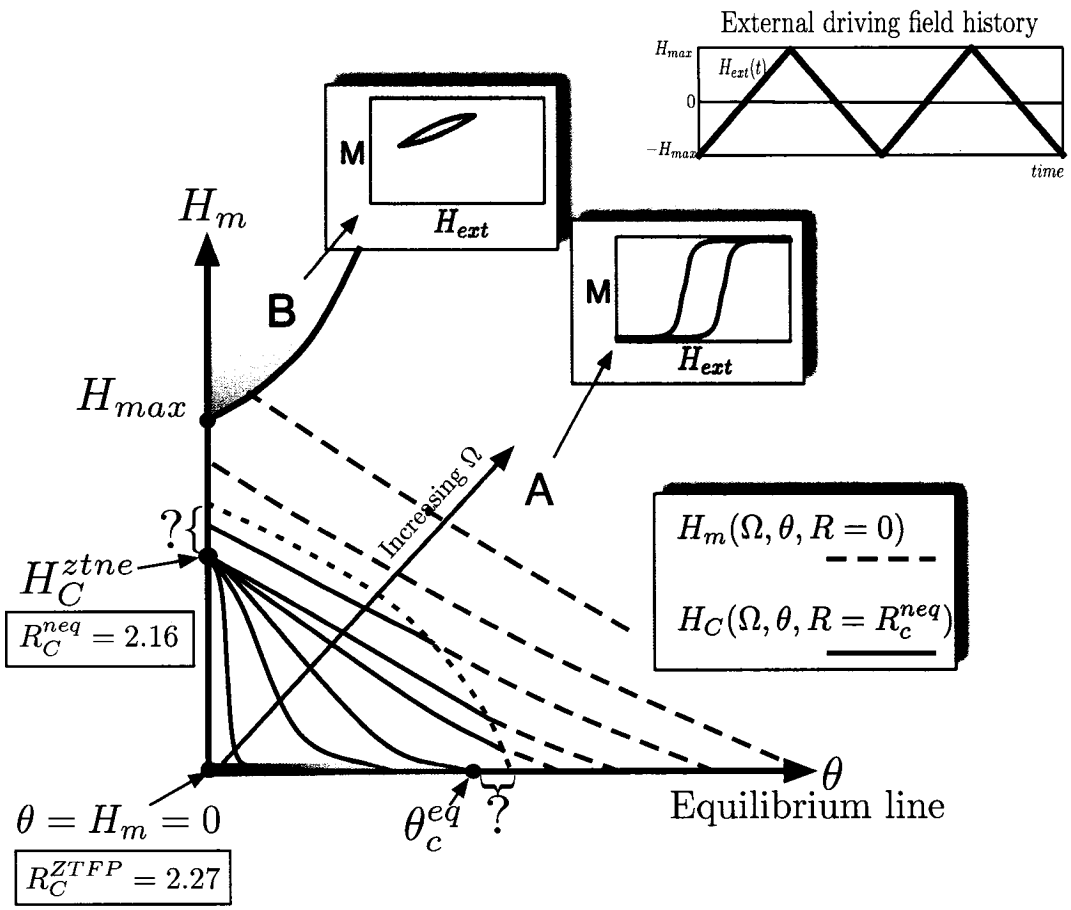

Figure C.2: A speculative sketch of the Iso-Sweeprate curves in $\theta - H$ at $R_c(\theta, \Omega, H_c)$. Schematic diagram of the external field, H_m at which the $M(H)$ curve has its maximum slope achieved by tuning the disorder in the system R. The value of H_m is approximately equal to the half-width of the hysteresis loop. When $\frac{M(H_m)}{dH}$ diverges we define $H_c \equiv H_m$. The Iso-Sweeprate curves of $H_c(\Omega, \theta)$ for increasing Ω in $\theta - H$ space are given by the solid lines. Dashed lines represent a saturation curve that cannot be made to have a diverging slope, even at $R = 0$. The dotted line separates the region in which we expect ztneRFIM like scaling all the way up to equilibrium (bottom) from a non-universal regime (top). For large enough sweeprates the hysteresis loop undergoes a dynamic phase transition from symmetric loops (A) to asymmetric loops (B) [90].

is deep in the paramagnetic phase). From eq. C.3 we obtain the slope of the $H_c(\theta, \Omega)$ curve near the equilibrium line for $\theta < \theta_c^{eq}$:

$$\frac{\partial H_c}{\partial \theta} \sim -\left(-\theta \log \Omega\right)^{-\frac{\beta\delta}{\nu\theta}-1}, \tag{C.5}$$

where $\frac{\beta\delta}{\nu\theta} \simeq 0.9(1)$ from numerical work on the equilibrium RFIM in 3 dimensions [70, 82]. Considering only small deviations from the $H_c = 0$ line we note $\Omega < \tau_{eq}^{-1}$ and $-\theta \log \Omega \gg 1$. Consequently, the H_c curve approaches the equilibrium line with a small negative slope that is concave up.

Near the H-axis, or the "far from equilibrium line", in the limit of $\Omega \to 0$, H_c must go from H_c^{ztne} to zero over a small temperature window $\theta = [0, \delta\theta]$. (*N.B.* Only in the zero field cooling history can the zero temperature ground state be approached in the RFIM on experimental timescales.) Thus we conclude that for $\Omega \to 0$ the iso-sweeprate curve has a diverging slope as it approaches H_c^{ztne}.

Extrapolating from requirements on the the H_c curves given above, we plot a speculative progression of all such curves for increasing sweeprates Ω. The solid curves represent saturation $M(H)$ curves that we suspect can be made to have diverging slopes by tuning R to a critical value $R_c(\theta, \Omega)$. The dashed curves represent saturation curves that are continuous for any value of R and achieve their maximum slopes when the disorder is zero. The dotted line separating the dashed from the solid region schematically isolates the regime in which we believe disorder induced nonequilibrium critical scaling is present for $H_c > 0$. We show the termination of the dotted line on the axes above the respective critical field H_c^{ztne} and temperature θ_c^{eq} to allow for the possibility that, at higher sweeprates, systems above those critical values may still exhibit the disorder induced critical scaling. How far above these values the dotted line terminates, as well as its shape are to be determined.

As the sweeprate increases, the system becomes unable to saturate and can get stuck in an anti-symmetric phase described in [90] and references therein. In this

"phase", the notion of maximum slope in the saturation history breaks down. We do not address this regime.

It must be noted, however, that by decreasing the amplitude of the driving field such that $H_{max} < H_c^{ztne}$ one could find one's self in very interesting territory, *e.g.*, small amplitude driving to measure the response of zero field cooled systems or in subloops that have thus far only been studied at $\theta = 0$, far from equilibrium [92].

We will call this entire regime below the mysterious dotted line the disorder induced critical regime (DICR) and argue the irrelevance of temperature in the next section. In the remainder of this appendix we discuss the dynamic scaling we expect to see in the DICR with special focus on the regime near the equilibrium line.

C.3 Irrelevance of temperature in the hysteresis loop regime: Some questions for future study.

In the DICR we assume that for every point along the Iso-Sweeprate curve there is a critical value of disorder R_c that we can tune to make the slope of the $M(H)$ response curve diverge at H_c. We now argue that, if one accepts this assumption, the effect of the finite temperature will be irrelevant to the universal scaling of the nonequilibrium disorder induced critical point.

Near H_c a slight change in the external field ΔH produces a divergent response (by definition of H_c). The time it takes to produce such a change in the external field is $\frac{\Delta H}{\Omega}$. This time scale is short compared to the equilibration timescale since an iso-Ω that would reach the equilibrium curve at θ_a, say, must traverse temperatures less than θ_a from H_c^{ztne} to $H_c = 0$. (Smaller temperatures yield slower equilibration times.) The length scales involved in thermal relaxation over this timescale are fixed and are not given the time to diverge as they would in the $\Omega \to 0$ limit. Consequently, the temporal fluctuations—in general a combination of thermal fluctuation

and driven dynamics—near the critical field are determined by driven dynamics alone when viewed on large length scales. Although the thermal fluctuations will have an impact on the details of the system in the approach to the critical field, we conjecture that any such effects can be folded into an "effective" static disorder of the system. This static disorder would consist of the quenched disorder captured by R and a thermal disorder which is static above a fixed lengthscale. This would manifest itself as a shift in the non-universal value of the critical disorder R_c.

We conjecture that the character of the effective disorder composed of contributions from both the quenched disorder and the static thermal disorder will not change the determinants of the universality class, such as symmetries, interaction range, relevant dimension or the dynamics. Accordingly, we believe the contribution to the static disorder that the temperature makes will be irrelevant, in the RG sense, to the disorder induced nonequilibrium critical behavior observed in the ztneRFIM.

C.4 Scaling near the equilibrium line

If we assume that the field of greatest slope H_c of the inner hysteresis loop is a fraction $f < 1$ of the field at which the system falls out of equilibrium, *i.e.*,

$$H_c = f H_{neq}, \tag{C.6}$$

it follows that the equilibration rate at the critical field of the hysteresis loop H_c goes to zero faster than the field sweeprate Ω. For small enough hysteresis loops (*i.e.*, in the limit of temperature and field sweeprate taken to zero) the energy barrier E_c to equilibration at H_c is expected to scale to zero $E_c \sim H_c^{-a} = f^{-a} H_{neq}^{-a}$ with $a = \nu\tilde{\theta}/(\beta\delta)$. We recall eq. C.3, $H_{neq} \sim (-\theta \log(\Omega))^{-\beta\delta/(\nu\tilde{\theta})}$ and obtain the equilibration rate at H_c:

$$\exp(-E_c/\theta) \sim \Omega^{f^{-a}} < \Omega \tag{C.7}$$

since $f^{-a} > 1$. In particular, as $\Omega \to 0$ and the hysteresis loop becomes assymptotically smaller and smaller the ratio of this equilibration rate to Ω also goes to zero, indicating that temperature is less and less relevant to the processes in the hysteresis loop, where the interesting nonequilibrium critical scaling is to be expected.

We thus conjecture that assymptotically for small Ω and small temperatures such that the hysteresis loop becomes small, there is an assymptotic scaling form for the hysteresis loop, given by the scaling behavior of the nonequilibrium zero temperature RFIM, with an additional field scale given by the size of the loop, given by $H_{neq} \sim (-\theta \log(\Omega))^{-1/a}$: In the nonequilibrium zero temperature RFIM, near the critical point ($R = R_c$ and $H = H_c$) the $M(H)$ curve scales as $M(H, R) \sim h^{1/\delta_n} \mathcal{M}(h/r^{\beta_n \delta_n})$, where $h \sim (H - H_c)$ and $r \sim (R - R_c)$ and symbols with subscript n refer to exponents or critical fiends of the nonequilibrium version of the model as given in [14, 1], and $\mathcal{M}$ is a universal scaling function of the nonequilibrium model. Similarly, using Widom scaling, we then conjecture for the assymptotically small hysteresis loop in the presence of temperature at finite field sweeprate that

$$M(R, H, T, \Omega) \sim (-\theta \log(\Omega))^{(-1/(a\delta_n))\mathcal{M}}(H/(-\theta \log(\Omega))^{-1/a}, h/r^{\beta_n \delta_n}), \qquad \text{(C.8)}$$

where R_c and H_c are non-universal functions of each other, θ, and Ω.

C.5 Combined power spectra over saturation history

Finally, we discuss the scaling behavior of the power spectrum $P(\omega)$ of the Barkhausen Noise that would be measured in such a system, which is really the power spectrum of the induction voltage given by the rate of flux or magnetization change with time dM/dt as the magnetic field is slowly ramped up or down. There are really two independent contributions to this spectrum: the nonequilibrium contribution P^{neq}

and the equilibrium contribution P^{eq} to the noise. We write the nonequilibrium contribution of the noise as the normalized loop integrated power spectrum previously obtained for the nonequilibrium random field Ising model [36] multiplied with the square of the total change of magnetization in the small hysteresis loop: $(\Delta M)^2 \sim (-\theta \log(\Omega))^{-2/(\delta a)}$. We then obtain for the scaling behavior of the power spectra of the entire curve where H is ramped from $-\infty$ to $+\infty$ or vice versa at rate Ω:

$$P(\omega) \sim (-\theta \log(\Omega))^{-2/(\delta a)} P^{neq}_{normalized}(\omega) + \int P^{eq}(\omega, H) dH. \qquad \text{(C.9)}$$

Here the integral over the equilibrium power spectra extends from $H = -\infty$ to $H = +\infty$ with exception of the part in the middle for $-H_{neq} < H < +H_{neq}$ where the system falls out of equilibrium, and whose contribution is captured by the first term in the sum.

C.6 Discussion

In this appendix we have introduced a theory for disorder induced critical behavior at finite temperature spanning the regimes characterized by far from equilibrium driven dynamics and equilibrium phase behavior. We have provided a perspective from which to view this regime with the speculative IsoΩ diagram as well as arguments for expected scaling behavior of the magnetization spectrum as the RFIM is driven slightly out of equilibrium.

A numerical investigation of the validity of this theory will require significant computational power as the DICR lies over a range that can only be reached by very slow sweeprates. Consequently we must rely on our own processors to think of creative ways to numerically probe this regime.

What about experiments? In the vast literature on hysteresis and glassy phenomenology there might be support for our thesis but since the disorder induced critical behavior observed in the ztneRFIM is relatively new and the ability to tune

the disorder in a material is generally difficult the search for this support is like finding pieces of needles in haystacks and then trying to put them together. Again, as with numerics, further thought is required to try to eke out consequences of this critical regime and map them to easily manipulatable experimental systems. Ferroelectric materials with hysteresis and significant thermal fluctuations may be a good example system.

Problems of validation aside we feel this theory provides a unique perspective that may complement the work being done in the interesting gap between equilibrium systems and far from equilibrium systems.

Appendix D

The effective nucleation field H_{eff}

In the absence of thermal fluctuations the external field nucleates avalanches when the nucleation spin's local field changes sign. We recall the local field H_i^{loc} of an Ising spin in terms of the external field $H(t)$, the random field h_i, and the nearest neighbor interaction from eq. 3.2:

$$H_i^{loc} = H(t) + \sum_{j_{n.n.}} J s_j + h_i. \tag{D.1}$$

Over the saturation history a spin s_i flips when H_i^{loc} changes sign. In other words, each individual spin's orientation is such that it minimizes its contribution $U = -s_i H_i^{loc}$ to the total energy of the system. This is, of course, in contrast to the equilibrium minimum energy condition where the global configuration of spins is such that it minimizes the free energy of the system as a whole.

Far from equilibrium we expect the local minimization condition to hold even in the presence of thermal fluctuations. This requires that we keep the system far from equilibrium by driving it at a rate $\Omega > \tau^{-1}$ where τ is the characteristic relaxation time to equilibrium. The particular Ω required to insure the system is kept far from equilibrium will depend on the temperature θ of the bath the system is contact with. High temperatures require high sweeprates to ensure the system does not equilibrate.

Considering only local relaxation in the presence of thermal fluctuations we first

focus on the nucleation events and ask: At fixed external field how many unique spins, on average, will the thermal fluctuations cause to flip to a higher energy state as a function of time?

D.1 Number of nucleation events $N_{\Omega=0}(t)$ as a function of time at fixed external field H_{ext}.

We assume Arrhenius transition rates for spins to be flipped into a higher energy state given by

$$\nu = e^{-\frac{2s_i\Delta H}{\theta}}, \tag{D.2}$$

where θ is the temperature, and ΔH is the difference between the external field H and the field at which the spin would have been field flipped at $\theta = 0$. Spins that cause no other spins to flip will flip back and forth because once thermally flipped they will be in an unstable state. Spins that nucleate avalanches will get stuck in the thermally flipped state due to the nearest neighbor interaction. In the saturation history, were all spins start in the $s_i = -1$ state and transition to the $s_i = +1$ state, we ignore spins that may cause avalanches of back flips from $s_i = 1$ to $s_i = -1$. Far from equilibrium these back flips have a negligible contribution as can be seen by the flat magnetization response observed in field reversals common to measurements of inner sub-loops of the saturation history [92].

Treating the Arrhenius transition rate as a probability that a spin ΔH away from the external field will flip in a single Monte Carlo time step, we find the number of spins n that will flip in one time step to be

$$n_1 = \int_0^\infty e^{-\frac{2H}{\theta}} a(H) dH, \tag{D.3}$$

where $a_o(H)$ is the nucleation spin density before the temperature has been "turned on". We have simplified the expression by setting the external field to zero, yielding

$\Delta H = -H$ and setting $s_i = +1$. After this step, the spins available to nucleate other avalanches, captured in the nucleation spin density, have been depleted and the resulting nucleation spin density after the first time step $a_1(H)$ is $a_o(H)\left(1 - e^{-\frac{2H}{\theta}}\right)$. In general, we let $a_t(H)$ denote the nucleation spin density after t time steps and note that

$$a_t(H) = a_{t-1}(H)\left(1 - e^{-\frac{2H}{\theta}}\right).$$

Solving this trivial recursion relation gives

$$a_t(H) = a_o(H)\left(1 - e^{-\frac{2H}{\theta}}\right)^t. \tag{D.4}$$

At each time step the number of unique spins that will be nucleated in that time step is

$$N_{\Omega=0}(t) = \int_0^\infty e^{\frac{-2H}{\theta}} a_t(H) dH. \tag{D.5}$$

To find the total number of unique spins N that have flipped after a time t we simply sum all n_i up to n_t, *i.e.*,

$$N_{\Omega=0}(t) = \sum_{i=1}^{t} n_i. \tag{D.6}$$

Expanding out this equation and approximating the sum over i with an integral over t' yields

$$\begin{aligned} N_{\Omega=0}(t) &\simeq \int_0^t n(t')dt' = \int_0^t \int_0^\infty e^{\frac{-2H}{\theta}} a_{t'}(H) dH dt' \\ &\simeq \int_0^t \int_0^\infty e^{\frac{-2H}{\theta}} a_o(H)\left(1 - e^{-\frac{2H}{\theta}}\right)^{t'} dH dt' \end{aligned} \tag{D.7}$$

$N_{\Omega=0}(t)$ is easily solved:

$$N_{\Omega=0}(t) = a_o(0)\theta ln(1+t) + O(a_o' f(t)). \tag{D.8}$$

D.2 Extracting H_{eff} from Ω and $N'(t)$

In the previous section we fixed the external field and asked how many spins $N_{\Omega=0}(t)$ are thermally flipped as a function of time. At zero temperature the number of spins

that are flipped as a function of time is $N_{\theta=0}(t) = \int_0^{t\Omega} a_o(H)dH$ or

$$N_{\theta=0}(t) = a_o(0)\Omega t + O(a_o'). \tag{D.9}$$

If we neglect the curvature of a_o for a moment (we will arrive at a criterion for justification later) we can represent the number of spins that are nucleated with time as $N_{\theta=0}(t) = a_o(0)H_{ext}(t)$. Likewise, from eq. D.8 we represent

$$N_{\Omega=0}(t) = a_o(0)\theta ln(1+t) = a_o(0)\tilde{H}t. \tag{D.10}$$

The calculations for $N_{\Omega=0}(t)$ are valid for a slowly moving reference field $H_{ext}(t)$ and $\tilde{H}(t)$ is measured with respect to that reference field. When the $\tilde{H}(t)$ is advancing at the same rate as the reference field, a steady state is reached. We interpret this steady state as an effective field H_{eff} which consists of the external field plus a temperature and sweeprate shift which leads the external field by an amount h_s determined by the steady state condition. By setting the time rate of change of the external field equal to the time rate of change of $\tilde{H}(t)$ we find

$$\Omega = \frac{\theta}{1+t_{ss}}, \tag{D.11}$$

where t_{ss} is the steady state time. Plugging this time back into $N_{\Omega=0}(t_{ss}) = a_o(0)\tilde{Ht}_{ss}$ and defining $h_s \equiv H(t_{ss})$ yields

$$h_s = \theta ln\left(\frac{\theta}{\Omega}\right). \tag{D.12}$$

If shift in the external field is small (*i.e.*, $h_s \ll 1$) the structure of $a_o(H)$ can safely be neglected. Consequently, for small h_s we can write the more general

$$N(t) = a_o(H)\left(H_{ext}(t) + h_s\right), \tag{D.13}$$

where $(H_{ext}(t) + h_s) = H_{eff}$, *i.e.*, the effective nucleation field.

References

[1] J. P. Sethna, K. A. Dahmen, and C. R. Myers. Crackling noise. *Nature*, 410:242, 2001.

[2] D. S. Fisher. Sliding charge-density waves as a dynamic critical phenomenon. *Phys. Rev. B*, 31:1396, 1985.

[3] G. Gruner. The dynamics of charge-density waves. *Rev. Mod. Phys.*, 60:1129, 1988.

[4] E. Altshuler and T. H. Johansen. Experiments in vortex avalanches. *Rev. Mod. Phys.*, 76:471, 2004.

[5] G. Blatter, M. V. Feigel'man, V. B. Geshkenbein, A. I. Larkin, and V. M. Vinokur. Vortices in high-temperature superconductors. *Rev. Mod. Phys.*, 66:1125, 1994.

[6] S. Zapperi G. Durin. The barkhausen effect. In G. Bertotti and I. Mayergoyz, editors, *The Science of Hysteresis*. Academic Press, 2005.

[7] H. Ji and M. O. Robbins. Percolative, self-affine, and faceted domain growth in random three-dimensional magnets. *Phys. Rev. B*, 46:14519, 1992.

[8] K. J. Wiese. The functional renormalization group treatment of disordered systems, a review. *Ann. Henri Poincaré*, 4:473–496, 2003.

[9] A. A. Middleton and D. S. Fisher. Critical behavior of pinned charge-density waves below the threshold for sliding. *Phys. Rev. Lett.*, 66:92–95, 1991.

[10] P. Bak, C. Tang, and K. Wiesenfeld. Self-organized criticality: An explanation of the 1/f noise. *Phys. Rev. Lett.*, 59:381, 1987.

[11] P. Bak, C. Tang, and K. Wiesenfeld. Self-organized criticality. *Phys. Rev. A*, 38:364–374, 1988.

[12] C. Tang and P. Bak. Critical exponents and scaling relations for self-organized critical phenomena. *Phys. Rev. Lett.*, 60:2347, 1988.

[13] J. P. Sethna, K. A. Dahmen, S. Kartha, J. A. Krumhansl, B. W. Roberts, and J. D. Shore. Hysteresis and hierarchies: Dynamics of disorder-driven first-order phase transformations. *Phys. Rev. Lett.*, 70:3347, 1993.

[14] O. Perković, K. Dahmen, and J.P. Sethna. Disorder-induced critical phenomena in hysteresis: Numerical scaling in three and higher dimensions. *Phys. Rev. B*, 59:6106, 1999.

[15] A. Berger, A. Inomata, J. S. Jiang, J. E. Pearson, and S. D. Bader. Experiemental observation of disorder-driven hysteresis-loop criticality. *Phys. Rev. Lett.*, 85:4176, 2000.

[16] H. Barkhausen. Zwei mit hilfe der neuen verstarker entdeckte erscheinugen. *Physik Z.*, 20:401, 1919.

[17] P. Weiss. Lhypothese du champ moleculaire et la propriete ferromagnetique. *J. de Phys.*, 6:661, 1907.

[18] G. Durin and S. Zapperi. Scaling exponents for Barkhausen avalanches in polycrystalline and amorphous ferromagnets. *Phys. Rev. Lett.*, 84:4705, 2000.

[19] S. Zapperi, C. Castellano, F. Colaiori, and G. Durin. Signature of effective mass in crackling-noise asymmetry. *Nature Physics*, 1:46–49, 2005.

[20] J. R. Petta, M. B. Weissman, and G. Durin. Barkhausen pulse structure in an amorphous ferromagnet: Characterization by high-order spectra. *Phys. Rev. E*, 57:6363, 1998.

[21] P. G. DeGennes. *Superconductivity of metals and alloys.* Benjamin, New York, 1966.

[22] S. Field, J. Witt, F. Nori, and X Ling. Superconducting vortex avalanches. *Phys. Rev. Lett.*, 74:1206, 1995.

[23] F. Omori. On the aftershocks of earthquakes. *J. College Sci. Imper. Univ. Tokyo*, 7:111–200, 1895.

[24] B. Gutenberg and C. F. Richter. *Seismicity of the Earth and associated phenomena.* Princeton University, Princeton, NJ, 1954.

[25] K. Dahmen, D. Ertas, and Y. Ben-Zion. Gutenberg-richter and characteristic earthquake behavior in simple mean-field models of heterogeneous faults. *Phys. Rev. E*, 58:1494–1501, 1998.

[26] Frank Spera. private communication, 2005.

[27] E. N. Parker. Nanoflares and the solar x-ray corona. *Astrophys. Journal*, 330:474, 1988.

[28] R. J. Hamilton E. T. Lu. Avalanches and the distribution of solar flares. *Astrophys. J. Lett*, 380:L89, 1991.

[29] M. S. Wheatland and I. J. D. Craig. Toward a reconnection model for solar flare statistics. *Astrophys. Journal*, 595:458–464, 2003.

[30] B. Alessandro, C. Beatrice, G. Bertotti, and A. Montorsi. Domain-wall dynamics and Barkhausen effect in metallic ferromagnetic materials. i. theory. *J. Appl. Phys.*, 68:2901, 1990.

[31] P. Cizeau, S. Zapperi, G. Durin, and H. E. Stanley. Dynamics of a ferromagnetic domain wall and the Barkhausen effect. *Phys. Rev. Lett.*, 79:4669, 1997.

[32] J. Marcos, E. Vives, L. Manosa, M. Acet, E. Duman, M. Morin, V. Novak, and A. Planes. Disorder-induced critical phenomena in magnetically glassy cu-al-mn alloys. *Phys. Rev. B*, 67(22):224406, 2003.

[33] F. Detcheverry, E. Kierlik, M. L. Rosinberg, and G. Tarjus. Local mean-field study of capillary condensation in silica aerogels. *Physical Review E (Statistical, Nonlinear, and Soft Matter Physics)*, 68(6):061504, 2003.

[34] M. C. Kuntz, O. Perkovic, K. A. Dahmen, B. W. Roberts, and J. P. Sethna. Hysteresis, avalanches, and noise. *Computing in Science & Engineering*, 1(4):73–81, 1999.

[35] K. A. Dahmen. *Hysteresis, Avalanches, and Disorder Induced Critical Scaling: A Renormalization Group Approach.* Ph.d. thesis, Cornell University, 1995.

[36] A. Travesset, R. A. White, and K. A. Dahmen. Crackling noise, power spectra, and disorder-induced critical scaling. *Phys. Rev. B*, 66(2):024430, 2002.

[37] M. Kuntz and J. P. Sethna. Noise in disordered systems: The power spectrum and dynamic exponents in avalanche models. *Phys. Rev. B*, 62:11699, 2000.

[38] A. P. Mehta, A. C. Mills, K. A. Dahmen, and J. P. Sethna. Universal pulse shape scaling function and exponents: Critical test for avalanche models applied to Barkhausen noise. *Physical Review E (Statistical, Nonlinear, and Soft Matter Physics)*, 65(4):046139, 2002.

[39] H. J. Williams, W. Shockley, and C. Kittel. Studies of the propagation velocity of a ferromagnetic domain boundary. *Phys. Rev.*, 80:1090–1094, 1950.

[40] J. R. Petta, M. B. Weissman, and G. Durin. Dependence of Barkhausen pattern reproducibility on hysteresis loop size. *Phys. Rev. E*, 56:2776, 1997.

[41] J. R. Petta, M. B. Weissman, and K. P. O'Brien. Multiple magnetization paths in Barkhausen noise. *Phys. Rev. E*, 54:R1029, 1996.

[42] A. C. Mills, F. M. Hess, and M. B. Weissman. Statistics of the pinning field in a soft metallic ferromagnet. *Phys. Rev. B*, 66(14):140409, 2002.

[43] S. Zapperi, P. Cizeau, G. Durin, and E. H. Stanley. Dynamics of a ferromagnetic domain wall: Avalanches, depinning transition, and the Barkhausen effect. *Phys. Rev. B*, 58:6353, 1998.

[44] R. C. Martin, E. D. Siggia, and H. A. Rose. Statistical dynamics of classical systems. *Phys. Rev. A*, 8:423, 1973.

[45] T. Nattermann, S. Stepanow, L. Tang, and H. Leschhorn. Dynamics of interface depinning in a disordered medium. *Journal de Physique II*, 2:1483–1488, 1992.

[46] O. Narayan and D. S. Fisher. Threshold critical dynamics of driven interfaces in random media. *Phys. Rev. B*, 48:7030–7042, 1993.

[47] K. Binder and D. W. Heermann. *Monte Carlo simulation in statistical physics.* Number 80 in Springer series in Solid-State Sciences. Springer-Verlag, Berlin, 1992.

[48] R. J. Glauber. Time-dependent statistics of Ising model. *J. Math. Phys.*, 4:294, 1963.

[49] G. Korniss, C. White, P. Rikvolda, and M. Novotny. Dynamic phase transition, universality, and finite-size scaling in the two-dimensional kinetic Ising model in an oscillating field. *Phys. Rev. E*, 63(016120), 2001.

[50] F. Colaiori, S. Zapperi, and G. Durin. Shape of a Barkhausen pulse. *J. Magn. Magn. Matt.*, 272:E533–E534, 2003.

[51] R. A. White and K. A. Dahmen. Driving rate effects on crackling noise. *Phys. Rev. Lett.*, 91(8), 2003.

[52] J. S. Urbach, R. C. Madison, and J. T. Markert. Interface depinning, self-organized criticality, and the Barkhausen effect. *Phys. Rev. Lett.*, 75:276, 1995.

[53] E. J. Gumbel. *Statistics of Extremes.* Columbia University Press, New York, 1958.

[54] S. Yang and J. L. Erskine. Domain wall dynamics and Barkhausen jumps in thin-film permalloy microstructures. *Phys. Rev. B*, 72(6):064433, 2005.

[55] N. R. Campbell. The study of discontinuous phenomena. *Math. Proc. Cambridge Phil. Soc*, 15:117–136, 1909.

[56] T. Hwa and M. Kardar. Avalanches, hydrodynamics, and great events in models of sandpiles. *Phys. Rev. A*, 45:7002–7023, 1992.

[57] S. L. A. deQueiroz and M. Bahiana. Finite driving rates in interface models of Barkhausen noise. *Phys. Rev. E*, 64:066127, 2001.

[58] B. Alessandro, C. Beatrice, G. Bertotti, and A. Montorsi. Domain-wall dynamics and Barkhausen effect in metallic ferromagnetic materials. ii. experiment. *J. Appl. Phys.*, 68:2908, 1990.

[59] G. Durin, A. Magni, and G. Bertotti. Measurements of the Barkhausen effect in $FeCoB$ amorphous alloys. *J. Magn. Magn. Mat.*, 160:299, 1996.

[60] P. Mazzetti. Study of nonindependent random pulse trains, with application to Barkhausen noise. *Il Nuovo Cimento*, 25:1322, 1962.

[61] P. Mazzetti. Correlation function and power spectrum of train of non-independent overlapping pulses having random shape. *Il Nuovo Cimento*, 31:88, 1964.

[62] H. Bittel. Noise in magnetic and dielectric materials. *Physica*, 83B:6–13, 1976.

[63] D. S. Fisher. Scaling and critical slowing down in random-field systems. *Phys. Rev. Lett.*, 56:416, 1986.

[64] A. J. Bray and M. A. Moore. Scaling theory of the random-field Ising model. *Journal of Physics C: Solid State Physics*, 18(28):L927–L933, 1985.

[65] P. Dutta, P. Dimon, and P. M. Horn. Energy scales for noise processes in metals. *Phys. Rev. Lett.*, 43:646, 1979.

[66] M. B. Weissman. 1/f noise and other slow, nonexponential kinetics in condensed matter. *Rev. Mod. Phys.*, 60:537–571, 1988.

[67] R. Street and J. C. Woolley. A study of magnetic viscosity. *Proc. Phys. Soc. A*, 62:562, 1949.

[68] K. Dahmen and J. P. Sethna. Hysteresis, avalanches, and disorder-induced critical scaling: A renormalization-group approach. *Phys. Rev. B*, 53:14872, 1996.

[69] J. S. Urbach, R. C. Madison, and J. T. Markert. Reproducibility of magnetic avalanches in an fe-ni-co ferromagnet. *Phys. Rev. Lett.*, 75:4694, 1995.

[70] A. Alan Middleton and Daniel S. Fisher. Three-dimensional random-field Ising magnet: Interfaces, scaling, and the nature of states. *Phys. Rev. B*, 65(13):134411, 2002.

[71] Alan Middleton. private communication, 2004.

[72] C. Frontera and E. Vives. Studying avalanches in the ground state of the two-dimensional random-field ising model driven by an external field. *Phys. Rev. E*, 62:7470–7473, 2000.

[73] F. Ritort and P. Sollich. Glassy dynamics of kinetically constrained models. *Adv. Phys.*, 52:219–342, 2003.

[74] J.-P. Bouchaud and G. Biroli. Nonlinear susceptibility in glassy systems: A probe for cooperative dynamical length scales. *Phys. Rev. B*, 72(6):064204, 2005.

[75] R. V. Hogg and A. T. Craig. *Introduction to Mathematical Statistics.* MacMillan, New York, 1978.

[76] D. Stauffer and A. Aharony. *Introduction to Percolation Theory.* Taylor & Francis, Philadelphia, PA, 1985.

[77] F. C. Montenegro, A. Rosales-Rivera, J. C. O. de Jesus, E. Montarroyos, and F. L. A. Machado. Random-field-crossover scaling in mn0.35zn0.65f2. *Phys. Rev. B*, 51:5849, 1995.

[78] R. J. Birgeneau, R. A. Cowley, G. Shirane, and H. Yoshizawa. Temporal phase transition in the three-dimensional random-field Ising model. *Phys. Rev. Lett.*, 54:2147, 1985.

[79] D. P. Belanger, A. R. King, and V. Jaccarino. Random-field critical behavior of a d=3 Ising system: Neutron scattering studies of Fe0.6Zn0.4F2. *Phys. Rev. B*, 31:4538, 1985.

[80] H. Yoshizawa, R. A. Cowley, and G. Shirane. Neutron scattering study of the effect of a random field on the three-dimensional dilute Ising antiferromagnet Fe0.6Zn0.4F2. *Phys. Rev. B*, 31:4548, 1985.

[81] S. Fishman and A. Aharony. Random field effects in disordered anisotropic antiferromagnets. *J. Phys. C.:Solid State Phys.*, 12:L729, 1979.

[82] A. T. Ogielski and D. A. Huse. Critical behavior of the three-dimensional dilute Ising antiferromagnet in a field. *Phys. Rev. Lett.*, 56:1298, 1986.

[83] A. P. Young and M. Nauenberg. Quasicritical behavior and first-order transition in the d=3 random-field Ising model. *Phys. Rev. Lett.*, 54:2429, 1985.

[84] M. Mezard and R. Monasson. Glassy transition in the threee-dimensional random-field Ising model. *Phys. Rev. B*, 50:7199, 1994.

[85] J. Villain. Nonequilibrium "critical" exponents in the random-field Ising model. *Phys. Rev. Lett.*, 52:1543–1546, 1984.

[86] J. Bricmont and A. Kupiainen. Lower critical dimension for the random-field Ising model. *Phys. Rev. Lett.*, 59:1829–1832, 1987.

[87] J. Z. Imbrie. The ground state of the three-dimensional random-field Ising model. *Comm. Math. Phys.*, 98:145–176, 1985.

[88] J. Z. Imbrie. Lower critical dimension of the random-field Ising model. *Phys. Rev. Lett.*, 53:1747–1750, 1984.

[89] D. S. Fisher and D. A. Huse. Ordered phase of short-range Ising spin-glasses. *Phys. Rev. Lett.*, 56:1601, 1986.

[90] B. K. Chakrabarti and M. Acharyya. Dynamic transitions and hysteresis. *Rev. Mod. Phys.*, 71:847–859, 1999.

[91] O. Perković, K. Dahmen, and J. P. Sethna. Disorder-induced critical phenomena in hysteresis: Numerical scaling in three and higher dimensions. *Phys. Rev. Lett.*, 75:4528, 1995.

[92] J. H. Carpenter, K. A. Dahmen, A. C. Mills, M. B. Weissman, A. Berger, and O. Hellwig. History-induced critical behavior in disordered systems. *Phys. Rev. B*, 72(5):052410, 2005.

Biographical sketch

The author was born to John and Kathie White on January 7, 1972 in Apple Valley, California. He graduated from California State University, Chico in 1998 with Bachelors degrees in Physics and Mathematics.